AN INVESTIGATION INTO THE TOTAL DISSOLVED GAS DYNAMICS OF THE WELLS PROJECT
(Total Dissolved Gas Investigation)

WELLS HYDROELECTRIC PROJECT

FERC NO. 2149

FINAL REPORT
REQUIRED BY FERC

April 2009

Prepared by:
M. Politano, A. Arenas Amado and L. Weber
IIHR-Hydroscience & Engineering
The University of Iowa
300 South Riverside Drive
Iowa City, Iowa 52242-1585

Prepared for:
Public Utility District No. 1 of Douglas County
East Wenatchee, Washington

For copies of this Study Report, contact:

Public Utility District No. 1 of Douglas County
Attention: Relicensing
1151 Valley Mall Parkway
East Wenatchee, WA 98802-4497
Phone: (509) 884-7191
E-Mail: relicensing@dcpud.org

Table of Contents

List of Tables

List of Figures

List of Appendices

ABSTRACT

The current Wells Hydroelectric Project (Wells Project) license will expire on May 31, 2012. As part of the Wells Project relicensing process, the Public Utility District No. 1 of Douglas County (Douglas PUD) is required to obtain a water quality certificate pursuant to Section 401 of the Clean Water Act. As part of the 401 certification process, the Washington State Department of Ecology (Ecology) must determine whether the Wells Project meets state water quality standards (WQS), including standards for total dissolved gas (TDG).

Douglas PUD examined TDG production dynamics at the Wells Project to comply with State water quality standards (WQS). As part of the relicensing of the Wells Project, Douglas PUD initiated a series of assessments aimed at gaining a better understanding of the effect of spill operations on the production, transport and mixing of TDG in the Wells Dam tailrace.

The primary methodology employed in this study was the development of an unsteady state three-dimensional (3D), two-phase flow computational fluid dynamics (CFD) tool to predict the hydrodynamics of gas saturation and TDG distribution within the Wells tailrace. Two models were used in the study; a volume of fluid (VOF) model and a rigid-lid two-phase flow model.

The VOF model predicts the flow regime and the free-surface characteristics, recognizing that a spillway jet may plunge to depth in the tailrace or remain closer to the surface depending upon the geometry of the outlet and the tailwater elevation. The VOF model boundary extended approximately 1,700 feet downstream of the dam.

The rigid-lid model included 16,500 feet of the Wells tailrace, from Wells Dam downstream to the TDG compliance monitoring station. This two-phase flow model characterizes the hydrodynamics and three-dimensional distribution of gas volume fraction, bubble size and TDG in the Wells tailrace. This model assumes that the free surface can be modeled using a rigid-lid non-flat boundary condition. The free-surface shape for the first 1,000 feet downstream of the dam was extracted from VOF computations and slopes derived from HEC-RAS simulations for the remaining downstream regions. The velocity profiles derived from the VOF model were input into the rigid-lid model. Predictions of the gas volume fraction, bubble diameter at the spillbays, and typical environmental conditions observed at high flow events (≥ 200 kcfs) are the external parameters of the model.

The model was calibrated and validated using field data collected in 2006 during a TDG production dynamics study (EES et al. 2007). Agreement was attained between the depth-averaged velocity data collected in the field and those generated by the model. A gas volume fraction of 3% and bubble diameter of 0.5 mm in the spillbays produced TDG values that bracketed the 2006 field observations.

Once calibrated, the predictive ability of the model was validated by running three different operational conditions tested in 2006. The model captured the lateral TDG distribution and the reduction of TDG longitudinally as observed in the field. The numerical results demonstrate that the model provides a reliable predictor of tailrace TDG and therefore can be used as a tool to identify Project operations that minimize TDG concentrations downstream of Wells Dam.

After validation and calibration, the model was used to analyze the sensitivity of TDG concentration to the operation of the Project. Nine runs were completed for four river flows in which spill was either spread across the spillbays or concentrated in one or more spillbays. Numerical results indicate that concentrated spill operations resulted in the lowest TDG concentration downstream of the dam. According to the model, concentrated spill operations reduce the TDG production and increase the degasification at the free surface.

Based on the results from the sensitivity simulations, the model was used to predict TDG in the tailrace using the preferred operating condition for a 7Q10 flow of 246 kcfs. The preferred operating condition utilized a spillway configuration where water was concentrated rather than spread evenly across the entire length of the spillway. Using environmental conditions expected to occur during the passage of a 7Q10 flow and using the preferred operating condition, the TDG values predicted by the model at the location of the compliance station was within the Washington State water quality standards (<120%). The results of this study indicate that specific changes in Project operations can be utilized to meet the numeric water quality standards for TDG under 7Q10 flows.

The numerical results of the model also confirm the findings of the 2005 and 2006 TDG studies indicating that TDG values at the compliance monitoring station downstream of Wells Dam are representative of the TDG production in the Wells tailrace.

1.0 INTRODUCTION

1.1 General Description of the Wells Hydroelectric Project

The Wells Hydroelectric Project (Wells Project) is located at river mile (RM) 515.6 on the Columbia River in the State of Washington (Figure 1.1-1). Wells Dam is located approximately 30 river miles downstream from the Chief Joseph Hydroelectric Project, owned and operated by the United States Army Corps of Engineers (COE), and 42 miles upstream from the Rocky Reach Hydroelectric Project, owned and operated by Public Utility District No. 1 of Chelan County (Chelan PUD). The nearest town is Pateros, Washington, which is located approximately 8 miles upstream from the Wells Dam.

The Wells Project is the chief generating resource for the Public Utility District No. 1 of Douglas County (Douglas PUD). It includes ten generating units with a nameplate rating of 774,300 kW and a peaking capacity of approximately 840,000 kW. The design of the Wells Project is unique in that the generating units, spillways, switchyard, and fish passage facilities were combined into a single structure referred to as the hydrocombine. Fish passage facilities reside on both sides of the hydrocombine, which is 1,130 feet long, 168 feet wide, with a top of dam elevation of 795 feet above mean sea level (msl).

The Wells Reservoir is approximately 30 miles long. The Methow and Okanogan rivers are tributaries of the Columbia River within the Wells Reservoir. The Wells Project boundary extends approximately 1.5 miles up the Methow River and approximately 15.5 miles up the Okanogan River. The surface area of the reservoir is 9,740 acres with a gross storage capacity of 331,200 acre-feet and usable storage of 97,985 acre feet at the normal maximum water surface elevation of 781 feet msl (Figure 1.1-1).

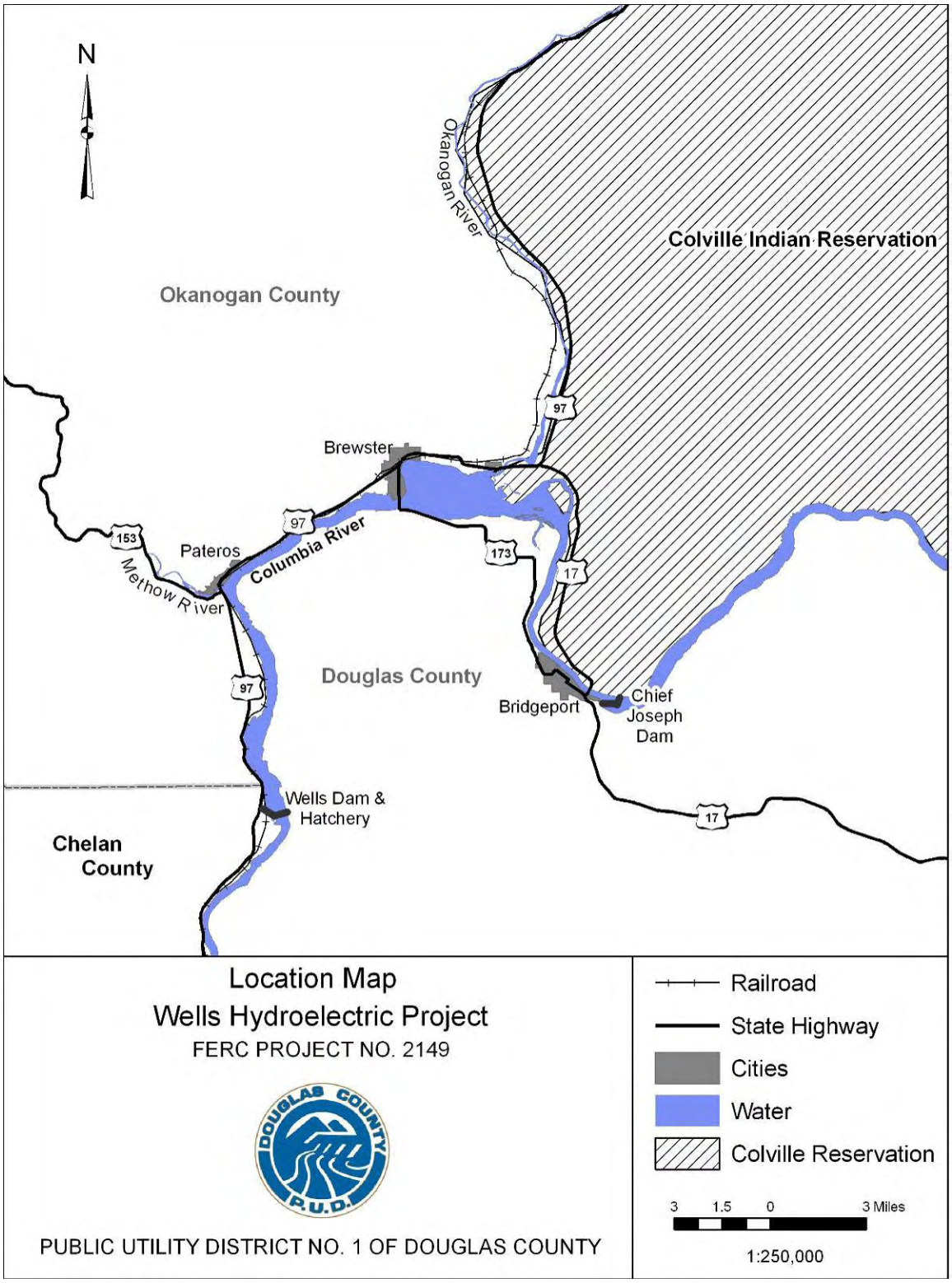

Figure 1.1-1 Location Map of the Wells Hydroelectric Project.

1.2 Relicensing Process

The current Wells Project license will expire on May 31, 2012. Douglas PUD is using the Integrated Licensing Process (ILP) promulgated by Federal Energy Regulatory Commission (FERC) Order 2002 (18 CFR Part 5). Stakeholders consisting of representatives from state and federal agencies, tribes, local governments, non-governmental organizations and the general public have participated in the Wells Project ILP, from a very early stage, to identify information needs related to the relicensing of the Wells Project.

In August 2005, Douglas PUD initiated a series of Resource Work Group (RWG) meetings with stakeholders regarding the upcoming relicensing of the Wells Project. This voluntary effort was initiated to provide stakeholders with information about the Wells Project, to identify resource issues and to develop preliminary study plans prior to filing the Notice of Intent (NOI) and Pre-Application Document (PAD). The RWGs were formed to discuss issues related to the Wells Project and its operations, identify information needs, and develop agreed-upon study plans.

The primary goals of the RWGs were to identify resource issues and potential study needs in advance of Douglas PUD filing the NOI and PAD. Through 35 meetings, each RWG cooperatively developed a list of Issue Statements, Issue Determination Statements and Agreed-Upon Study Plans. An Issue Statement is an agreed-upon definition of a resource issue raised by a stakeholder. An Issue Determination Statement reflects the RWG's efforts to apply the FERC's seven study criteria to mutually determine the applicability of each individual Issue Statement. Agreed-Upon Study Plans are the finished products of the informal RWG process.

Douglas PUD submitted the NOI and PAD to the FERC on December 1, 2006. The PAD included the RWGs' 12 Agreed-Upon Study Plans. The filing of these documents initiated the relicensing process for the Wells Project under the FERC's regulations governing the ILP.

On May 16, 2007, Douglas PUD submitted a Proposed Study Plan (PSP) Document. The PSP Document consisted of the Applicant's Proposed Study Plans, Responses to Stakeholder Study Requests and a schedule for conducting the Study Plan Meeting. The ILP required Study Plan Meeting was conducted on June 14, 2007. The purpose of the Study Plan Meeting was to provide stakeholders with an opportunity to review and comment on Douglas PUD's PSP Document, to review and answer questions related to stakeholder study requests and to attempt to resolve any outstanding issues with respect to the PSP Document.

On September 14, 2007, Douglas PUD submitted a Revised Study Plan (RSP) Document. The RSP Document consisted of a summary of each of Douglas PUD's RSPs and a response to stakeholder PSP Document comments.

On October 11, 2007, the FERC issued its Study Plan Determination based on its review of the RSP Document and comments from stakeholders. The FERC's Study Plan Determination required Douglas PUD to complete 10 of the 12 studies included in its RSP Document. Douglas PUD has opted to complete all 12 studies to better prepare for the 401 Water Quality Certification process conducted by the Washington State Department of Ecology (Ecology) and to fulfill its commitment to the RWGs who collaboratively developed the 12 Agreed-Upon Study

Plans with Douglas PUD. On October 15, 2008, Douglas PUD filed with the FERC the ISR Document that contained final reports for eight of the 12 studies and interim progress reports for four of the 12 studies. The ISR Document included results from all ten of the studies required by the FERC in the October 11, 2007 Study Plan Determination. The ISR Document also included results from two studies voluntarily conducted by Douglas PUD for the reasons stated above. On November 24, 2008, Douglas PUD filed a letter correcting a water temperature figure within the original ISR Document. On December 2, 2008, Douglas PUD filed the final Traditional Cultural Property Study for the Wells Project, which was prepared by the Confederated Tribes of the Colville Reservation under a contract with Douglas PUD.

The deadline for stakeholder comment on the ISR Document was December 15, 2008 pursuant to the approved Process Plan and Schedule for the Wells Project. Comments were filed by the City of Pateros on November 7, 2008 and by the City of Brewster on December 5, 2008.

On January 14, 2009, Douglas PUD filed a letter containing its responses to the comments from the cities on the ISR Document and proposed revisions to the schedule for the Wells ILP. On February 4, 2009, the FERC issued a determination on the requests for modification to the Wells Study Plan and on Douglas PUD's proposed revisions to the schedule. The FERC concluded that there was no need to modify the Wells Study Plan. The FERC also approved Douglas PUD's proposed modifications to the Wells ILP schedule.

This report is the final report for the Total Dissolved Gas Investigation. There were no variances from the FERC approved study plan for the Total Dissolved Gas Investigation.

1.3 Overview of Total Dissolved Gas at Wells Dam

Wells Dam, owned and operated by Douglas PUD, is located at RM 515.6 on the Columbia River, Washington (Figure 1.3-1). The spillway gates at Wells Dam are used to pass water when river flows exceed the maximum turbine hydraulic capacity (forced spill), to assist outmigration of juvenile salmonids (fish bypass spill), and to prevent flooding along the mainstem Columbia River (flood control spill). The Wells Project can pass approximately 22 kcfs through each operating turbine (220 kcfs through 10 turbines) with an additional 10-11 kcfs used to operate the juvenile fish bypass system and 1.0 kcfs to operate the adult fish ladders (ASL Environmental Sciences Inc. 2007). Therefore, spill is forced when inflows are higher than 232 kcfs. Spill may occur at flows less than the hydraulic capacity when the volume of water is greater than the amount required to meet electric system loads. Hourly coordination among hydroelectric projects on the mid-Columbia River was established to minimize unnecessary spill.

Wells Dam is a hydrocombine-designed dam with the spillway situated directly above the powerhouse. Research at Wells Dam in the mid-1980s showed that a modest amount of spill would effectively guide between 92 percent and 96 percent of the downstream migrating juvenile salmonids through the Juvenile Bypass System (JBS) and away from the turbines (Skalski et al., 1996). The operation of the Wells JBS utilizes five spillways that have been modified with constricting barriers to improve the attraction flow while using modest levels of water (Klinge 2005). The JBS will typically use approximately 6-8 percent of the total river flow for fish guidance. The high level of fish protection at Wells Dam has won the approval of the fisheries

agencies and tribes and was vital to Douglas PUD meeting the survival standards contained within the Anadromous Fish Agreement and Habitat Conservation Plan (HCP).

State of Washington water quality standards require TDG levels to not exceed 110% at any point of measurement. Due to air entrainment in plunge pools below spillways of hydroelectric dams, TDG levels can sometimes exceed the state standard during spill events at dams. In the State of Washington, there are exceptions allowed to the State's TDG standard. TDG levels are allowed to exceed the standard in order to (1) pass flood flows at the Project of 7Q10 or greater and (2) pass voluntary spill to assist out migrating juvenile salmonids. The 7Q10 flood flow, which is defined as the highest average flow that occurs for seven consecutive days in a once-in-ten-year period, is 246 kcfs at the Wells Project.

Figure 1.3-1 Map of Washington showing the location of the Wells Dam

2.0 GOALS AND OBJECTIVES

The goal of this study was to develop a numerical model capable of predicting the hydrodynamics and TDG concentrations in the tailrace of the Wells Project. The purpose of the model was to assist in the understanding of the underlying dynamics of TDG production allowing the evaluation of the effectiveness of spill type and plant operations in reducing TDG concentrations at Wells Dam.

3.0 STUDY AREA

The study area includes approximately 16,500 ft of the Wells tailrace, extending from Wells Dam downstream to transect TW3 (Transect T3) (Figure 3.0-1). Transect TW3 coincides with the Wells TDG compliance monitoring station.

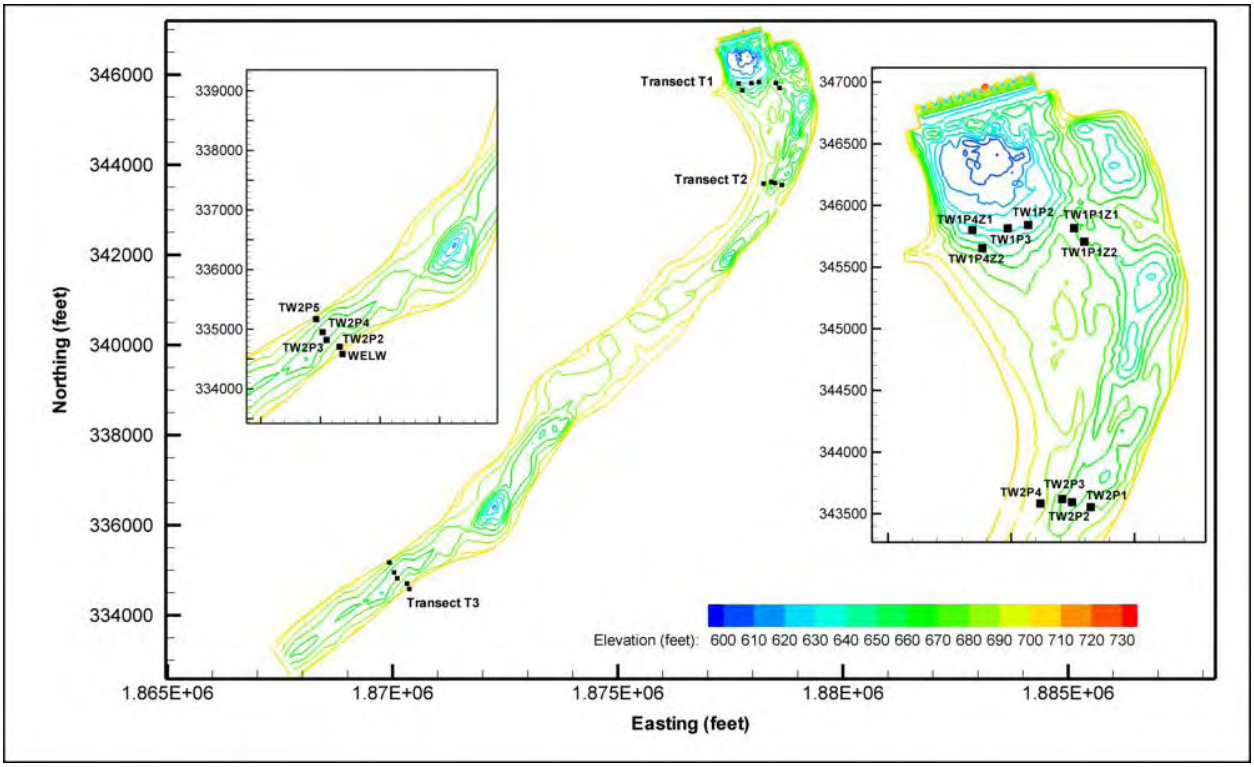

Figure 3.0-1 Study Area for the TDG model

4.0 BACKGROUND AND EXISTING INFORMATION

4.1 Summary of TDG studies in the Wells Tailrace

Douglas PUD conducted a series of assessments aimed at gaining a better understanding of TDG production dynamics resulting from spill operations at Wells Dam. Each year from 2003 to 2008, Douglas PUD has performed experimental spill operations to document the relationship between water spilled over the dam and the production of TDG.

In 2003 and 2004, Columbia Basin Environmental (CBE) deployed TDG sensors along two transects downstream of Wells Dam. The objectives of this study were to determine the effectiveness of the tailwater sensor and to better understand the relationship between spillway releases and TDG production (CBE 2003, 2004). In a two-week period, the studies showed that the tailwater station provided a reliable record of daily average TDG values in the Wells Dam tailrace.

In spring 2005, Douglas PUD conducted a study to measure TDG pressures resulting from various spill patterns at Wells Dam (CBE, 2006). An array of water quality data loggers was installed in the Well tailrace for a period of two weeks between May 23, 2005 and June 6, 2005. The Wells powerhouse and spillway were operated through a controlled range of operational scenarios that varied both total flow and allocation of the spillway discharge. A total of eight configurations were tested including flat spill patterns (near equal distribution of spill across the entire spillway), crowned spill patterns (spill is concentrated towards the center of the spillway), and spill over loaded and unloaded generating units. Results from the study indicated that spill from the west side of the spillway resulted in consistently higher TDG saturations than similar spill from the east side. Flat spill patterns yielded higher TDG saturations than crowned spill for similar total discharges. The results of this study also indicated that TDG levels of powerhouse flows may be influenced by spill.

In 2006, Douglas PUD continued TDG assessments at the Wells Project by examining alternative spill configurations and project operations to minimize the production of TDG. The purpose of the 2006 study was to evaluate how the Project could be operated to successfully pass the 7Q10 river flow while remaining in compliance with Washington State TDG standards. Thirteen sensors were placed along transects in the tailrace located at 1,000, 2,500 and 15,000 feet below Wells Dam. There were also three sensors placed across the forebay. The sensors were programmed to collect data in 15 minute intervals for both TDG and water temperature. Each test required the operations of the dam to maintain stable flows through the powerhouse and spillway for at least a three hour period. While there were 30 scheduled spill events, there were an additional 50 events in which the powerhouse and spillway conditions were held constant for a minimum three hour period. These additional events provided an opportunity to collect TDG data on a variety of Project operations that met study criteria. These are included in the results of the 2006 TDG Abatement Study (EES et al., 2007). Spill amounts ranged from 5.2 to 52.0% of project flow and flows ranged from 2.2 to 124.7 kcfs for spill and 16.4 to 254.0 kcfs for total discharge. There were six tests that were performed at flows that exceeded the Wells Dam 7Q10 flows of 246 kcfs. Results of the study indicated that two operational scenarios, spread spill and concentrated spill (spill from 1 or 2 gates), produced the lowest levels of TDG.

The 2006 study also indicated that the current location of the tailwater TDG compliance monitoring station is appropriate in providing representative TDG production information both longitudinally and laterally downstream of Wells Dam.

4.2 Numerical studies of TDG in Tailraces

Early studies to predict TDG below spillways were based on experimental programs and physical models (Hibbs and Gulliver 1997; Orlins and Gulliver 2000). The primary shortcoming of this approach is that the laboratory models cannot quantitatively predict the change in TDG due to model scaling issues. The approach relies on performance curves that relate flow conditions with past field experiences. This has led to inconsistent results at hydroelectric projects, some being quite successful while others less successful.

Computational fluid dynamics (CFD) modeling offers a powerful tool for TDG and hydrodynamics prediction. In the application to powerhouse and spillway flows, an understanding of the underlying physics and the capability to model three-dimensional physical phenomena is of paramount importance in performing reliable numerical studies. The most important source of TDG production is the gas transfer from the entrained bubbles, therefore a TDG predictive model must account for the two-phase flow in the stilling basin and the mass transfer between bubbles and water.

The TDG concentration depends on complex processes such as air entrainment in the spillway (pre-entrainment), entrainment when the jet impacts the tailwater pool, breakup and coalescence of entrained bubbles, mass transfer between bubbles and water, degasification at the free surface, and bubble and TDG transport. In addition, tailrace flows in the region near the spillway cannot be assumed to have a flat air/water interface which results in the required computation of the free surface shape. Moreover, it has been demonstrated that surface jets may cause a significant change in the flow pattern since they attract water toward the jet region, a phenomenon referred to as water entrainment (Liepmann 1990; Walker and Chen 1994; Walker 1997). Water entrainment leads to mixing and modification of the TDG field. As an additional complexity, the presence of bubbles has a strong effect on water entrainment. Bubbles reduce the density (and pressure) and effective viscosity in the spillway region and affect the liquid turbulence.

Free surface models can predict the shape and development of the free surface and, though costly, have feasible application to complex three dimensional (3D) flows. In the field of hydraulic engineering, free surface models are not yet widely applied but are steadily developing (Turan et al., 2008; Ferrari et. al., 2008). However, direct simulation of individual bubbles in a spillway/tailrace environment is well beyond current computer capabilities. Therefore, a two-fluid model with space-time averaged quantities that do not resolve the interface is needed to model the effect of the bubbles on the flow field and bubble dissolution. Numerical simulations of two phase flows using two-fluid models have been extensively used, mainly in the chemical and nuclear engineering community. Jakobsen et al. (2005) provided an extensive review of the state-of-the-art of two-phase flow modeling. Politano et al. (2007a) used a two-dimensional (2D) two-fluid model assuming isotropic turbulence to predict the gas distribution and TDG concentration in a cross-section passing through a spillway bay at Wanapum Dam. The model was compared against field data measured before deflector installation. The model allowed

examination of the effect of the bubble size on TDG concentration. However, 2D simulations cannot capture the water entrainment caused by deflectors and therefore the TDG dilution due to powerhouse flows could not be predicted with the model. Turan et al. (2007) conducted the first numerical study to predict the hydrodynamics and water entrainment in a hydropower tailrace. The authors used an anisotropic mixture model that accounts for the gas volume fraction and attenuation of normal fluctuations at the free surface. Politano et al. (2007b) used an anisotropic mixture model for the 3D prediction of the two phase flow and TDG in the tailrace of Wanapum Dam. The simulations captured the measured water entrainment in the tailrace of Wanapum Dam. In this study, quantitative agreement between predicted and measured TDG was obtained for two different operational conditions.

4.3 Aquatic Resource Work Group

As part of the relicensing process for the Wells Project, Douglas PUD established an Aquatic Resource Work Group (Aquatic RWG) which began meeting informally in November, 2005. This voluntary effort was initiated to provide stakeholders with information about the Wells Project, to collaboratively identify potential resource issues related to Project operations and relevant to relicensing, and to develop preliminary study plans to be included in the Wells Pre-Application Document (PAD) (DCPUD, 2006).

Through a series of meetings, the Aquatic RWG cooperatively developed a list of Issue Statements, Issue Determination Statements and Agreed-Upon Study Plans. An Issue Statement is an agreed-upon definition of a resource issue raised by a stakeholder. An Issue Determination Statement reflects the RWGs' efforts to review the existing project information and to determine whether an issue meets the requirements of the FERC's seven study plan criteria and would be useful for informing future relicensing decisions. Agreed-Upon Study Plans are the finished products of the voluntary RWG process.

Based upon these meetings and discussions, the Aquatic RWG proposed to conduct studies of the TDG dynamics of Wells Dam. The need for this study was agreed to by all members of the Aquatic RWG, including Douglas PUD. These studies are intended to inform future relicensing decisions, including the water quality certification process.

The Issue Statement and Issue Determination Statement listed below were included in the PAD (section number included) filed with the FERC on December 1, 2006:

4.3.1 Issue Statement (PAD Section 6.2.1.5)

Wells Dam may affect compliance with Total Dissolved Gas (TDG) standards in the Wells tailrace and Rocky Reach forebay.

4.3.2 Issue Determination Statement (PAD Section 6.2.1.5)

Wells Dam can have an effect on compliance with the TDG standard. The resource work group believes that additional information is necessary in the form of continued monitoring and that these data will be meaningful with respect to the State 401 Water Quality Certification process.

Douglas PUD has been implementing studies at Wells Dam to address TDG production dynamics.

4.4 Project Nexus

TDG concentrations may become a water quality concern when gases supersaturate a river, lake or stream. The plunging water caused by spill at hydroelectric facilities may elevate TDG to levels that may result in impaired health or even death for aquatic life residing or migrating within the affected area.

The Washington State Department of Ecology is responsible for the protection and restoration of the state's waters. Ecology has adopted water quality standards that set limits on pollution in lakes, rivers, and marine waters in order to protect water quality. On July 1, 2003, Ecology completed the first major overhaul of the state's water quality standards in a decade. A significant revision presented in the 2003 water quality standards classifies fresh water by actual use, rather than by class as was done in the 1997 standards. These revisions were adopted in order to make the 2003 standards less complicated to interpret and provide future flexibility as the uses of a water body evolve. The applicable water quality standards (WQS) for TDG at hydroelectric projects states that total dissolved gas shall not exceed 110 percent of saturation at any point of sample collection.

However, as discussed in Section 4.0, an exception to the above standard is allowed to aid fish passage over hydroelectric dams when it is determined that this action is consistent with an Ecology-approved gas abatement plan. The information collected during this study will assist Douglas PUD in operating the Wells Project in a manner that minimizes TDG in the Wells tailrace and Rocky Reach forebay.

5.0 METHODOLOGY

5.1 Model Overview

The models used in this study are based upon the general purpose CFD code FLUENT, which solves the discrete Reynolds Averaged Navier Stokes (RANS) equations using a cell centered finite volume scheme. Two models were used to predict the hydrodynamics and TDG distribution within the tailrace of the Wells Project: a volume of fluid (VOF) model and a rigid-lid non-flat lid model.

The VOF model predicted the flow regime and free-surface for the first 1,000 feet downstream of the dam. The free-surface shape was then used to generate a grid conformed to this geometry and fixed throughout the computation (rigid, non-flat lid approach). After the statistically-steady state was reached, the VOF solution that minimizes the difference between measured and predicted tailwater elevation was selected. Water surface elevations and local slopes derived from simulations using the Hydrologic Engineering Centers River Analysis System (HEC-RAS) were used at the downstream region of the model. The HEC-RAS computations were performed using geometric input files provided by Douglas PUD with a roughness coefficient of 0.035.

The rigid-lid model allowed proper assessment of water entrainment and TDG concentration. The model assumed one variable bubble size, which could change due to local bubble/water mass transfer and pressure. The air entrainment (gas volume fraction and bubble size) was assumed to be a known inlet boundary condition. It must be noted that the choice of bubble size and volume fraction at the spillway bays has an important effect on the level of entrainment and TDG distribution. In this study a reasonable single-size bubble diameter and volume fraction were used at the spillway gates to bracket the experimental TDG data during the model calibration and the same values are used for all computations.

Specific two phase flow models and boundary conditions were implemented into FLUENT through User Defined Functions (UDFs). Two-phase User Defined Scalars (UDSs) transport equations were used to calculate the distribution of TDG and bubble number density.

The model included the main features of the Wells Dam, including the draft tube outlets of the generating units, spillway, top spill in bays 2 and 10 and fish passage facilities (Figure 5.1-1). Bathymetric data supplied by Douglas PUD were used to generate the river bed downstream of the dam. Detail of Figure 5.1-1 shows a cross section through a spillway unit illustrating the Wells Hydrocombine.

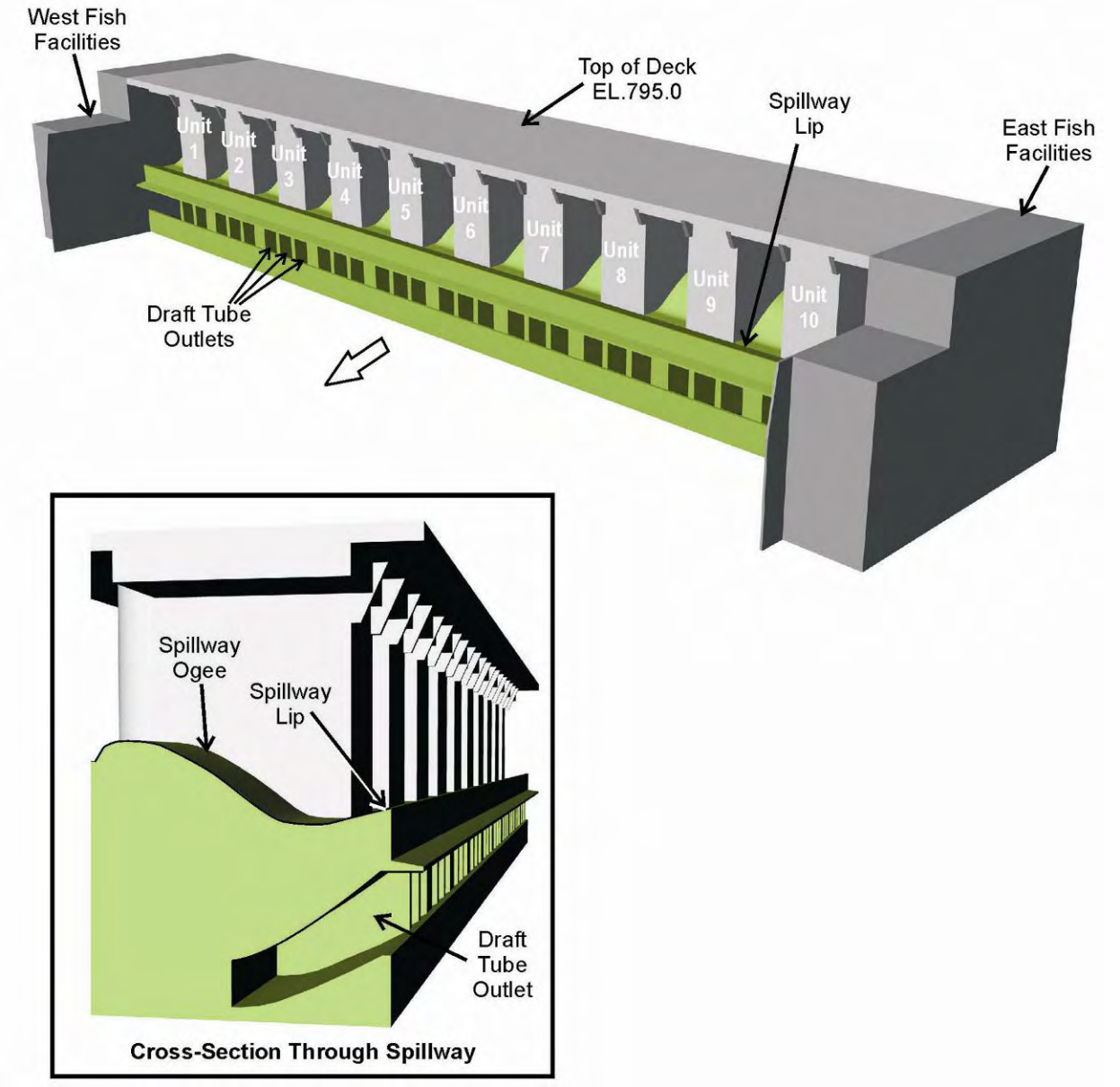

Figure 5.1-1 Structures included in the TDG model

5.2 VOF Model

5.2.1 Mathematical Model

In the VOF model, the interface between fluids is calculated with a water volume fraction (α_w) transport equation:

$$\frac{\partial \alpha_w}{\partial t} + \vec{v} \cdot \nabla \alpha_w = 0 \qquad (1)$$

Mass conservation requires that $\sum \alpha_i = 1$. The jump conditions across the interface are embedded in the model by defining the fluid properties as: $\varphi = \sum \alpha_i \varphi_i$, where φ is either the density or the viscosity. In the VOF approach, each control volume contains just one phase (or the interface). Points in water have $\alpha_w = 1$, points in air have $\alpha_w = 0$, and points near the interface have $0 < \alpha_w < 1$. The free surface was generally defined in the VOF using an α_w of 0.5.

5.2.2 Grid Generation

The domain was divided into a number of blocks and a structured mesh was generated in each block with common interfaces between the blocks. Each individual block consists of hexahedral cells. To resolve the critical regions of interest, the grids were refined near the solid boundaries, near the turbine intakes and spillway where large accelerations are expected, and near the free surface. The grids containing between 6×10^5 to 8×10^5 nodes were generated using Gridgen V15. Grid quality is an important issue for free surface flow simulations. As fine grids are needed near the interface to minimize numerical diffusion, each simulation required the construction of a particular grid. The grids were constructed nearly orthogonal in the vicinity of the free surface to improve convergence. Figure 5.2-1 shows an overall 3D view of the grid used for the June 5, 2006 simulation. An extra volume at the top of the grid was included to accommodate the air volume for the VOF method.

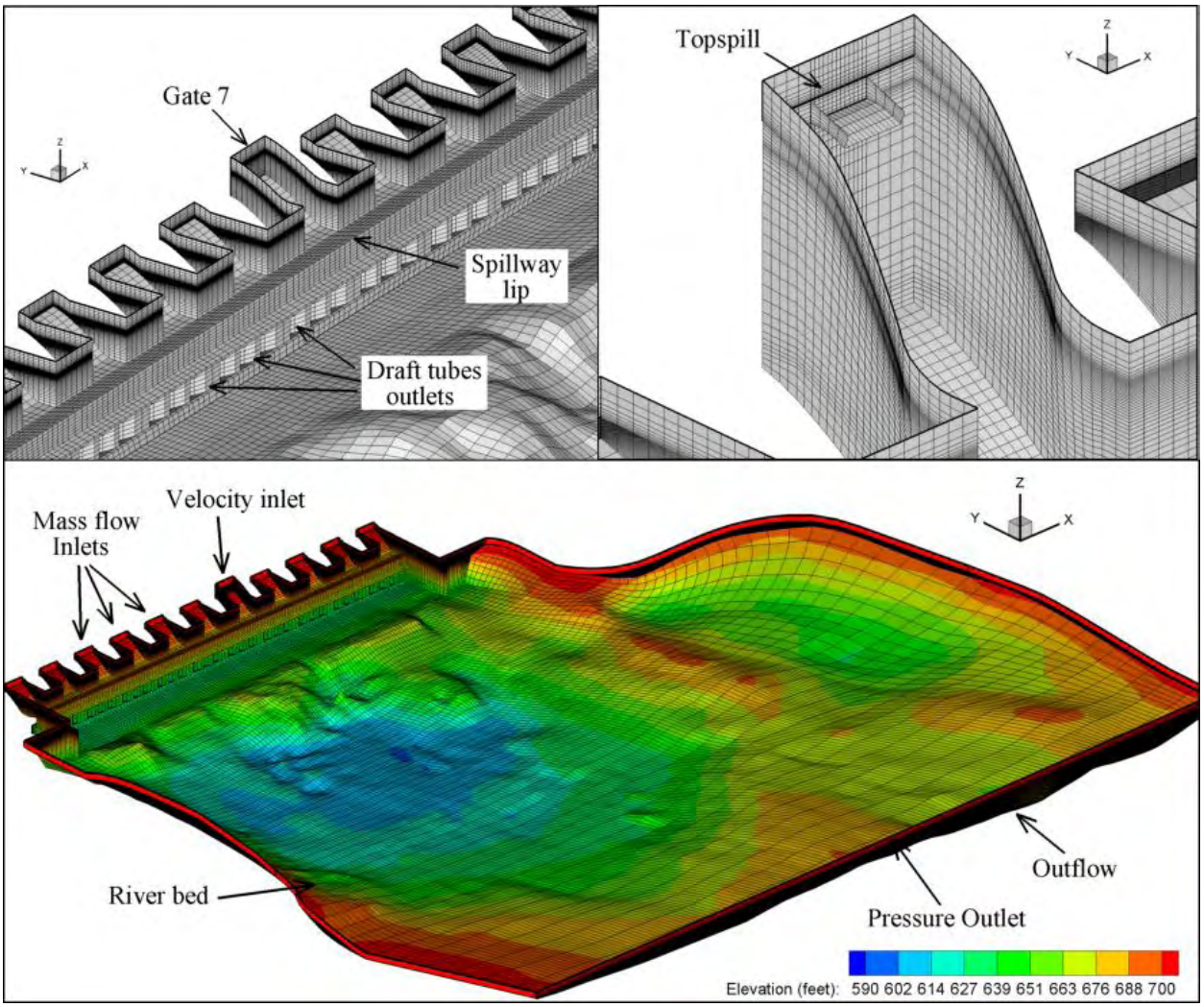

Figure 5.2-1 3D view of a typical grid used for the VOF simulations

5.2.3 Boundary Conditions

5.2.3.1 Inlet

A given mass flow rate of water assuming uniform velocity distribution was used at each of the turbine units and spillway bays.

5.2.3.2 Walls and River Bed

A no-slip (zero velocity) surface condition was imposed on all walls and tailrace bed.

5.2.3.3 Exit

The free water surface elevation (WSE) was imposed by specifying the water volume fraction distribution. The WSE measured at the tailwater elevation gage was used at the exit (outflow condition in Figure 5.2-1). A hydrostatic pressure was imposed at the outflow using a UDF. At the top of the outflow a pressure outlet boundary condition was used to avoid air pressurization.

5.2.3.4 Top Surface

A pressure outlet boundary condition with atmospheric pressure was applied at the top to allow free air flow and avoid unrealistic pressure.

5.3 Rigid-lid Model

The rigid-lid model is an algebraic slip mixture model (ASMM) (Mannheim et al. 1997) that accounts for buoyancy, pressure, drag and turbulent dispersion forces to calculate the gas volume fraction and velocity of the bubbles. The model considers the change of the effective buoyancy and viscosity caused by the presence of the bubbles on the liquid and the forces on the liquid phase due to the non-zero relative bubble-liquid slip velocity.

5.3.1 Mathematical Model

5.3.1.1 Mass and Momentum Conservation for the Mixture

The two phase model provides mass and momentum equations for the liquid and gas phases (Drew & Passman 1998). Summing the mass and momentum equations for each phase results in continuity and momentum equations for the mixture gas-liquid phase:

$$\frac{\partial \rho_m}{\partial t} + \nabla \cdot \left[\rho_m \, \vec{u}_m \right] = 0 \tag{2}$$

$$\frac{\partial}{\partial t}\left(\rho_m \, \vec{u}_m \right) + \nabla \cdot \left(\rho_m \, \vec{u}_m \, \vec{u}_m \right) = -\nabla P + \nabla \cdot \left[\boldsymbol{\sigma}_m^{\mathrm{Re}} + \boldsymbol{\tau}_m \right] + \rho_m \, \vec{g} - \nabla \cdot \left(\sum_{k=g,l} \alpha_k \, \rho_k \, \vec{u}_k \, \vec{u}_{dr,k} \right) \tag{3}$$

where P is the total pressure, $\vec{g}$ is the gravity acceleration, and $\boldsymbol{\sigma}_m^{\mathrm{Re}}$ and $\boldsymbol{\tau}_m = \rho_m \nu_m \left(\nabla \vec{u}_m + \nabla \vec{u}_m^T \right)$ are the turbulent and molecular shear stresses, respectively. ρ_m, μ_m and $\vec{u}_m$ are the mixture density, viscosity and mass-averaged velocity defined as $\rho_m = \sum_{k=g,l} \alpha_k \, \rho_k$, $\mu_m = \sum_{k=g,l} \alpha_k \, \mu_g$ and $\vec{u}_m = \frac{1}{\rho_m} \sum_{k=g,l} \alpha_k \, \rho_k \, \vec{u}_k$, with α_g the gas volume fraction. The subscripts *g, l* and *m* denote gas, liquid and mixture, respectively. $\vec{u}_{dr,k}$ is the drift velocity defined as the velocity of the phase k relative to the mixture velocity.

The gas density is calculated using the ideal gas law $\rho_g = M\,P/(RT)$ with P the pressure, M the molecular weight of air, R the universal gas constant, and T the absolute temperature.

5.3.1.2 Mass Conservation for the Gas Phase

The continuity equation for the gas phase is (Drew & Passman, 1998):

$$\frac{\partial}{\partial t}\left(\alpha_g\,\rho_g\right)+\nabla\cdot\left(\alpha_g\,\rho_g\,U_{g,i}\right)=-S \tag{4}$$

where $\vec{u}_g$ is the bubble velocity and S is a negative gas mass source; in this application the TDG source due to the air transfer from the bubbles to the liquid.

5.3.1.3 Momentum Conservation for the Gas Phase

The ASMM assumes that the inertia and viscous shear stresses are negligible compared to pressure, body forces and interfacial forces in the momentum equation of the gas phase (Antal et al., 1991; Lopez de Bertodano et al., 1994; Manninen et al., 1997):

$$0=-\alpha_g\,\nabla P+\alpha_g\,\rho_g\,\vec{g}+\vec{M}_g \tag{5}$$

where $\vec{M}_g$ represents the interfacial momentum transfer between the phases.

5.3.1.4 Bubble Number Density Transport Equation

Most of the two fluid models in commercial codes (Fluent, CFX, CFDLib, among others) assume a mean constant bubble size with a given relative velocity (Chen et al., 2005). In tailrace flows the use of a mean constant bubble size for the evaluation of the bubble-liquid mass transfer and interfacial forces is not valid. As a consequence of the complex processes of generation, breakup, and coalescence, the bubbles resulting from air entrainment have different sizes. These processes occur at the plunging jet region immediately after the spillway, where the gas volume fraction and turbulence can be large. The model used in this study is intended for the region downstream of the plunging jet, where bubble size changes mainly due to mass transfer and pressure variations, and therefore bubble breakup and coalescence processes can be neglected. This assumption is considered a reasonable hypothesis for low gas volume fractions (Politano et al. 2007b).

Let $f\,dm\,d\vec{r}$ represent the number of bubbles with original (at the insertion point, before any physical process modifies the bubble mass) mass m, located within $d\vec{r}$ of $\vec{r}$ at time t. The Boltzmann transport equation for f is:

$$\frac{\partial f}{\partial t}+\nabla\cdot\left[\vec{u}_g\,f\right]+\frac{\partial}{\partial m}\left[\frac{\partial m}{\partial t}\,f\right]=0 \tag{6}$$

Note that this is a Lagrangian representation, and thus *f* has a different interpretation than the usual Eulerian approach (Guido-Lavalle et al., 1994; Politano et al., 2000). Integration of Eq. (6) for bubbles of all masses results in a transport equation for the bubble number density N :

$$\frac{\partial N}{\partial t} + \nabla \cdot \left[\vec{u}_g \, N \right] = 0 \tag{7}$$

The bubble radius is calculated from $R = \left[3\alpha / (4\pi N) \right]^{1/3}$.

5.3.1.5 Two-phase TDG Transport Equation

TDG is calculated with a two-phase transport equation (Politano et al. 2007b):

$$\frac{\partial \alpha_l C}{\partial t} + \nabla \cdot \left(\vec{u}_l \, \alpha_l \, C \right) = \nabla \cdot \left(\left(\nu_m + \frac{\nu_t}{Sc_C} \right) \alpha_l \, \nabla C \right) + S \tag{8}$$

where C is the TDG concentration, and ν_m and ν_t are the molecular and turbulent kinematic viscosity, respectively. In this study, a standard Schmidt number of $Sc_C = 0.83$ is used.

5.3.1.6 Turbulence Closure

In this study a Reynolds Stress Model (RSM) was used. The ASMM assumes that the phases share the same turbulence field. The turbulence in the mixture phase is computed using the transport equations for a single phase but with properties and velocity of the mixture. The transport equations for the Reynolds stresses $\boldsymbol{\sigma}_{i,j}^{\mathrm{Re}} = \rho_m \overline{u'_{m,i} \, u'_{m,j}}$ are:

$$\frac{\partial \boldsymbol{\sigma}^{\mathrm{Re}}}{\partial t} + \left(\nabla \cdot \vec{u}_m \right) \boldsymbol{\sigma}^{\mathrm{Re}} + \vec{u}_m \left(\nabla \cdot \boldsymbol{\sigma}^{\mathrm{Re}} \right) = \nabla \cdot \left[\rho_m \frac{\nu_m^t}{\sigma_R} \nabla \boldsymbol{\sigma}^{\mathrm{Re}} \right] - \mathbf{P} + \boldsymbol{\varphi} + \boldsymbol{\varepsilon} + \mathbf{S}_{\boldsymbol{\sigma}} \tag{9}$$

where the stress production tensor is given by $\mathbf{P} = \boldsymbol{\sigma}^{\mathrm{Re}} \cdot \nabla \vec{u}_m^T + \left(\boldsymbol{\sigma}^{\mathrm{Re}} \cdot \nabla \vec{u}_m^T \right)^T$, $\boldsymbol{\varepsilon} = 2/3 \, \mathbf{I} \, \rho_m \, \varepsilon$ and $\sigma_R = 0.85$. The pressure-strain tensor $\boldsymbol{\varphi}$ is calculated using the models proposed by Gibson and Lander (1978), Fu et al. (1987) and Launder (1989). In this study, $\mathbf{S}_{\boldsymbol{\sigma}}$ represents the effect of the bubbles on the Reynolds stresses. The transport equation for the turbulent dissipation rate reads:

$$\frac{\partial}{\partial t} \left(\rho_m \, \varepsilon \right) + \nabla \cdot \left(\rho_m \, \vec{u}_m \, \varepsilon \right) = \nabla \cdot \left[\rho_m \left(\nu_m + \frac{\nu_m^t}{\sigma_\varepsilon} \right) \nabla \varepsilon \right] - C_{\varepsilon 1} \, \rho_m \, \frac{1}{2} \mathrm{Tr}\left(\mathbf{P} \right) \frac{\varepsilon}{k} - C_{\varepsilon 2} \, \rho_m \, \frac{\varepsilon^2}{k} + S_\varepsilon \tag{10}$$

with $C_{\varepsilon 1} = 1.44$, $C_{\varepsilon 2} = 1.92$, and $\sigma_\varepsilon = 1$. The turbulent kinetic energy is defined as $k = \frac{1}{2\rho_m}\mathrm{Tr}(\boldsymbol{\sigma})$. The source term S_ε accounts for the effect of the bubbles on the turbulent dissipation rate. The turbulent kinematic viscosity is computed as in the $k-\varepsilon$ models using $\nu_t = C_\mu k^2/\varepsilon$, with $C_\mu = 0.09$.

5.3.1.7 Constitutive Equations

In order to close the model, interfacial transfer terms emerging from the relative motion between the bubbles and the continuous liquid need to be modeled.

Interfacial momentum

Since in this particular application there are no significant velocity gradients or flow accelerations (in the bubble scale), most interfacial forces such as lift and virtual mass are negligible compared with drag and turbulent dispersion forces:

$$\vec{M}_g = \vec{M}_g^D + \vec{M}_g^{TD} \tag{11}$$

where $\vec{M}_g^D$ and $\vec{M}_g^{TD}$ are the drag and turbulent dispersion terms. The drag force can be modeled as (Ishii and Zuber, 1979):

$$\vec{M}_g^D = -\frac{3}{8}\rho_m \alpha_g \frac{C^D}{R}\vec{u}_r|\vec{u}_r| \tag{12}$$

where $\vec{u}_r$ is the relative velocity of the gas phase respect to the liquid phase. Most of the numerical studies use drag correlations based on rising bubbles through a stagnant liquid proposed by Ishii & Zuber (1979) (see Lane et al., 2005):

$$C^D = \begin{cases} \dfrac{24}{\mathrm{Re}_b} & if\ R < 0.0002 \\ \dfrac{24\left(1+0.15\,\mathrm{Re}_b^{0.867}\right)}{\mathrm{Re}_b} & if\ 0.0002 < R < 0.0011 \end{cases} \tag{13}$$

where $\mathrm{Re}_b = 2\rho_l|\vec{u}_r|R/\mu_l$ is the bubble Reynolds number. The turbulent dispersion term is modeled as (Carrica et al., 1999):

$$\vec{M}_g^{TD} = -\frac{3}{8}\frac{\nu^t}{Sc_b}\rho_m \frac{C^D}{R}|\vec{u}_r|\nabla\alpha_g \tag{14}$$

where $Sc_b = \nu^t / \nu^b$ is the bubble Schmidt number. Following Carrica et al. (1999), $Sc_b = 1$ is used.

Bubble dissolution and absorption

The rate of mass transfer is computed considering that the air is soluble in water and obeys Henry's law and that the air molar composition is that of equilibrium at atmospheric pressure, which implies that the air is considered a single gas with molar averaged properties. The mass flux from gas to liquid can be expressed by (Deckwer 1992; Politano et al. 2007b):

$$S = 4\pi N R^2 k_l \left(\frac{P + \sigma/R}{He} - C \right) \tag{15}$$

where σ is the interfacial tension and He is the Henry constant. The second term on the RHS of Eq. (15) accounts for the effect of the interfacial tension on the equilibrium concentration. The effect of temperature on the Henry constant is modeled using the Van 't Hoff equation:

$$He(T) = He(T_o) \exp\left[-C_T \left(\frac{1}{T} - \frac{1}{T_o} \right) \right] \tag{16}$$

where T is the absolute temperature and T_o refers to the standard temperature (298 K). A constant for air $C_T = 1388\,K$ is used in this model.

Takemura and Yabe (1998) proposed a correlation for the mass transfer coefficient of spherical rising bubbles, where the turbulence is generated by the rising bubbles:

$$k_l^{rb} = \frac{D\, Pe_b^{0.5}}{\sqrt{\pi} R} \left(1 - \frac{2}{3\left(1 + 0.09\, \mathrm{Re}_b^{2/3}\right)^{0.75}} \right) \tag{17}$$

where D is the molecular diffusivity and the bubble Peclet number is $Pe_b = 2 \left| \overrightarrow{u_r} \right| R / D$.

External turbulence could be important in flows downstream of spillways, mainly in regions of high shear near the walls and where the plunging jet impacts and enhances the mass transfer. In this application, the mass transfer coefficient can be calculated using the expression proposed by Lamont and Scott (1970):

$$k_l^t = 0.4\, Sc^{-1/2} (\nu \varepsilon)^{1/4} \tag{18}$$

where $Sc = D/\nu$. In this study, the same order of magnitude is obtained from Eqs. (17) and (18), thus the maximum mass transfer coefficient between bubbles rising in stagnant liquid (k_l^{rb}) and bubbles in turbulent flow (k_l^t) is used: $k_l = \max\left(k_l^{rb}, k_l^t\right)$.

5.3.2 Grid Generation

The Wells tailrace structures and the bathymetry are meshed with structured and unstructured multi-block grids containing only hexahedral elements, using Gambit and Gridgen V15. Typical grid sizes are in the range of 7 10^5 to 1 10^6 nodes. Figure 5.3-1 shows typical grids used for the rigid-lid model. Details (a) and (b) show free surface shapes for spread and concentrated flows, respectively. Detail (c) shows the unstructured grid, extended from approximately 1,500 feet to 3,500 feet downstream of the Wells Dam, used to reduce grid size and improve aspect ratio.

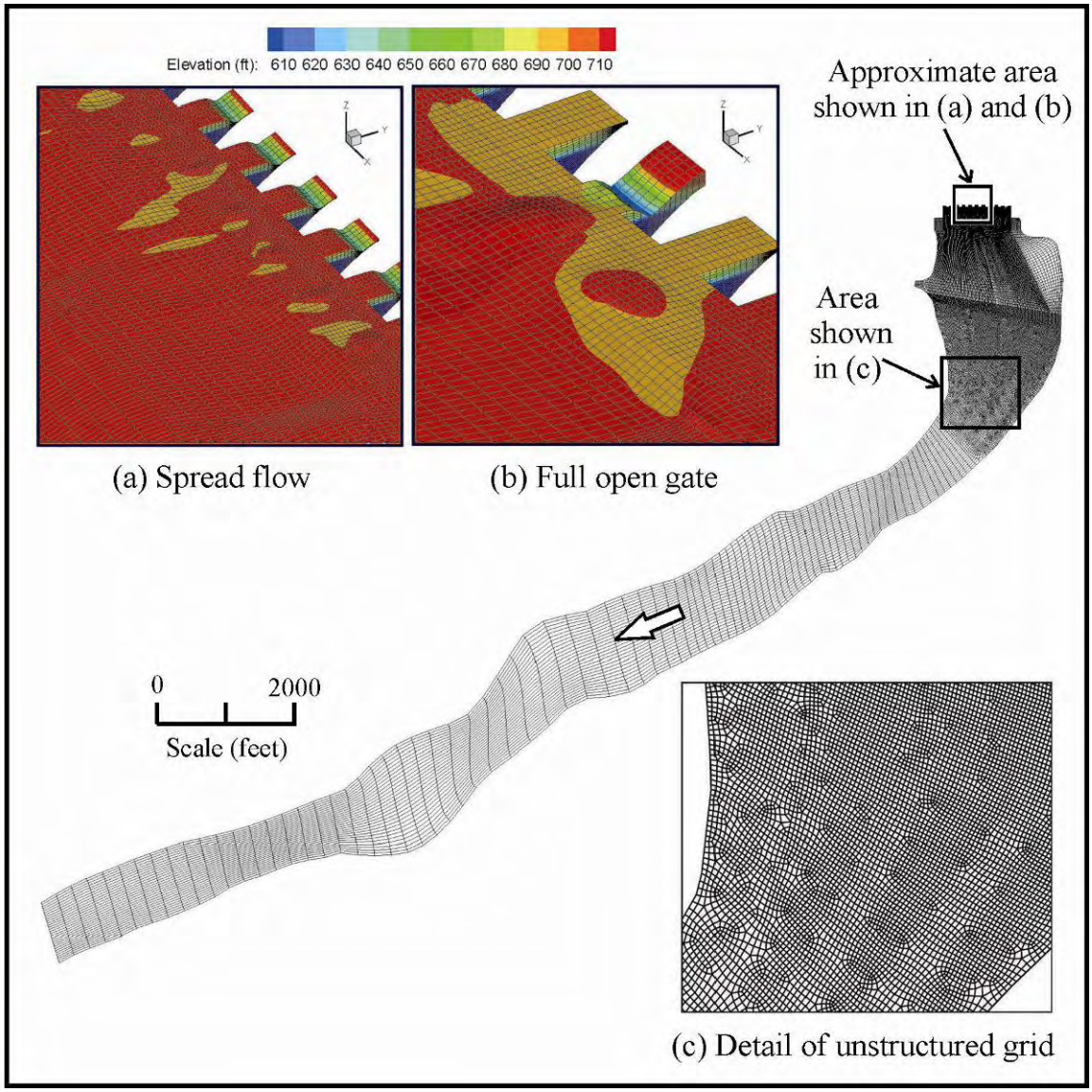

Figure 5.3-1 3D view of a typical grid used for the rigid-lid simulations

5.3.3 Boundary Conditions

5.3.3.1 Free Surface

Kinematic and dynamic boundary conditions enforcing zero normal velocity fluctuations at the free surface are programmed through UDFs. Details of the implementation of the boundary conditions used for the Reynolds stress and velocity components are found in Turan et al. (2007).

In order to allow the gas phase to flow across the interface, the normal component of the gas velocity at the free surface is calculated using a mass balance for the gas phase in each control volume contiguous to the interface. The resulting equation is implemented using UDFs.

For the TDG concentration, a Neumann boundary condition is used. A mass transfer coefficient at the free surface of $k_l = 0.0001$ m/s as measured by DeMoyer et al. (2003) for tanks and bubble columns is used.

5.3.3.2 Walls and River Bed

The sides and the river bed are considered impermeable walls with zero TDG flux. For the gas phase, no penetration across walls is imposed.

5.3.3.3 Exit

The river exit is defined as an outflow. A zero gradient condition was programmed for the TDG concentration and bubble number density.

5.3.3.4 Spillbays and Powerhouse Units

Uniform velocities with constant gas volume fraction of $\alpha = 0.03$ and bubble diameter 5 mm are used for the 11 bays in the spillway region.

It is assumed that air is not entrained with the turbine inflow. The TDG concentration measured in the forebay is used at the spillway bays and powerhouse units.

5.4 Modeling Assumptions and Model Inputs

5.4.1 Model Assumptions

The model used in this study assumes that:

- Gas and liquid phases are interpenetrating continua. Since the volume of a phase cannot be occupied by the other phases, the concept of volume fraction is used.
- A local equilibrium over short spatial length scale is assumed. Therefore, the gas-liquid relative velocity can be calculated with algebraic equations.
- The liquid phase is considered incompressible.
- The turbulence can be described by the RSM turbulence model.
- The free surface shape is not affected by the presence of bubbles.

- The air is considered a unique gas with molar averaged properties.
- Bubble size changes mainly due to mass transfer and pressure and breakup and coalescence are negligible.

5.4.2 Model Inputs

The bubble size and gas volume fraction at the inlet (spillway bay gates) are model parameters selected based upon the calibration of the model.

Environmental factors such as forebay TDG, forebay elevation, and water temperature are based upon historical data relative to the choice of values for modeling the most likely 7Q10 conditions. The conditions were based on hourly observations recorded between April and September throughout the ten-year period 1999-2008 (daily average flows ≥ 200 kcfs did not occur outside of the April to September time frame; DART Hourly Water Quality Composite Report www.cbr.washington.edu/dart/hgas_com.html).

5.4.2.1 Environmental Conditions

The environmental data described above (43,200 hourly records) were subsequently filtered to include values in which outflow was equal to or greater than 200 kcfs to represent high flow conditions at Wells Dam (2,941 hourly records). Temporal distribution of hourly values (by week of the year) range from early April to early September, with the middle quartiles (25% to 75%) occurring between weeks 23 and 26 (4-June and 25-June). Median values of the distribution occur at week 24. Hourly flow measurements averaged 221 kcfs (±18 kcfs SD) during these 'high flow' events, though 50% (median) of flows were ≤ 215 kcfs and only 12% of values exceeded 246 kcfs. Water temperatures during these occurrences range from 4.1-19.7 °C, with a median temperature of 13.0 °C (Figure 5.4-1). Forebay TDG during these occurrences (≥ 200 kcfs) range from 99.9-120.1% with a median TDG of 112.5 % (Figure 5.4-2). Average daily forebay elevations were also collected from DART throughout the same period (1999-2008; www.cbr.washington.edu/dart/river.html). When average daily flows were ≥ 200 kcfs, forebay elevation ranges from 775-781 feet, with a median elevation of 779.6 feet (Figure 5.4-3; note that the five outliers ~ 775 feet occurred consecutively between June 4th and June 8th, 2002). Since the distributions of the three values needed for model input (water temperature, forebay TDG, and forebay elevation) have a slightly negative or 'left' skew (that is, mean values are slightly less than median values), the median values, rounded to the nearest whole number or percent, were used to best represent environmental conditions under high-flow events.

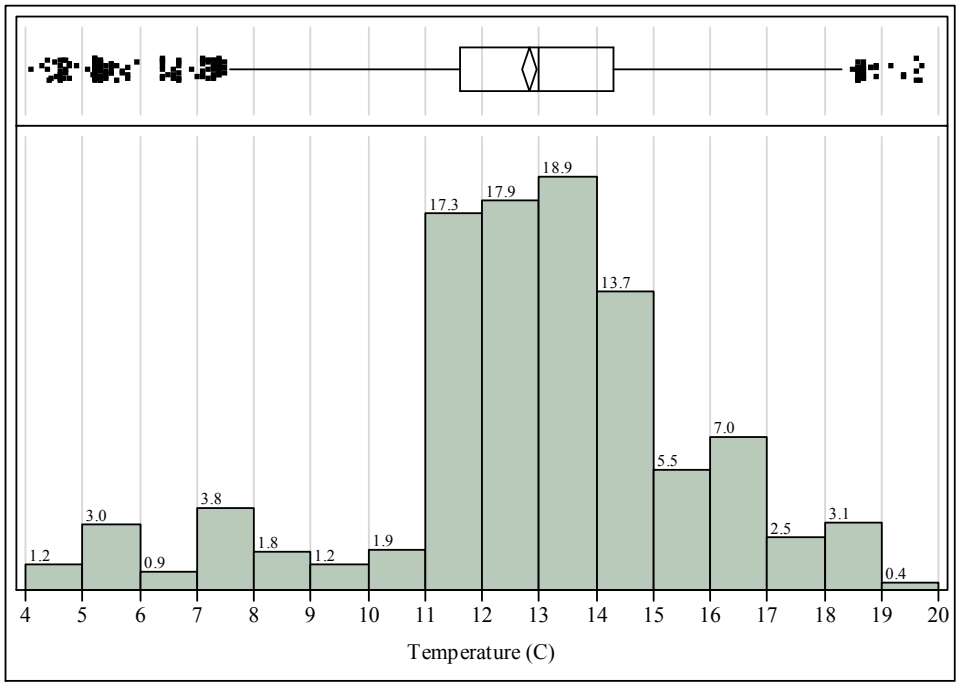

Figure 5.4-1 Distribution of water temperatures (°C) during flows equal to or greater than 200 kcfs between April and September, 1999-2008. Percent occurrence of values is shown above histogram bars.

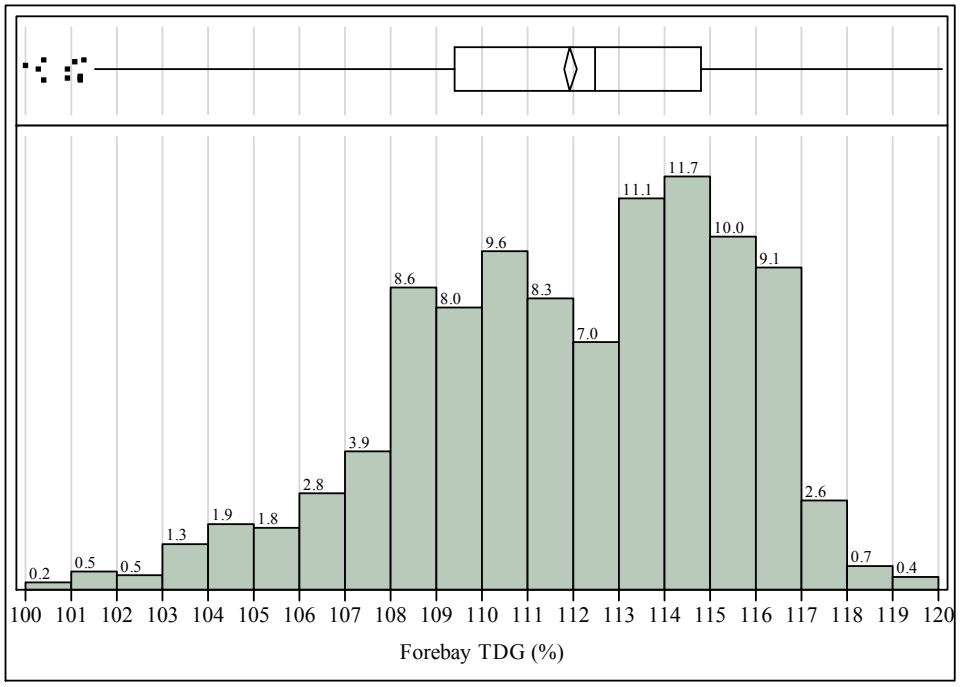

Figure 5.4-2 Distribution of forebay TDG (%) during flows equal to or greater than 200 kcfs between April and September, 1999-2008. Percent occurrence of values is shown above histogram bars.

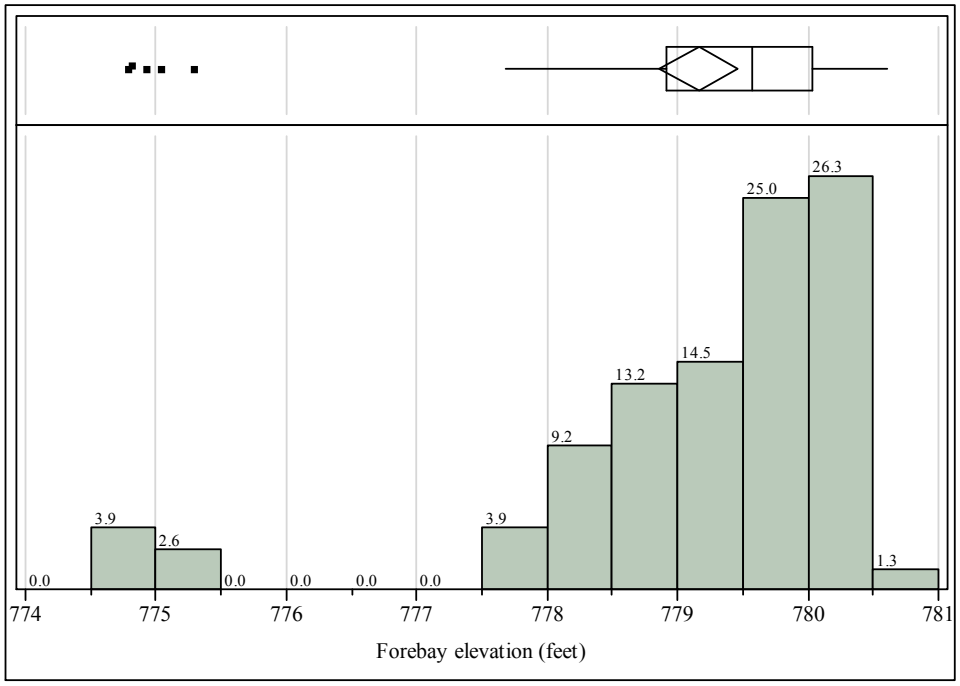

Figure 5.4-3 Distribution of forebay elevations (feet) during daily average flows equal to or greater than 200 kcfs, 1999-2008. Percent occurrence of values is shown above histogram bars.

6.0 NUMERICAL METHOD

The computations were performed using 4 processors of a Linux cluster with 2 GB of memory per processor and in three dual socket dual core Xeon Mac Pro systems.

6.1 VOF Model

The discrete RANS equations and Eq. (1) were solved sequentially (the segregated option in Fluent) and coupled to a realizable $k-\varepsilon$ model with wall functions for turbulence closure. The pressure at the faces is obtained using the body force weighted scheme. The continuity equation was enforced using a Semi-Implicit Method for Pressure-Linked (SIMPLE) algorithm. A modified High Resolution Interface Capturing (HRIC) scheme was used to solve the gas volume fraction.

Unsteady solutions were obtained using variable time-step between 0.001 to 0.01 seconds. Typically, two to three nonlinear iterations were needed within each time step to converge all variables to a L_2 norm of the error $<10^{-3}$. The flow rate at the exit and the elevation at the tailwater elevation gauge location were selected as convergence parameters.

6.2 Rigid-lid Model

The ASMM model equations were solved sequentially. The VOF and rigid-lid simulations were performed using the same discretization schemes for the continuity and pressure equations. A first order upwind scheme was used for the gas volume fraction and Reynolds stress components.

Unsteady solutions were obtained using a fixed time-step of 10 seconds. In order to improve convergence, the model was first run assuming single-phase flow and then bubbles were injected into the domain. The rigid-lid model was computed in typically 7 hours (2 days of computation time) to obtain a steady condition for the flow field and TDG concentration.

7.0 VALIDATION AND CALIBRATION OF THE MODEL

7.1 Simulation Conditions

The ability of the model to predict the TDG distribution and hydrodynamics was evaluated using field data collected for a period of six weeks between May 14, 2006 and June 28, 2006, during the TDG production dynamics study (EES et al., 2007). Velocities were measured on three transects in the near field region of the Wells tailrace on June 4, 2006 and June 5, 2006. Figure 3.0-1 shows the 15 stations where TDG sensors were deployed during the field study.

7.1.1 Calibration

The model was calibrated with data collected on June 4 and June 5, 2006, referred to as treatments 46 and 47 in the report by EES et al. (2007). The spillway flow was spread across all spillbays on June 4 and concentrated in a single spillbay on June 5. Total river flows during these treatments were 172.4 kcfs and 222.3 kcfs, respectively. Tables in Appendix A summarize plant operations, TDG saturation in the forebay, and tailwater elevation on these days. Powerhouse and spillway units are numbered from west to east.

7.1.2 Validation

The predictive ability of the numerical model was validated using three different spillway conditions tested in 2006. The three spillway conditions are: treatment 1-Full Gate (FG); treatment 11-FG; and treatment 63-Concentrated (C). The FG designates the use of a single spill bay whereas C designates a crowned spill pattern. Total river flows during these treatments were 120.4 kcfs, 157.2 kcfs and 205.5 kcfs, respectively. Plant operation and tailwater elevations associated with each of the treatments are tabulated on Tables in Appendix A.

7.2 VOF Model Results

The objectives for the calibration and verification VOF simulations were to establish a steady state solution that yield a flow field, including spillway jet regimes, consistent with that was observed in the field.

7.2.1 Calibration

The calibration cases were run in a domain of approximately 3,000 ft downstream of the dam. Zero velocities and turbulence were used as initial conditions in the entire domain.

The convergence parameters for the calibration cases were:

$$46S - June\ 4,2006 \rightarrow (\ flowrate : 172.4\ kcfs, WSE : 717.3\ ft)$$
$$47FG - June\ 5,2006 \rightarrow (\ flowrate : 222.3\ kcfs, WSE : 720.2\ ft)$$

Horizontal lines in Figure 7.2-1 show the target flow rate (blue line) and WSE at the tailwater elevation gage (green line). The evolution of the simulations for the calibration cases is illustrated in Figure 7.2-1; blue lines represent the flow rate at the exit and the green lines the free surface elevation. It was found that statistically steady solutions were obtained at approximately 30 minutes, which required about 60 days of computation time.

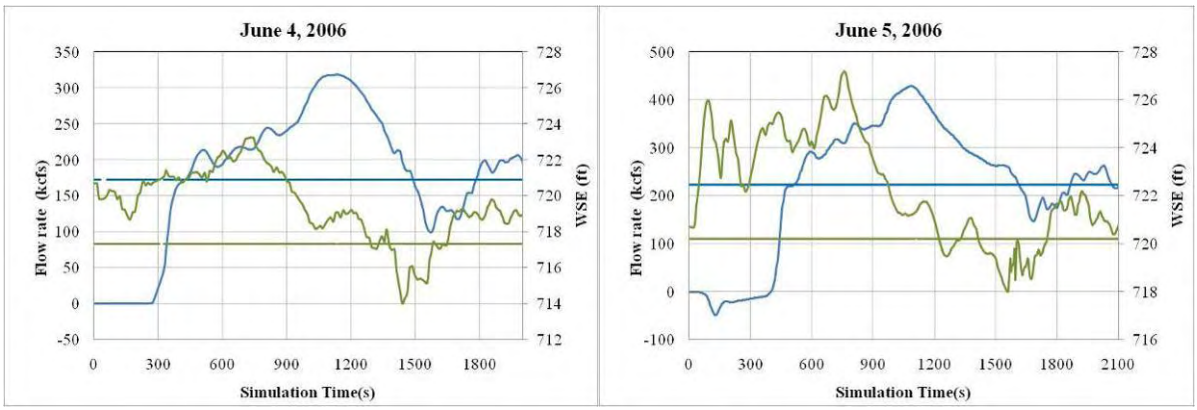

Figure 7.2-1 Evolution of the flow rate at the exit (blue line) and free surface elevation (green line) for June 4, 2006 and June 5, 2006. Horizontal lines represent target values.

Figure 7.2-2 shows an isosurface of gas volume fraction $\alpha_w = 0.5$ representing the free-surface location used to create the top of the rigid-lid grid for the June 4, 2006 simulation. In Figure 7.2-3 a horizontal slice at 27 ft from the free-surface (top) and a vertical section at the center of spillway bay 7 (bottom) show the predicted flow field with the VOF method. Red and blue contours represent water and air, respectively. For clarity, predicted velocity vectors were interpolated in structured uniform grids. Almost uniform flow is observed close to the spillway during the spread flow operation. Surface jets are predicted in all the spillway bays due to elevated tailwater levels. In addition, water flow from the powerhouse units prevented the spillway jet from plunging to depth within the stilling basin.

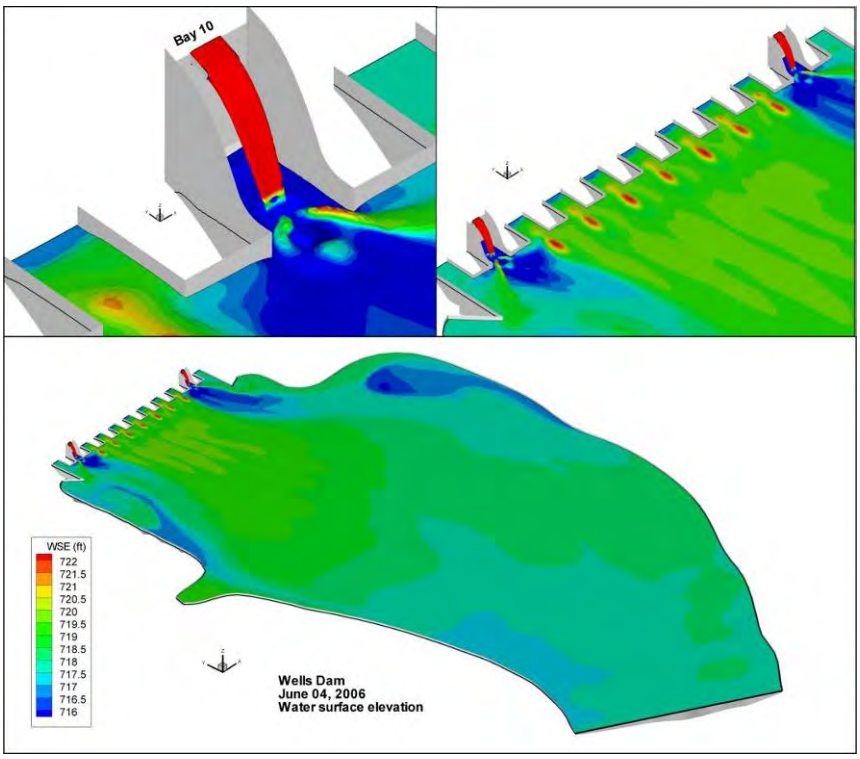

Figure 7.2-2 Predicted free surface shape for June 04, 2006

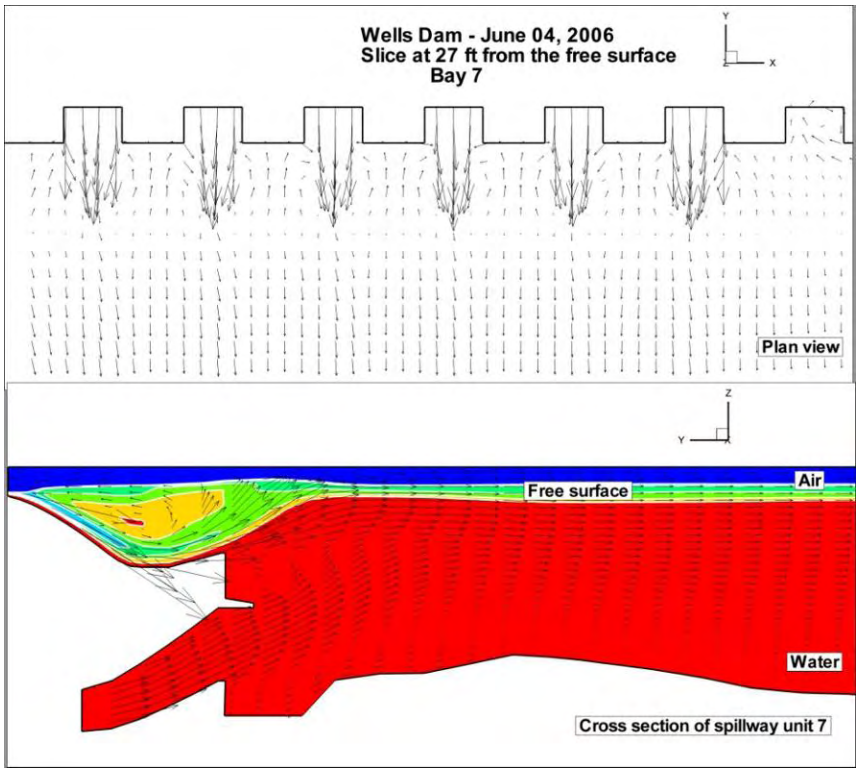

Figure 7.2-3 Predicted flow field for June 4, 2006

The free surface used to create the rigid-lid grid for June 5, 2006 is shown in Figure 7.2-4. The top of Figure 7.2-5 shows the water attraction toward the surface jet on bay 7 (water entrainment) caused by the full open gate operation. The water entrainment causes the formation of two large eddies near the east and west bank of the Wells tailrace. As observed on June 4, 2006, the strong surface jet originated in bay 7 remains close to the free surface (see bottom picture in Figure 7.2-5) due to the favorable tailwater elevation and plant operation on this day.

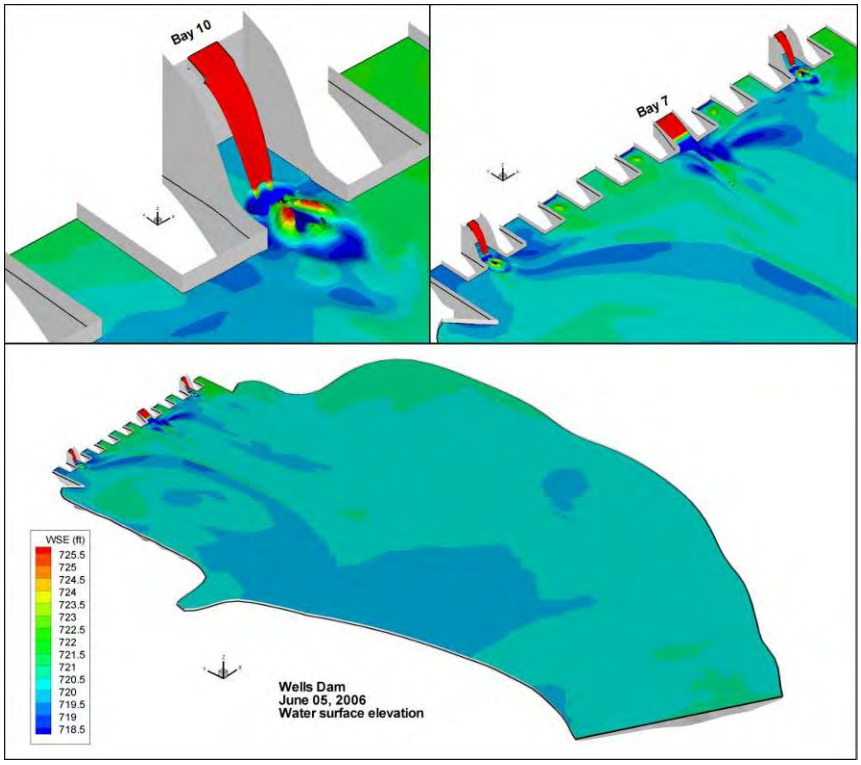

Figure 7.2-4 Predicted free surface shape for June 5, 2006

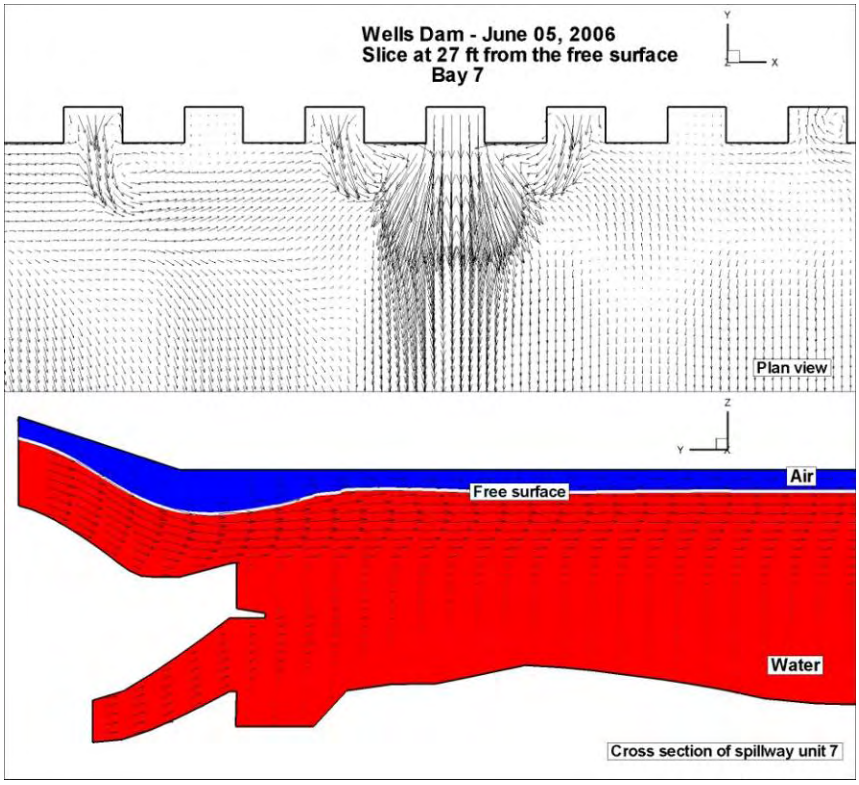

Figure 7.2-5 Predicted flow field for June 5, 2006

7.2.2 Validation

The domain used to simulate the validation cases was reduced to 1,700 ft downstream of the dam with the purpose of speeding up the VOF computations. During the calibration it was observed that the effect of the top spill on the free surface shape is limited to a small region near spillway bays 2 and 10. Therefore the validation cases assumed that spillway bays 2 and 10 were closed and the free surface shape obtained during the calibration process was used near the top spills.

The numerical solution (pressure, velocity, free surface location and turbulent quantities) obtained on June 5, 2006 was used as an initial condition for the validation cases.

The convergence parameters for the calibration cases were:

$$1FG-May\ 14,2006 \rightarrow (\ flowrate:120.4\ kcfs, WSE:711.5\ ft)$$

$$11FG-May\ 17,2006 \rightarrow (\ flowrate:157.2\ kcfs, WSE:715.4\ ft)$$

$$63C-June\ 17,2006 \rightarrow (\ flowrate:205.5\ kcfs, WSE:718.6\ ft)$$

Figure 7.2-6 shows the evolution of the flow rate and WSE at the tailwater elevation gauge for the validation cases. Blue and green lines represent the flow rate and WSE, respectively. The above mentioned simplifications allowed the calibration cases to reach the statistically steady solutions in typically 20 minutes using 30 days of computation time.

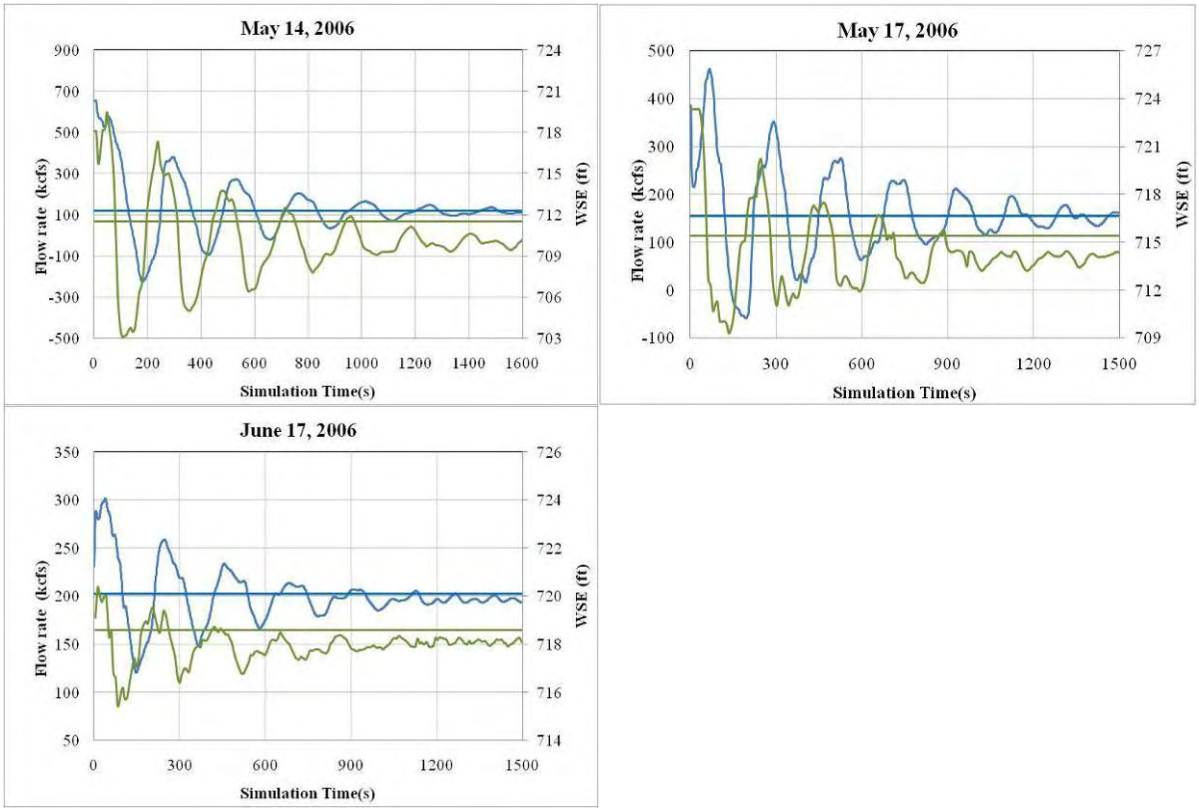

Figure 7.2-6 Evolution of the flow rate at the exit (blue line) and free surface elevation (green line) for May 14, 2006, May 17, 2006, and June 17, 2006. Horizontal lines represent target values.

7.3 Rigid-lid Model Results

7.3.1 Hydrodynamics

Figures 7.3-1 and 7.3-2 show depth-averaged velocity data collected in the field on June 4, 2006 and June 5, 2006 and those predicted by the rigid-lid model. Good agreement between observed and predicted velocity vectors was found, especially at the downstream transect where flow conditions were more stable and the Acoustic Doppler Current Profiler (ADCP) velocity data are less affected by turbulence and non-steady conditions.

As observed in the field, the model captured the counterclockwise eddy near the east bank and the almost uniform profile at the most downstream transect.

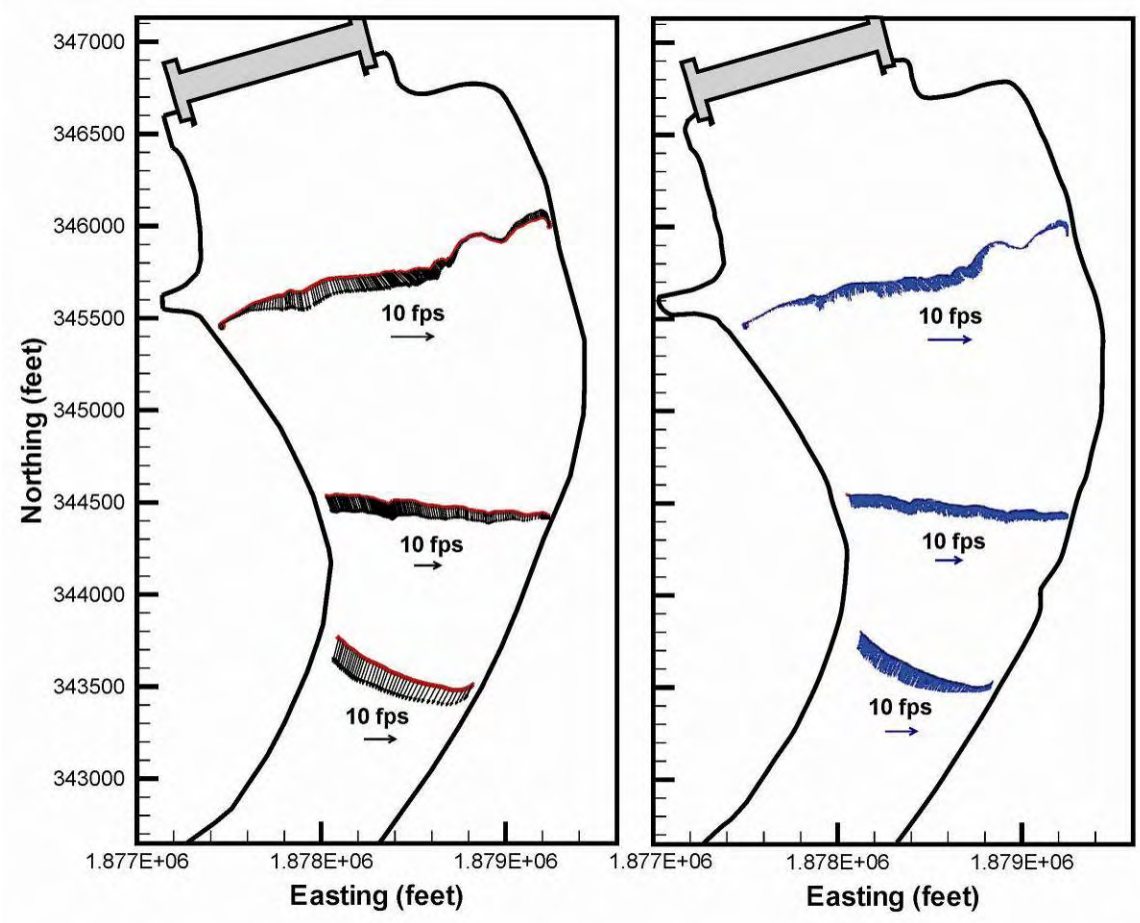

Figure 7.3-1 **Flow field on June 4, 2006. Black vectors: rigid-lid model predictions and blue vectors: velocity field data**

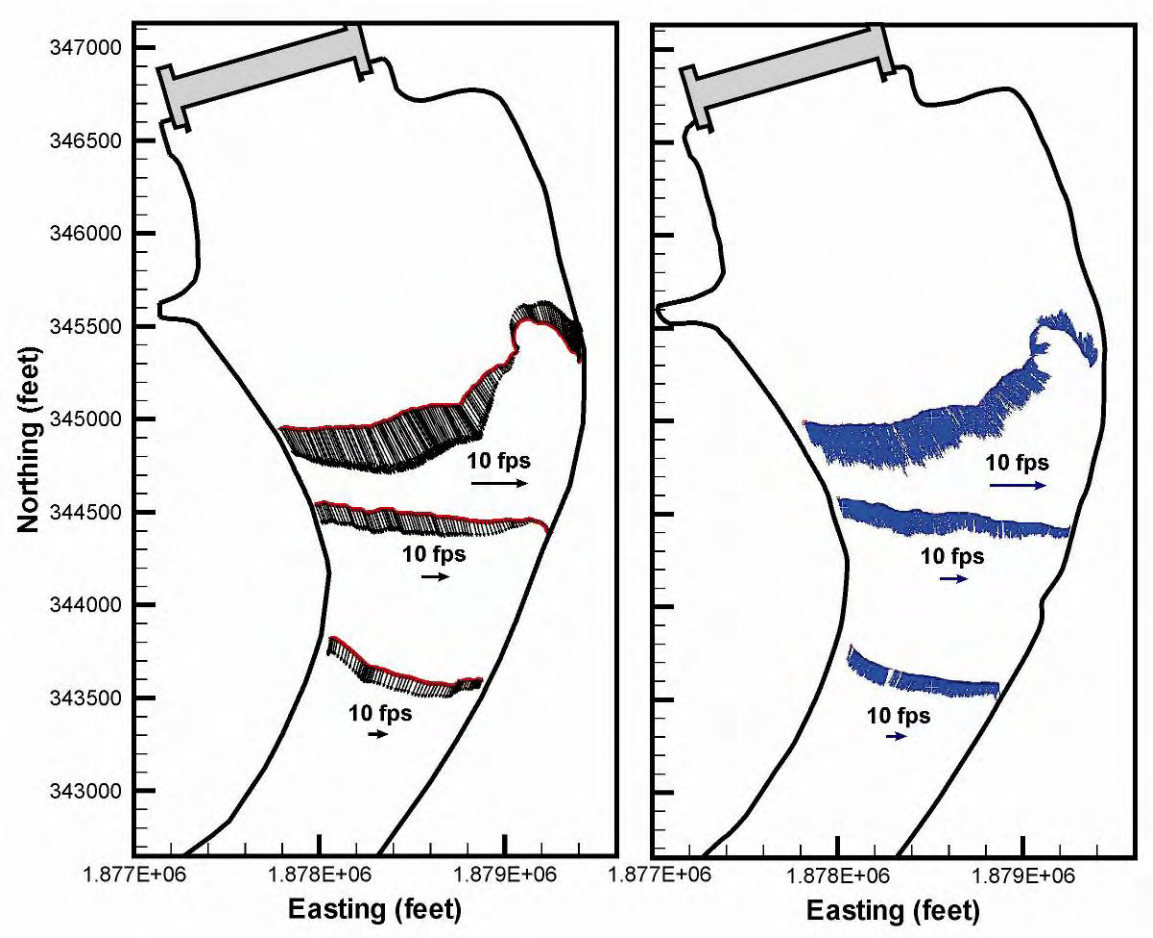

Figure 7.3-2 Flow field on June 5, 2006. Black vectors: rigid-lid model predictions and blue vectors: velocity field data

7.3.2 TDG Model

The percent saturation of TDG measured in the field at each station and the mean TDG in each of the three transects together with the values generated by the CFD model for the calibration and validation cases are shown in Appendix B. Figures 7.3-3 to 7.3-7 show measured and predicted values at each probe location. A bubble diameter of 0.5 mm and gas volume fraction of 3% in the spillbays produced TDG values that bracketed field observations.

The model captures the reduction of TDG with distance downstream and the lateral gradient observed in the field. As measured, the highest predicted TDG value at Transect TW1 occurred in the center of the channel and the lateral gradients in transects TW2 and TW3 were negligible.

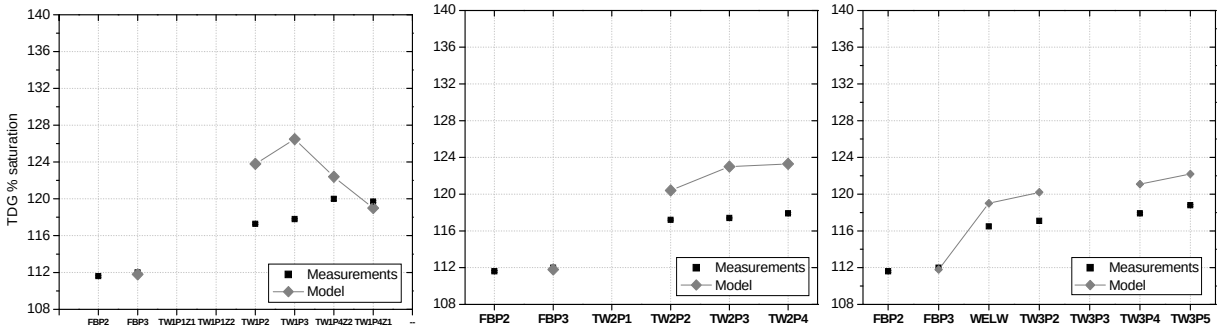

Figure 7.3-3 Comparison between measured and predicted TDG on June 4, 2006. Gray diamonds represent TDG model predictions and black squares represent field observations.

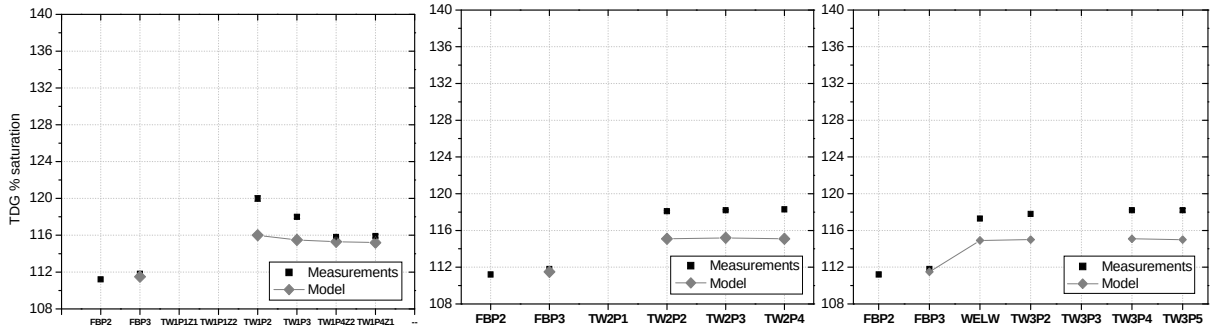

Figure 7.3-4 Comparison between measured and predicted TDG on June 5, 2006. Gray diamonds represent TDG model predictions and black squares represent field observations.

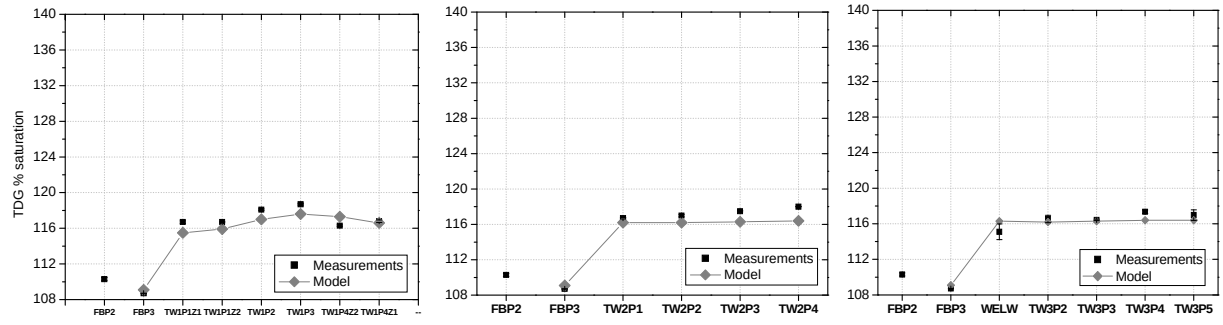

Figure 7.3-5 Comparison between measured and predicted TDG on May 14, 2006. Gray diamonds represent TDG model predictions and black squares represent field observations.

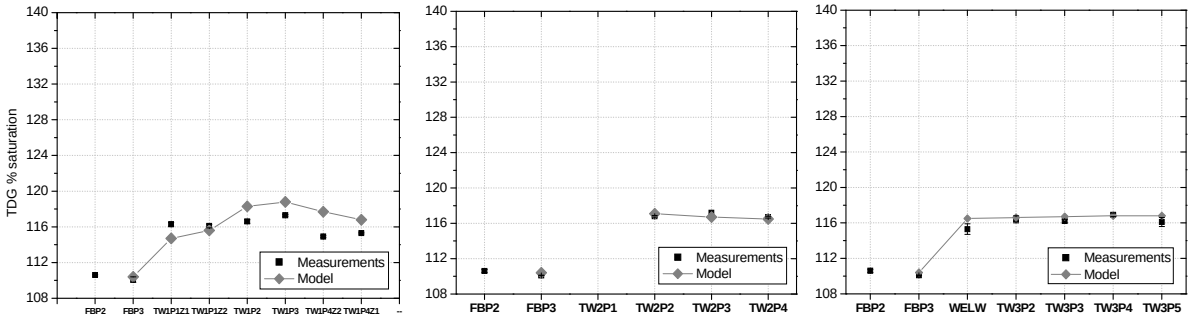

Figure 7.3-6 Comparison between measured and predicted TDG on May 17, 2006. Gray diamonds represent TDG model predictions and black squares represent field observations.

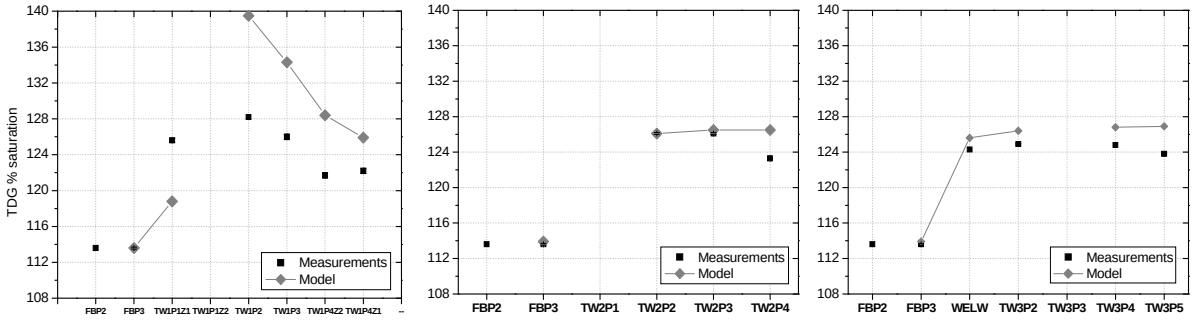

Figure 7.3-7 Comparison between measured and predicted TDG on June 17, 2006. Gray diamonds represent TDG model predictions and black squares represent field observations.

Figures 7.3-8 and 7.3-9 show isosurfaces of TDG, gas volume fraction and bubble diameter for June 4, 2006 and June 5, 2006 where the spill operation was adjusted to test both a spillway discharge pattern that was spread across the spill bays (Figure 7.3-8) and a concentrated spill pattern (Figure 7.3-9). As shown by the gas volume fraction isosurfaces, the model predicts uniformly distributed bubbles on the spillway region during spread spill operations. On the other hand, bubbles concentrate near the center of the spillway for full open gate operation. The maximum TDG occurs at the center region due to the exposure of water to the aerated flow as it travels within the stilling basin (see TDG isosurfaces). The rate of mass exchange depends on the gas volume fraction, the bubble size and the difference in concentration between the bubble boundary and the water. The gas dissolution region occurs mainly within 500 to 1,000 ft downstream of the spillway; afterwards the bubbles moved up to regions of lower pressure and the dissolution rate decreased. The bubbles shrink near the bed due to the air mass transfer and high pressure. The smaller the bubble size the stronger its tendency to dissolve. Substantial desorption of TDG takes place near the free surface downstream of the spillway. Once the air bubbles are vented back into the atmosphere the rate of mass exchange decreases significantly. The TDG concentration reaches a developed condition approximately 1,300 ft from the spillway. According to the simulation results, the draft tube deck extensions and spillway lip, tend to act as deflectors for the spill, and powerhouse operation prevented spilled flow from plunging deep, reducing the exposure of bubbles to high pressure.

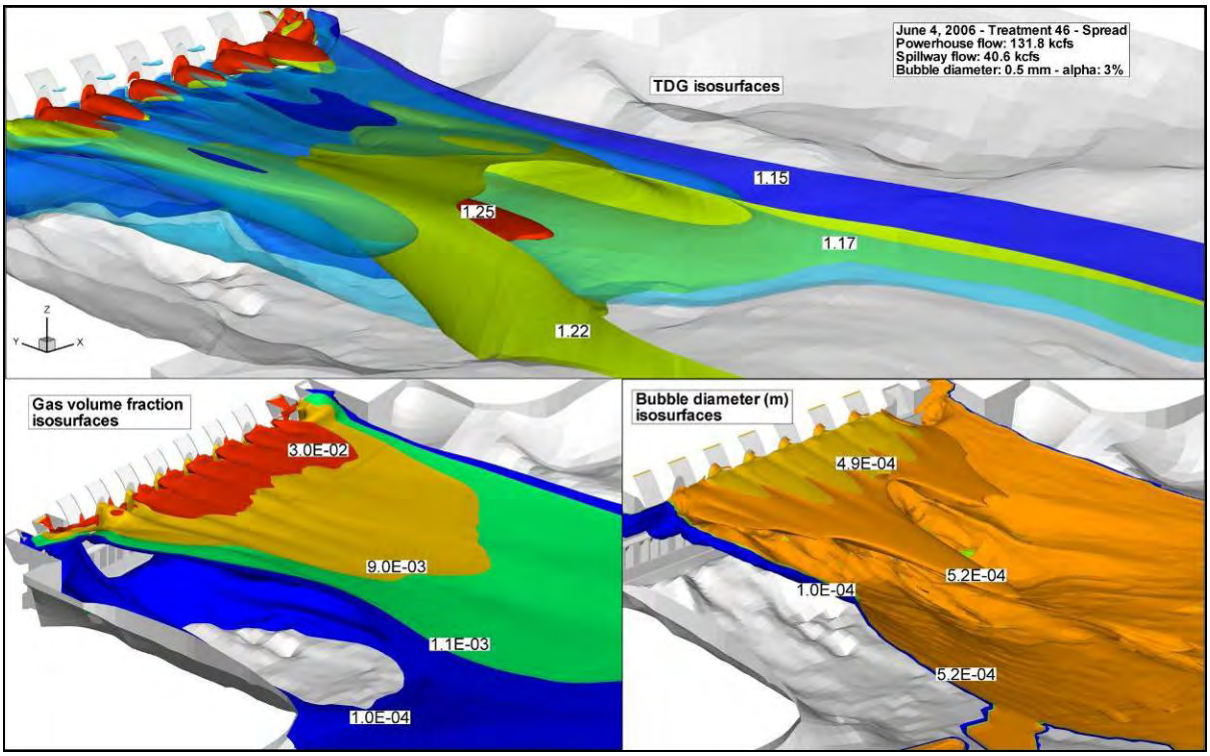

Figure 7.3-8 TDG, gas volume fraction and bubble diameter isosurfaces for June 4, 2006

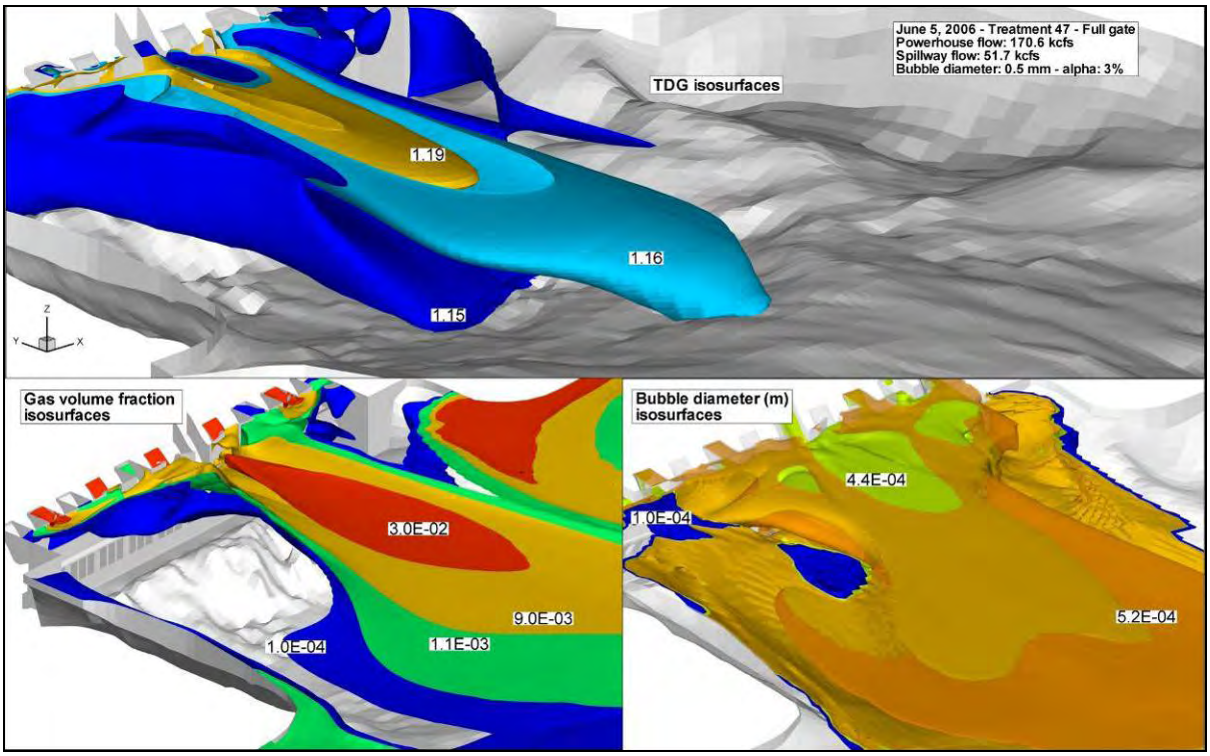

Figure 7.3-9 TDG, gas volume fraction and bubble diameter isosurfaces for June 5, 2006

Table 7.3-1 summarizes simulation conditions and averaged predicted TDG at transects T1, T2 and T3. The last column in the table shows the difference between averaged TDG at transect T3 and forebay TDG, $\Delta TDG = TDG_{T3} - TDG_{forebay}$ indicating the approximate net production of TDG in the tailrace.

Table 7.3-1 Averaged predicted TDG in Transects 1, 2 and 3 for the calibration and validation cases

Case	Date	Spill (kcfs)	Total Q (kcfs)	% Spilled	Unit Spill (kcfs/ft)	Tailwater Elevation (feet)	Spillway Submergence (feet)	% TDG Forebay	% TDG Transect 1	% TDG Transect 2	% TDG Transect 3	Difference % TDG Forebay to Transect 3
46 S	4-Jun	40.6	172.4	23.5	0.11	717.3	26.3	111.8	122.9	122.2	120.7	8.9
47 FG	5-Jun	51.7	223.3	23.2	0.77	720.2	29.2	111.5	115.5	115.1	115.0	3.5
1 FG	14-May	44.6	120.4	37.0	0.62	711.5	20.5	109.1	116.7	116.3	116.3	7.2
11FG	17-May	42.6	157.2	27.1	0.60	715.4	24.4	110.4	117.0	116.9	116.7	6.3
63C	17-Jun	87.4	205.5	42.5	0.55	718.6	27.6	113.9	130.5	126.4	126.4	12.5

8.0 SENSITIVITY SIMULATIONS

8.1 Simulation Conditions

Nine model runs (MR) with two spillway configurations (spread and concentrated spill) and four total river flows were simulated to analyze the sensitivity of TDG production as a function of total flow, spill releases, and tailwater elevation. These simulations were run assuming forebay TDG was 115% and water temperature was 14 ^{o}C. Tables in Appendix A summarize plant operations, TDG saturation in the forebay, and tailwater elevation used for these simulations.

Numerical results of the MR simulations confirmed what seemed to be demonstrated by field data, that is, saturation of gases in the tailrace could be minimized by concentrating the spill through one or more gates rather than spread across the spillway. This lead to further model runs in which various spill patterns were tested with the objective of reducing TDG production in the Wells Tailrace. In Section 9, the Preferred Operating Conditions are discussed and presented.

8.2 VOF Model Results

The free surface shape for the sensitivity simulations was extracted from VOF computations in a domain extending about 1,700 ft downstream of the dam. The convergence parameters for these simulations were:

$MR1 \text{ and } MR5 \rightarrow (\ flowrate : 208.5\ kcfs, WSE : 718.8\ ft)$

$MR2,\ MR6 \text{ and } MR8 \rightarrow (\ flowrate : 246.0\ kcfs, WSE : 721.4\ ft)$

$MR3 \text{ and } MR7 \rightarrow (\ flowrate : 128.0\ kcfs, WSE : 713.4\ ft)$

$MR4 \text{ and } MR9 \rightarrow (\ flowrate : 165.5\ kcfs, WSE : 715.9\ ft)$

The initial conditions from the MR simulations were obtained from interpolation of the numerical solutions for the calibration/validation cases. The MR cases reached the statistically steady solutions in typically 20 to 30 minutes (30 to 45 days of computation time).

8.3 Rigid-lid Model Results

8.3.1 MR Simulations

Tables in Appendix C show the percent saturation of TDG predicted by the model at each station and the mean TDG in each of the three transects for the MR simulations. Figures 8.3-1 to 8.3-3 show predicted TDG values at each probe location. Table 8.3-1 summarizes simulation conditions, averaged predicted TDG at transects T1, T2, T3 and ΔTDG .

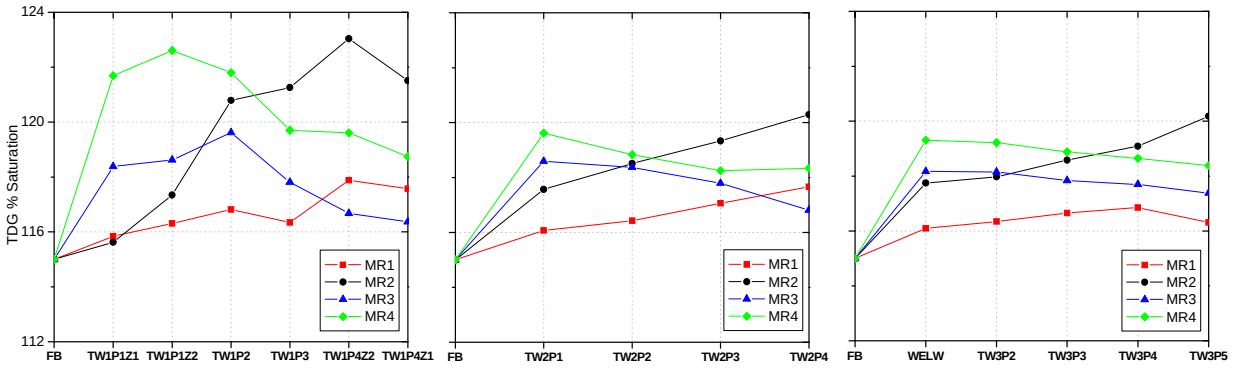

Figure 8.3-1 Predicted TDG concentration for spread operation

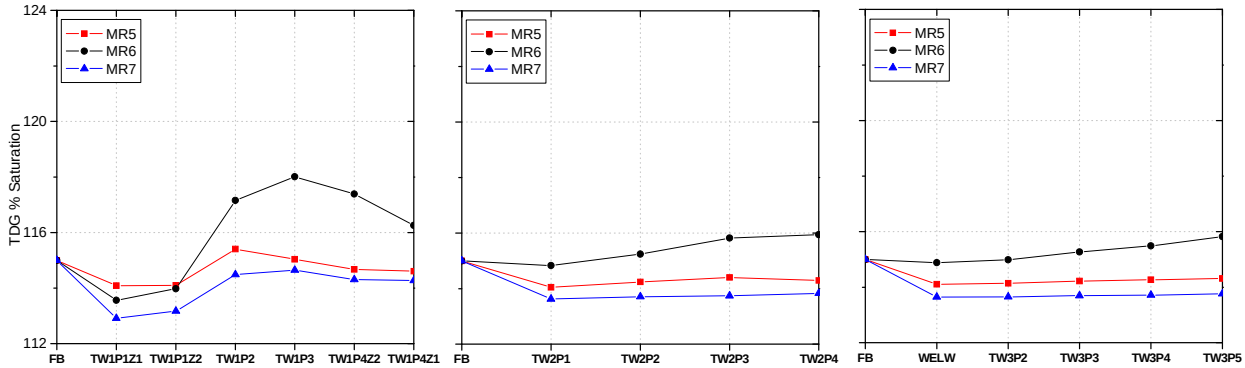

Figure 8.3-2 Predicted TDG concentration for full open gate operation

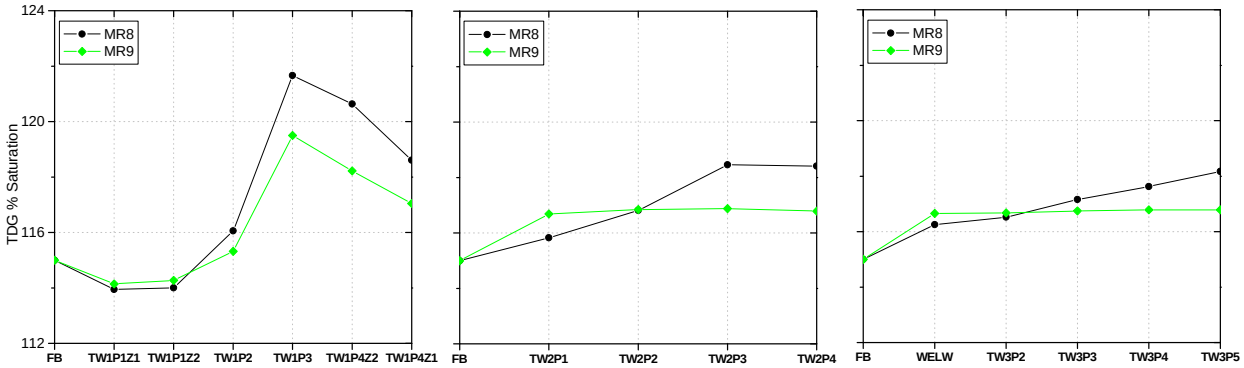

Figure 8.3-3 Predicted TDG concentration for two full open gates operation

Table 8.3-1 Averaged predicted TDG in Transects 1, 2 and 3 for the sensitivity simulations.

Case	Type	Spill (kcfs)	Total Q (kcfs)	% Spilled	Unit Spill (kcfs/ft)	Tailwater Elevation (feet)	Spillway Submergence (feet)	% TDG Forebay	% TDG Transect 1	% TDG Transect 2	% TDG Transect 3	Difference % TDG Forebay to Transect 3
1	S	23.0	208.5	11.0	0.07	718.8	27.8	115.0	117.3	118.1	117.9	2.9
2	S	60.5	246.0	24.6	0.19	721.4	30.4	115.0	123.7	124.1	123.7	8.7
3	S	23.0	119.0	19.3	0.07	713.4	22.4	115.0	121.3	120.7	120.7	5.7
4	S	60.5	156.5	38.7	0.19	715.9	24.9	115.0	126.3	124.5	124.7	9.7
5	1-FG	23.0	208.5	11.0	0.50	718.8	27.8	115.0	116.0	116.8	116.7	1.7
6	1-FG	60.5	246.0	24.6	1.32	721.4	30.4	115.0	121.1	121.4	121.3	6.3
7	1-FG	23.0	119.0	19.3	0.50	713.4	22.4	115.0	117.5	117.1	117.3	2.3
8	2-FG	60.5	246.0	24.6	0.66	721.4	30.4	115.0	121.2	123.0	122.6	7.6
9	2-FG	60.5	156.5	38.7	0.66	715.9	24.9	115.0	122.2	122.9	122.9	7.9

In order to understand the effect of plant operations on TDG production and mixing, the simulations were grouped as follow:

1. Simulations with the same spill and powerhouse flows:
   $\{[\text{MR1 and MR5}],\ [\text{MR2, MR6 and MR8}],\ [\text{MR3 and MR7}],\ \text{and}\ [\text{MR4 and MR9}]\}$

2. Simulations with the same spill operation (concentrated or spread spill) and same powerhouse flows:
   $\{Spread:[\text{MR1(S=23 kcfs) and MR2(S=60.5 kcfs)}]\ \text{and}\ [\text{MR3(S=23 kcfs) and MR4(S=60.5 kcfs)}]\}$
   $\{FG:[\text{MR5(S=23 kcfs) and MR6(S=60.5 kcfs)}]\}$

3. Simulations with the same spill operation (concentrated or spread spill) and same spilled flows:
   $\{Spread:[\text{MR1(P=185.5 kcfs) and MR3(S=96 kcfs)}]\ \text{and}\ [\text{MR2(S=185.5 kcfs) and MR4(S=96 kcfs)}]\}$
   $\{FG:[\text{MR5(S=185.5 kcfs) and MR7(S=96 kcfs)}]\}$

where S and P denote spillway and powerhouse flows, respectively.

Simulations with the same spill and powerhouse flows

Substantial differences in downstream TDG levels were observed with spread or full open gate operations. Numerical results indicate that, for the same spill and powerhouse flows, full open gate operation resulted in the lowest TDG concentration. On the other hand, the highest TDG concentrations were observed with spread flow operation. Simulations MR6 and MR8 show that distributing the same spill flow into two gates produced more TDG than concentrating the flow through a single bay.

To understand the underlying physics that cause larger TDG concentrations with spread operation, the volume of air available for dissolution and TDG sources for simulations MR1 (spread) and MR5 (FG) were analyzed at two transects downstream of the dam.

Figure 8.3-4 shows the cumulative volume of air in bubbles per unit length and cumulative TDG source per unit length as a function of the distance from the free surface at 50 m downstream of

the dam. Solid lines show the cumulative volume of air in bubbles per unit length for simulations MR1 and MR5. Almost no air was present below 10 m. Note that the amount of air available for dissolution for concentrated spill operation (MR5) is always smaller than that for spread flows (MR1). The distribution of gas volume fraction and TDG at a vertical slice at 50 m from the dam for both types of operation is shown in 8.3-5. Note that the gas volume fraction, and consequently the TDG, is significantly larger for spread operation. As shown in Figure 8.3-6, for the simulated flow rates, the spread operation produces a submerged jet while the full open gate operation produces a surface jump. The residence time of bubbles entrained in a submerged jet is longer than those entrained in a surface jump. Bubbles reach the free surface more quickly in a surface jump because, on average, they travel closer to the free surface and because the water depth on the spillway face is smaller. In addition, large vertical liquid velocities downstream of the spillway lip help bubbles leave the tailrace more quickly for the concentrated spill operation.

The dotted lines in Figure 8.3-4 show the cumulative TDG source for simulations MR1 and MR5. Since the amount of air in bubbles available to produce TDG is larger for the spread operation, both the degasification (negative source of TDG) and production of TDG (positive source of TDG) are increased for this case. The net TDG production for spread and concentrated spill operations are approximately 0.15 kg air/(s m) and 0.06 kg air/(s m), respectively.

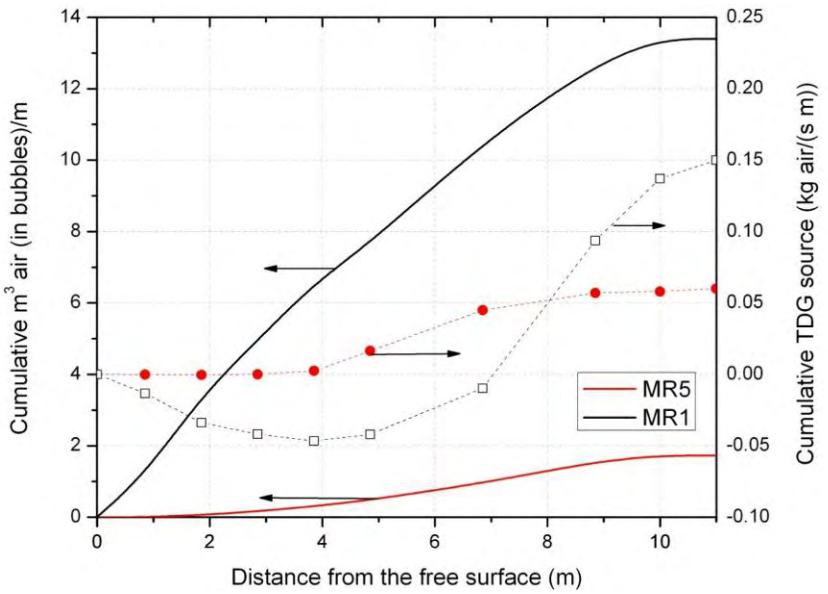

Figure 8.3-4 **Cumulative volume of air in bubbles per unit length (left) and cumulative TDG source per unit length (right) as a function of the distance from the free surface at a plane at 50 m from the dam.**

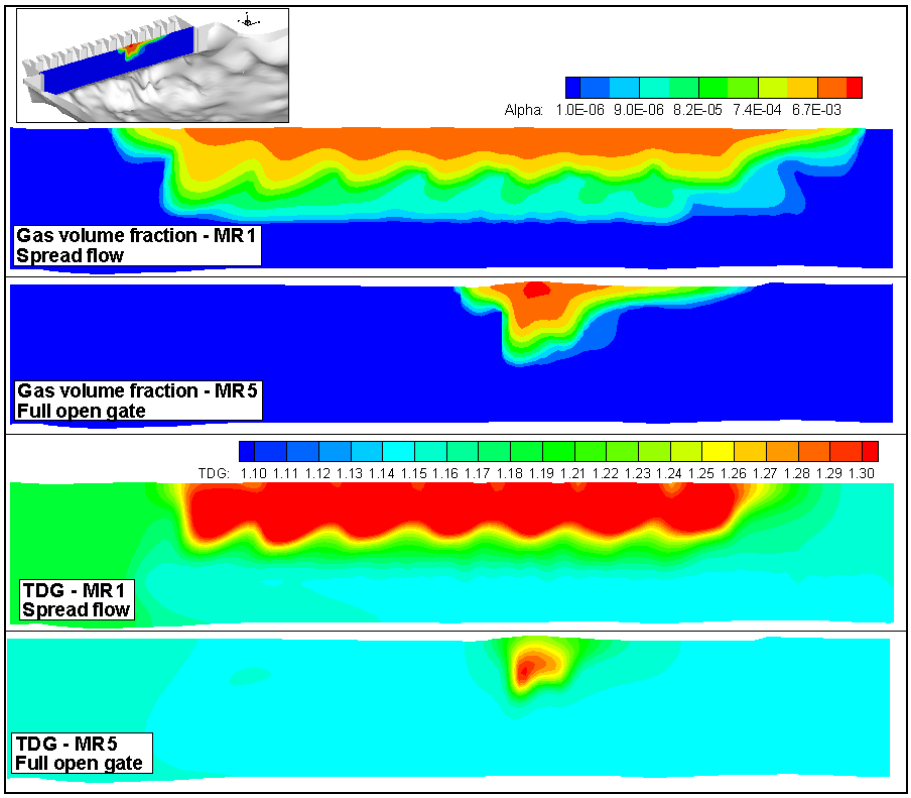

Figure 8.3-5 **Contours of gas volume fraction and TDG at 50 m from the dam for simulations MR1 and MR5.**

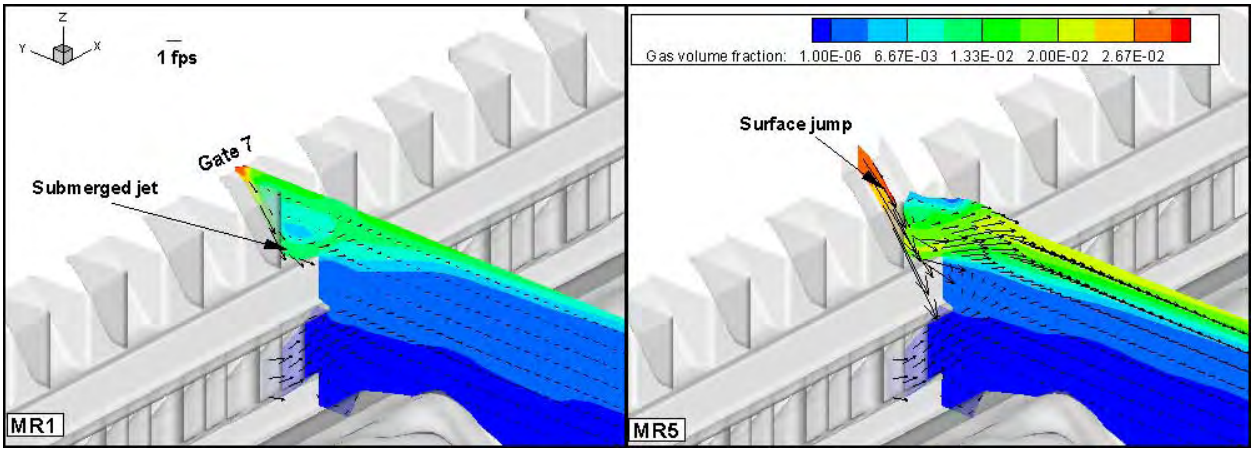

Figure 8.3-6 **Contours of gas volume fraction and velocity vectors at a slice through gate 7 for MR1 (top) and MR5 (bottom).**

Figure 8.3-7 shows the cumulative curves at Transect 1 location, 370 m downstream of the dam. Contrary to observations at 50 m from the dam, more bubbles are present at transect T1 for concentrated spill operation than for spread flows. The distributions of gas volume fraction and resulting TDG for MR1 and MR5 are shown in Figure 8.3-8. Higher liquid velocities with

concentrated spill operation transport bubbles further in the tailrace. In addition, higher turbulent dispersion, created by a stronger jet in a full open gate operation, entrains bubbles deeper into the tailrace increasing bubble residence times. Note that 100% of the bubbles at Transect T1 are 2m or less from the free surface for the spread operation. On the other hand, due to turbulent dispersion, about 65% of the bubbles are 2 m from the free surface for full open gate operation. The TDG source is negative (degasification) for both type of operations. However, more degasification is observed with concentrated spill due to more availability of gas and an elevated mass transfer coefficient at the free surface for higher turbulent flows. As shown in Figure 8.3-8, TDG is higher for the spread operation as a result of more TDG production and less degasification at the free surface.

The flow pattern and TDG distribution in the tailrace for cases MR1 and MR5 are shown with streamlines colored by TDG concentration in Figures 8.3-9 and 8.3-10, respectively.

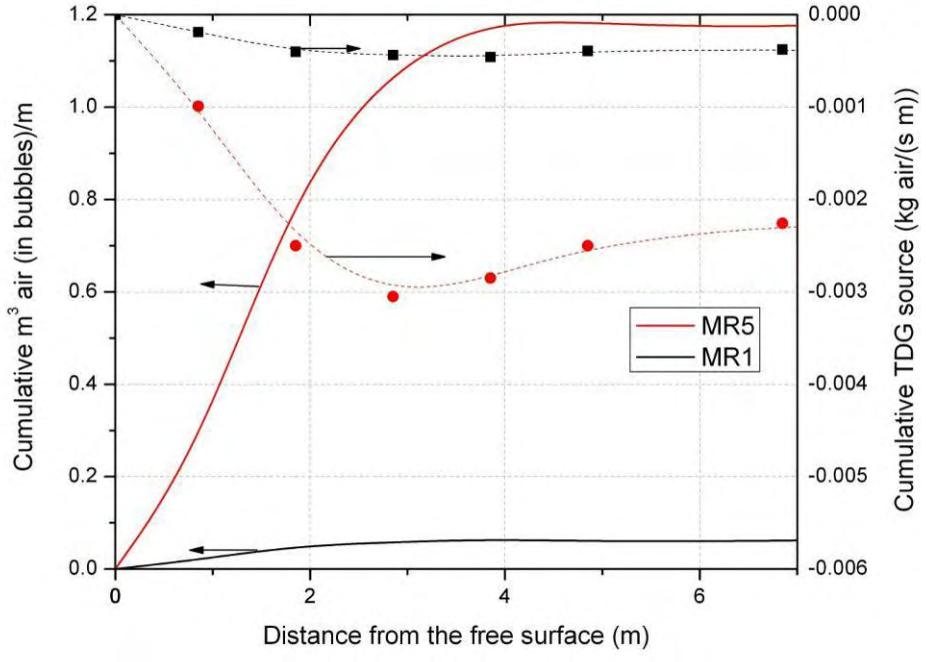

Figure 8.3-7 **Cumulative volume of air in bubbles per unit length (left) and cumulative TDG source per unit length (right) as a function of the distance from the free surface at a plane at 370 m from the dam.**

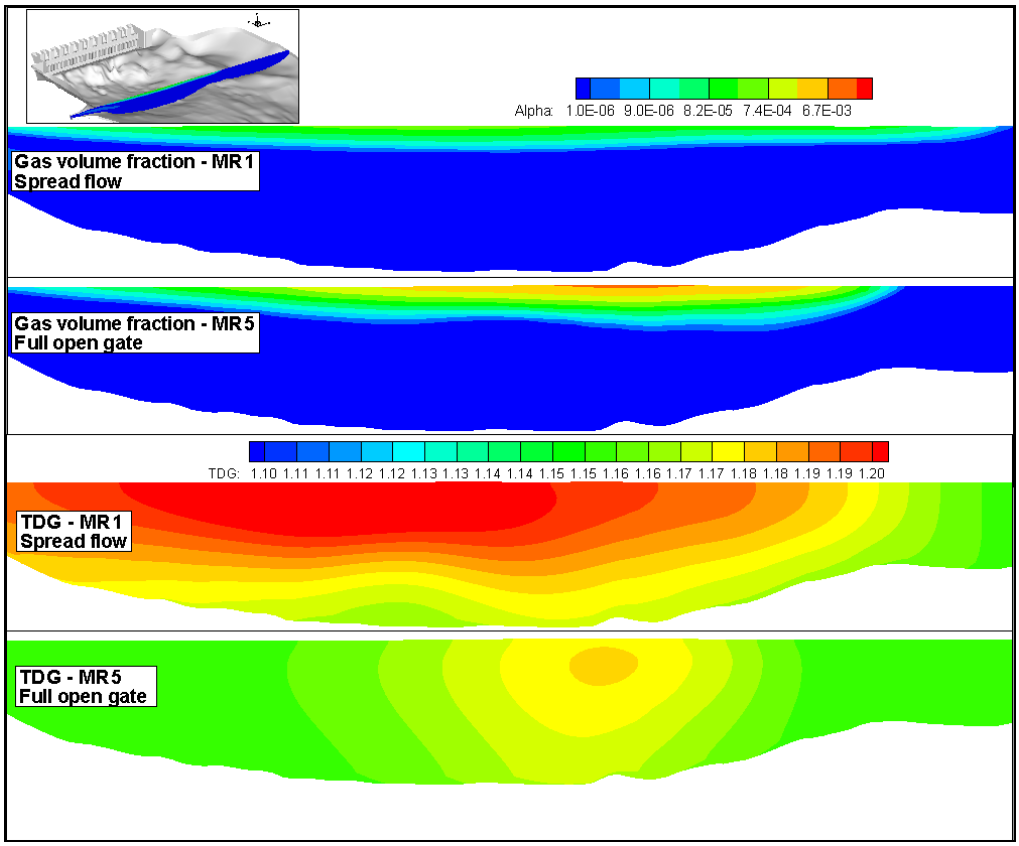

Figure 8.3-8 **Contours of gas volume fraction and TDG at 370 m from the Dam for simulations MR1 and MR5.**

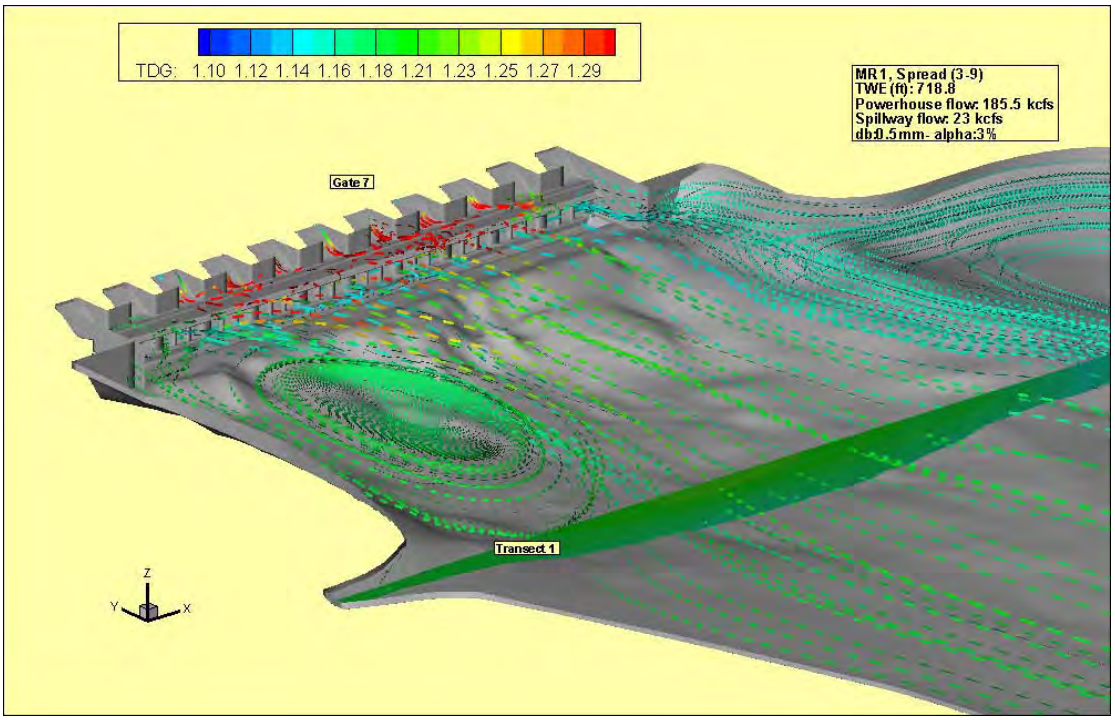

Figure 8.3-9 Streamlines colored by TDG concentration for MR1.

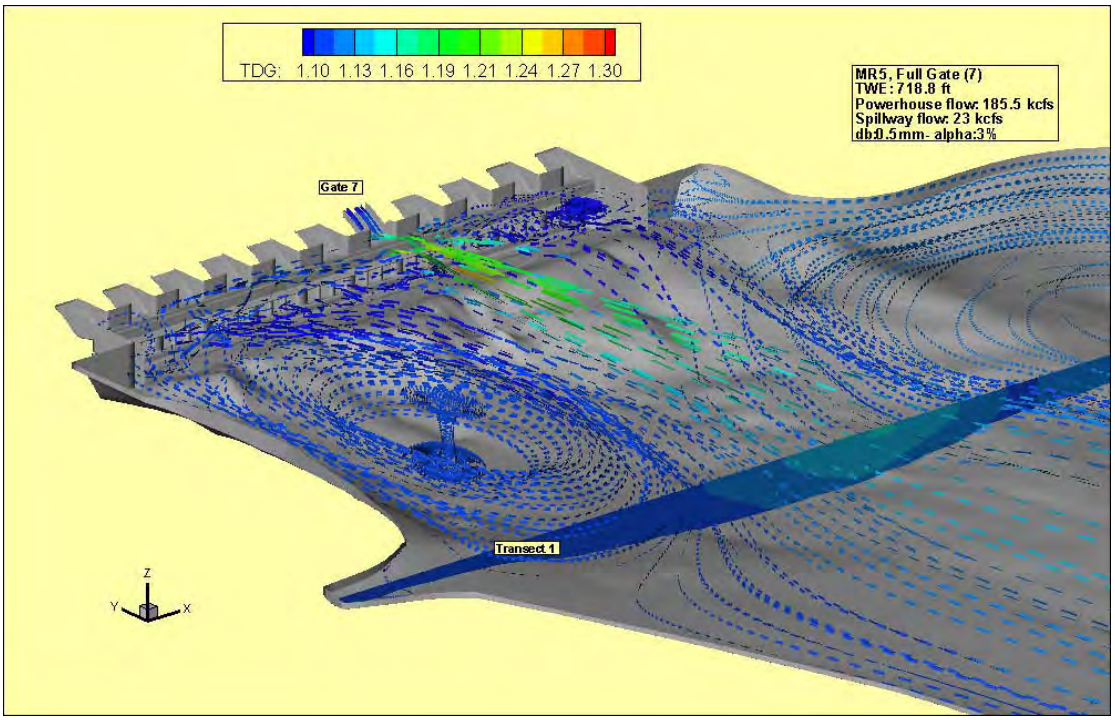

Figure 8.3-10 Streamlines colored by TDG concentration for MR5.

Simulations with the same spill operation and same powerhouse flows

Downstream TDG levels depend on the percentage of spilled water. For constant powerhouse flows, the greater the amount of spill, the greater the amount of bubbles entrained and the turbulence generated in the tailrace, and therefore, the greater the TDG production. Thus, the simulations for spread flows MR1 and MR3 with 23 kcfs spill flow produces less TDG than the equivalent MR2 and MR4 simulations with 60.5 kcfs (see Figure 8.3-1). Streamlines colored by TDG show the flow pattern and TDG distribution for MR1 (Figure 8.3-1) and MR2 (Figure 8.3-11). For these cases, the maximum TDG levels occurred at the west bank of the Wells tailrace.

Figures 8.3-12 and 8.3-13 show the submergence depth of the flip lip as a function of spill per unit width for full open gate and spread operations, respectively. The submergence depth is defined as the tailwater elevation minus the elevation of the top of the flip lip (691 ft) and the spill per unit width is:

$$\text{Spill per unit width} = \frac{1}{S_T W} \sum_i S_i^2 \qquad (19)$$

where W is the width of the spillbay, S_T is the total spill, and S_i is the spill of a generic bay i. Orange triangles represent field data black stars: predicted data at the model calibration/validation, black squares: sensitivity simulations. Labels indicate ΔTDG values. Data were grouped based on the percentage spill between 0 to 19%, 20 to 39%, 40 to 59%, and 60 to 100%. These plots confirm that the TDG production is strongly dependent on the percentage of spilled water.

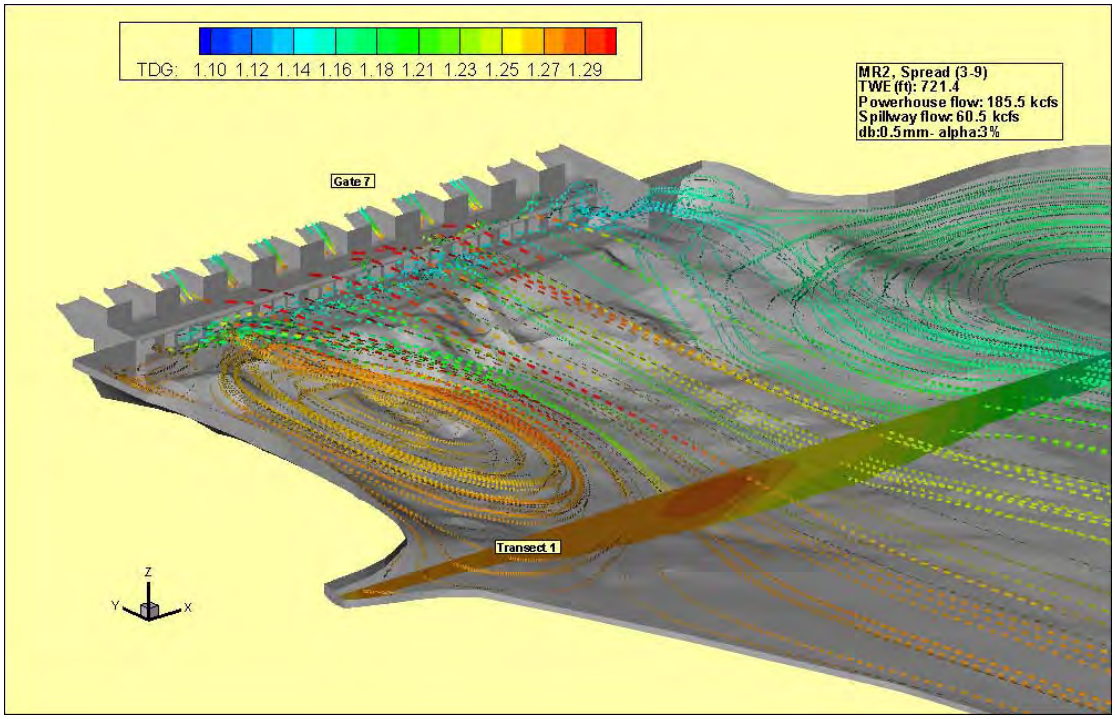

Figure 8.3-11 Streamlines colored by TDG concentration for MR2.

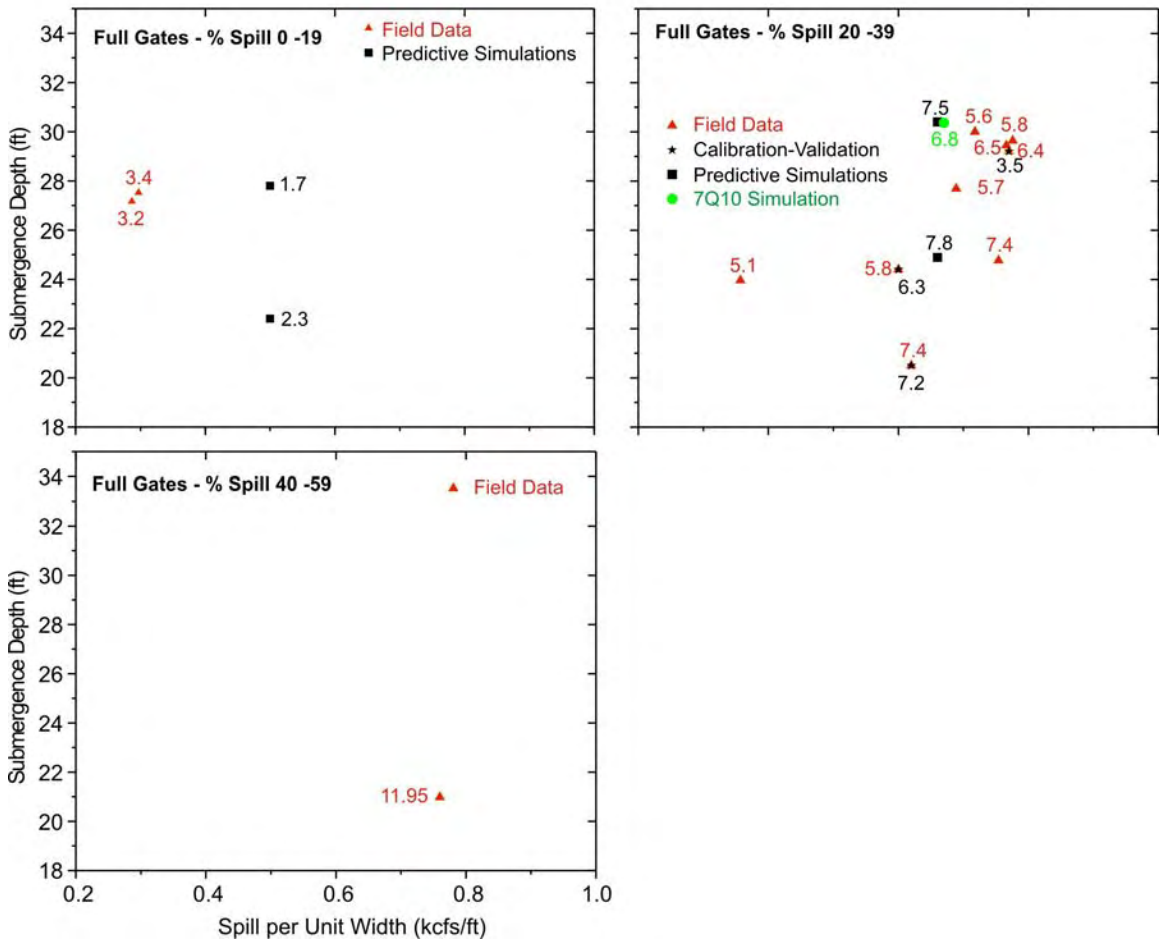

Figure 8.3-12 **Submergence depth as a function of spill per unit width for full open gate operation for percentage spill between 0 to 19%, 20 to 39%, and 40 to 59%. Red triangles: field data, black stars: predicted data at the model calibration/validation, black squares: sensitivity simulations, and green circle 7Q10 simulation. Labels indicate ΔTDG values.**

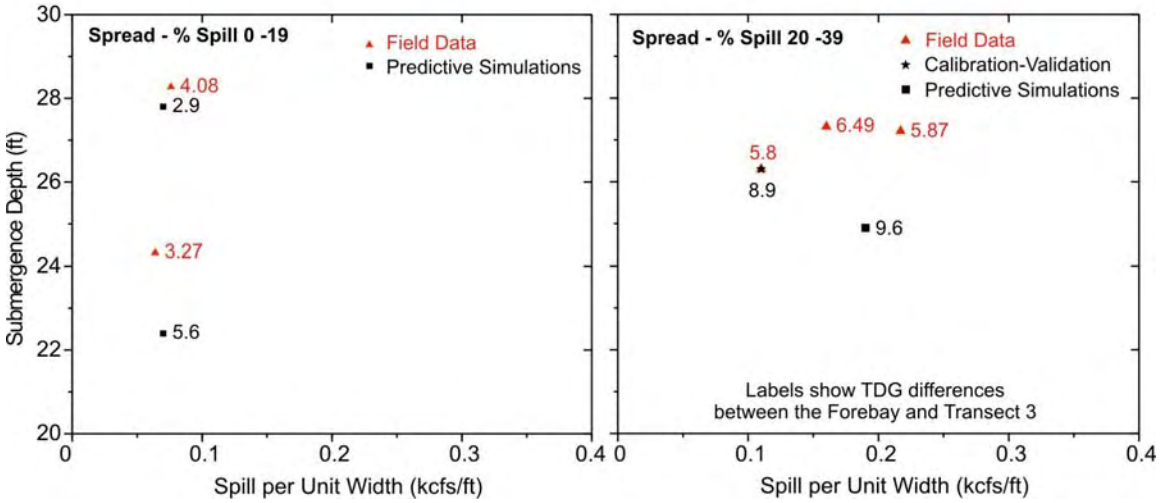

Figure 8.3-13 Submergence depth as a function of spill per unit width for spread operation for percentage spill between 0 to 19% and 20 to 39. Red triangles: field data, black stars: predicted data at the model calibration/validation, and black squares: sensitivity simulations. Labels indicate ΔTDG values.

Simulations with the same spill operation and spilled flows

Mixing and dilution from increased powerhouse flows resulted in reduced TDG levels downstream for both spread and concentrated spill operations. The most notable effect of the powerhouse flow reduction was the increment of TDG values at the east bank for spread flows. The TDG distribution predicted in simulation MR4 with 96 kcfs powerhouse flow compared with the predicted values for MR2 with 185.5 kcfs powerhouse flow are shown in Figures 8.3-14 and 8.3-11, respectively.

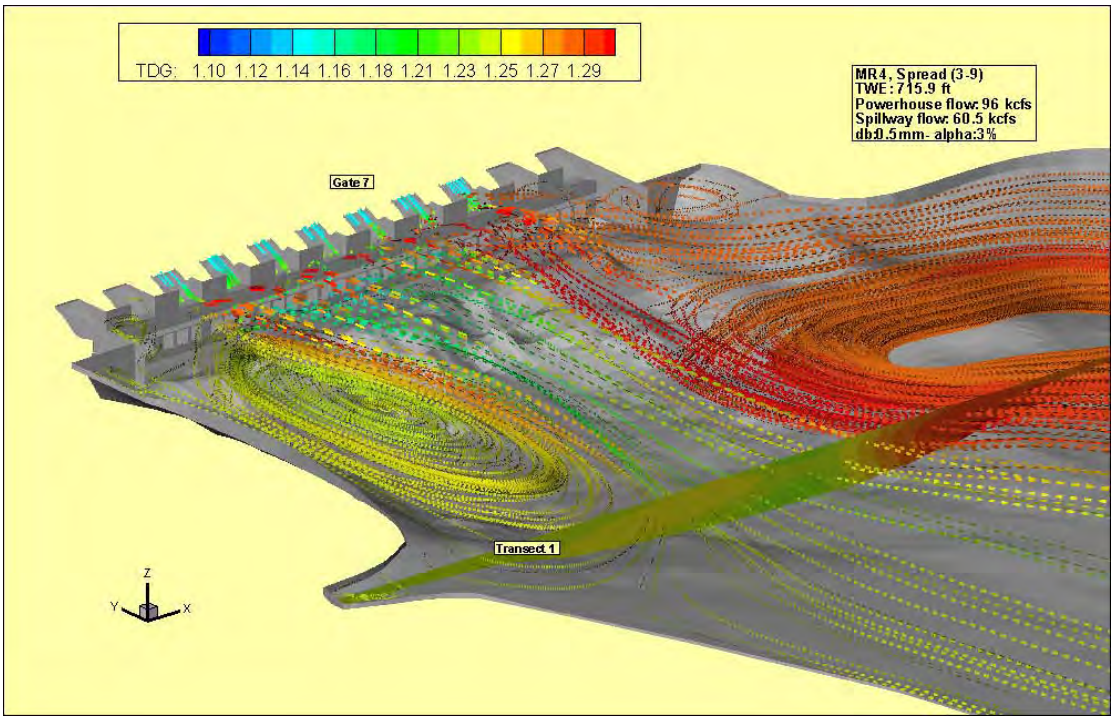

Figure 8.3-14 Streamlines colored by TDG concentration for MR4.

9.0 PREFERRED OPERATING CONDITION - 7Q10 FLOW SIMULATION

9.1 Simulation Conditions

Based upon the results of the sensitivity simulations, several additional operating configurations were tested toward identification of a Preferred Operating Condition (POC) for a 7Q10 flow at Wells Dam. The environmental conditions used for these model runs were different than the sensitivity simulations because the environmental parameters consistent with high flow events (>200 kcfs) are very different than the environmental conditions observed during average operating conditions. Because of these differences, the inputs for the 7Q10 preferred operating simulation included forebay TDG of 113% and water temperature equal to 13 ^{o}C. Table 9.1-1 shows simulation conditions used for the 7Q10 run. Operational conditions included operating only 9 of 10 turbine units[1], (each unit running at 20 kcfs[2]), 10 kcfs running through the Juvenile

[1] Ecology has requested that the TDG model be operated utilized only 9 of the 10 available turbine units at Wells Dam. This request was intended to simulate a condition where one turbine unit is off-line for maintenance.

[2] Note that the maximum flow for each of the 10 turbines at Wells Dam is 22.6 kcfs for a total powerhouse capacity of 226 kcfs. The TDG model used a more conservative 20 kcfs per turbine which represents a more normal operation condition when flows at Wells Dam are approaching the hydraulic capacity of the powerhouse (>200 kcfs).

Bypass System[3], and 1 kcfs flowing down the fish ladders, and 54.6 kcfs through the spillways (combined spillway and bypass flow of 64.6 kcfs).

Table 9.1-1 Conditions used for the POC-7Q10 numerical simulation

POC-7Q10 Simulation									
Forebay TDG: 113.0%									
Tailwater Elevation: 721.4 ft									
Powerhouse Unit Discharge (kcfs)									
U1	U2	U3	U4	U5	U6	U7	U8	U9	U10
0.0	20.0	20.0	20.0	20.0	20.0	20.0	20.0	20.0	20.0
Powerhouse Total: 180.0 kcfs									
Spillway Unit Discharge (kcfs)									
S1	S2	S3	S4	S5	S6	S7	S8	S9	S10
0.0	1.7	0.0	2.2	0.0	8.0	43.0	8.0	0.0	1.7
Spillway Total: 64.6 kcfs									
Fishway Flow: 1 kcfs									
Total River Flow: 245.6 kcfs									

9.2 VOF Model Results

The convergence parameters for the POC-7Q10 simulations were:

$$POC-7\text{Q10 S} \rightarrow \left(flowrate : 246\ kcfs, WSE : 721.4\ ft \right)$$

The numerical solution of MR6 was used as an initial condition for the 7Q10 simulation. This case reached the statistically steady solution in approximately 15 minutes (21 days of computation time).

Figure 9.2-1 shows the spillway jet characteristics predicted with the VOF method for the 7Q10 simulation. Similar to observations on June 5, 2006, the surface jet originating from bay 7 attracts water toward the center of the dam. The cross section of spillway 7 in Figure 9.2-1 shows that the surface jet remains close to the free surface minimizing air entrainment. On the other hand, submerged jumps are predicted at bays 6 and 8 (see cross section of spillway unit 6 in Figure 9.2-1). Though surface jumps may entrain more bubbles in the tailrace, minor contributions to TDG production are expected from these bays because of their relatively small volume of spilled water.

[3] Note that the Juvenile Bypass System uses up to 11 kcfs of water when operating through all five bottom gates. The TDG model assumed that only 10 kcfs of water was used to operate the Juvenile Bypass System. This can be achieved by running the system in a top spill configuration on gates 2 and 10 and in bottom spill configuration for gates 4, 6 and 8.

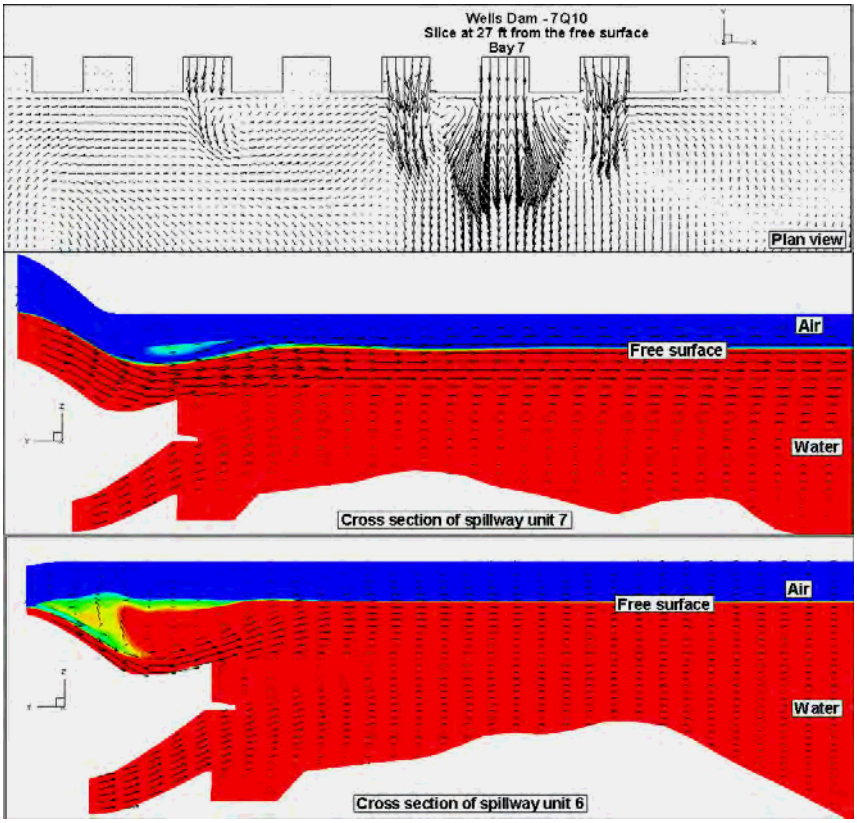

Figure 9.2-1 Predicted flow field for the POC-7Q10 simulation

9.3 Rigid-lid Model Results

Tables in Appendix B show the percent saturation of TDG predicted by the model at each station for the preferred operating conditions during a 7Q10 flow event. Figure 9.3-1 shows TDG values predicted by the model at each probe location. The TDG distribution at the Wells tailrace together with the predicted TDG at each station is shown in Figure 9.3-2. The main process affecting TDG production and mixing occurs upstream of transect T2, after which TDG production reaches a developed condition with minor changes associated with small mass transfer at the free surface. Table 9.3-1 shows the average TDG at transects T1, T2 and T3. According to the model, the average gas saturation does not exceed 120% at any of the three transects.

Figure 9.3-3 show isosurfaces of TDG, gas volume fraction and bubble diameter for the preferred operating condition to address flows up to 7Q10 (246 kcfs). The highest TDG isosurfaces are observed directly below spillbay 7 corresponding with the zone of higher gas volume fraction (aerated zone). In this area, the entrained bubbles generate high levels of TDG. However, the supersaturated water quickly degasses by mass exchange with bubbles near the free surface and mass transfer at the turbulent free surface near the spillway. Moreover, as shown the streamlines of Figure 9.3-4, strong lateral currents caused by the surface jet on bay 7 directed water toward the center of the dam contributing further to fully mixed flow and TDG dilution.

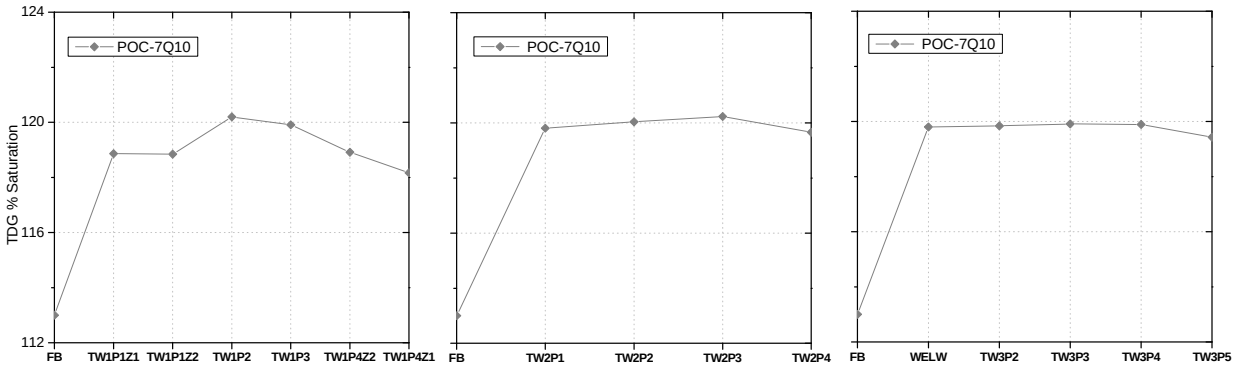

Figure 9.3-1 Predicted TDG concentration for the POC-7Q10.

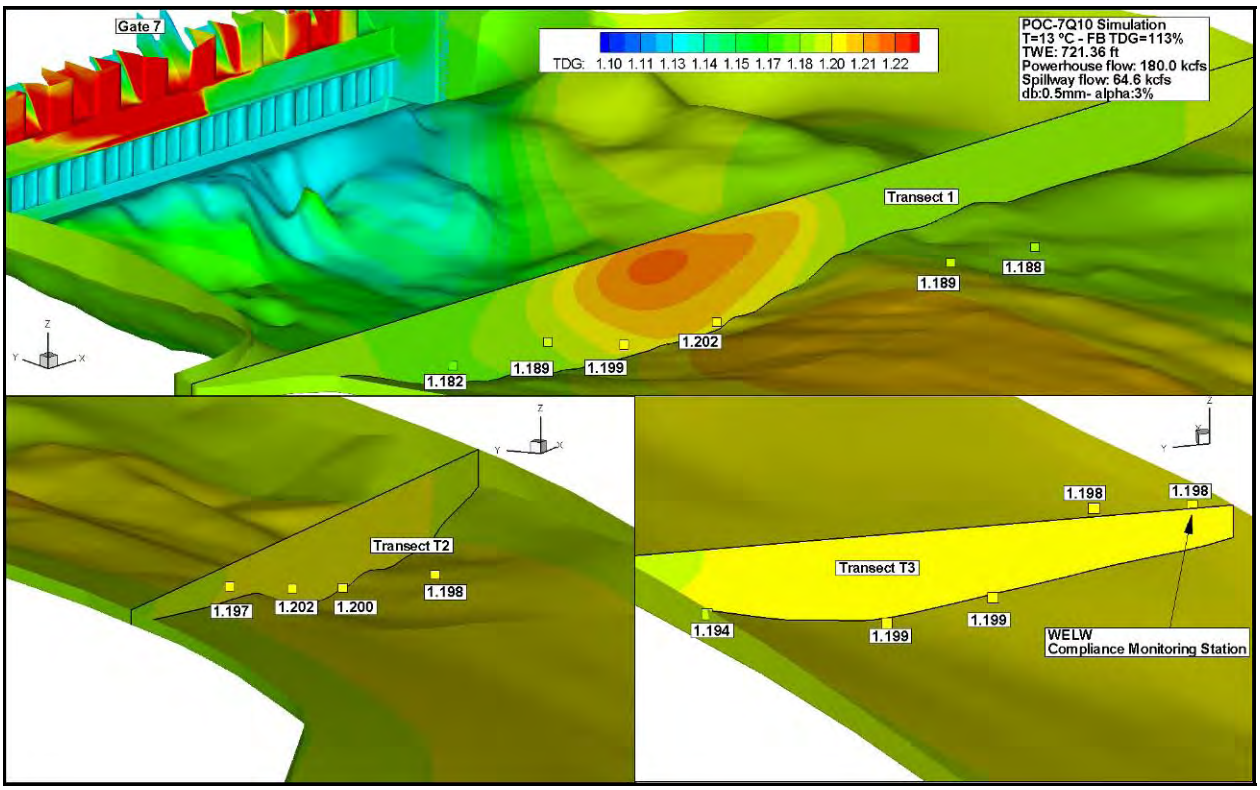

Figure 9.3-2 TDG distribution for the POC-7Q10 simulation.

Table 9.3-1 Averaged predicted TDG in Transects 1, 2 and 3 for the POC-7Q10 simulation.

Case	Type	Spill (kcfs)	Total Q (kcfs)	% Spilled	Unit Spill (kcfs/ft)	Tailwater Elevation (feet)	Spillway Submergence (feet)	% TDG Forebay	% TDG Transect 1	% TDG Transect 2	% TDG Transect 3	Difference % TDG Forebay to Transect 3
7Q10 Simulation	1-FG	64.6	245.6	26.3	0.67	721.4	30.4	113.0	119.2	119.9	119.8	6.8

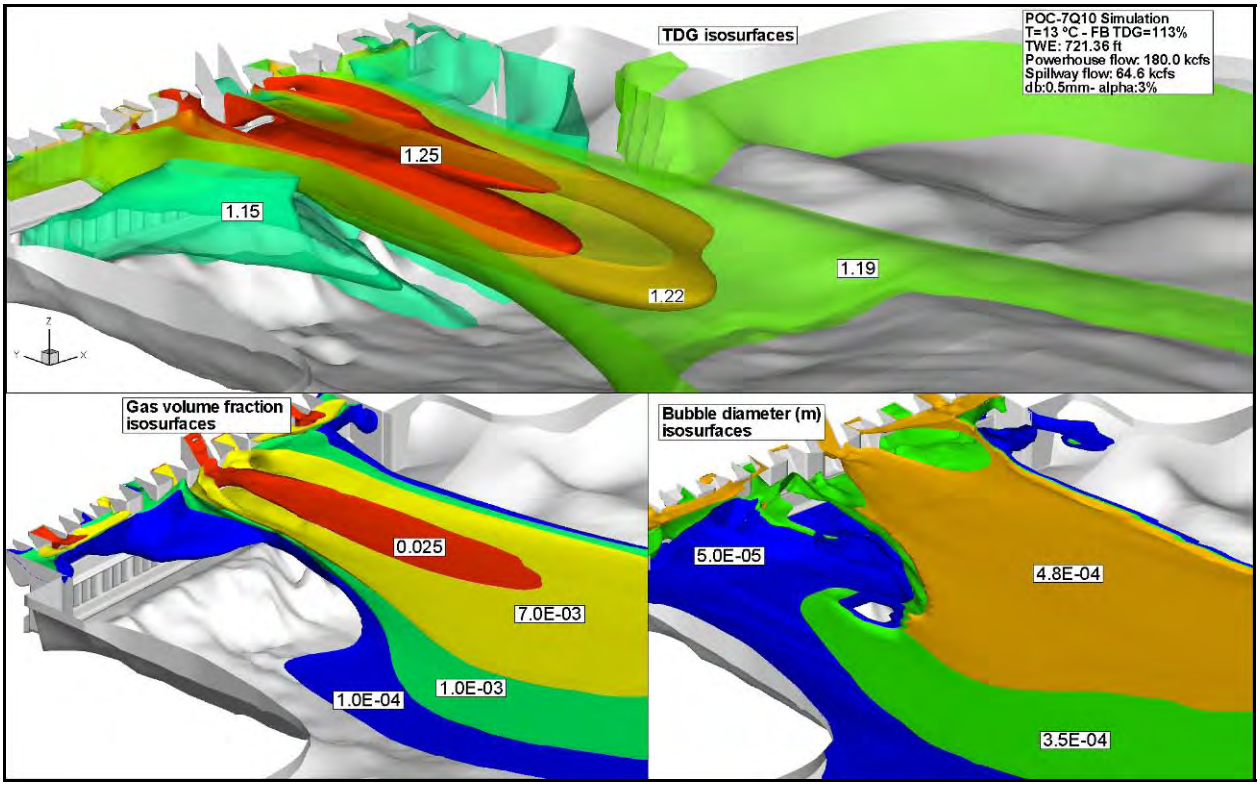

Figure 9.3-3 Streamlines colored by TDG concentration for the POC-7Q10 simulation.

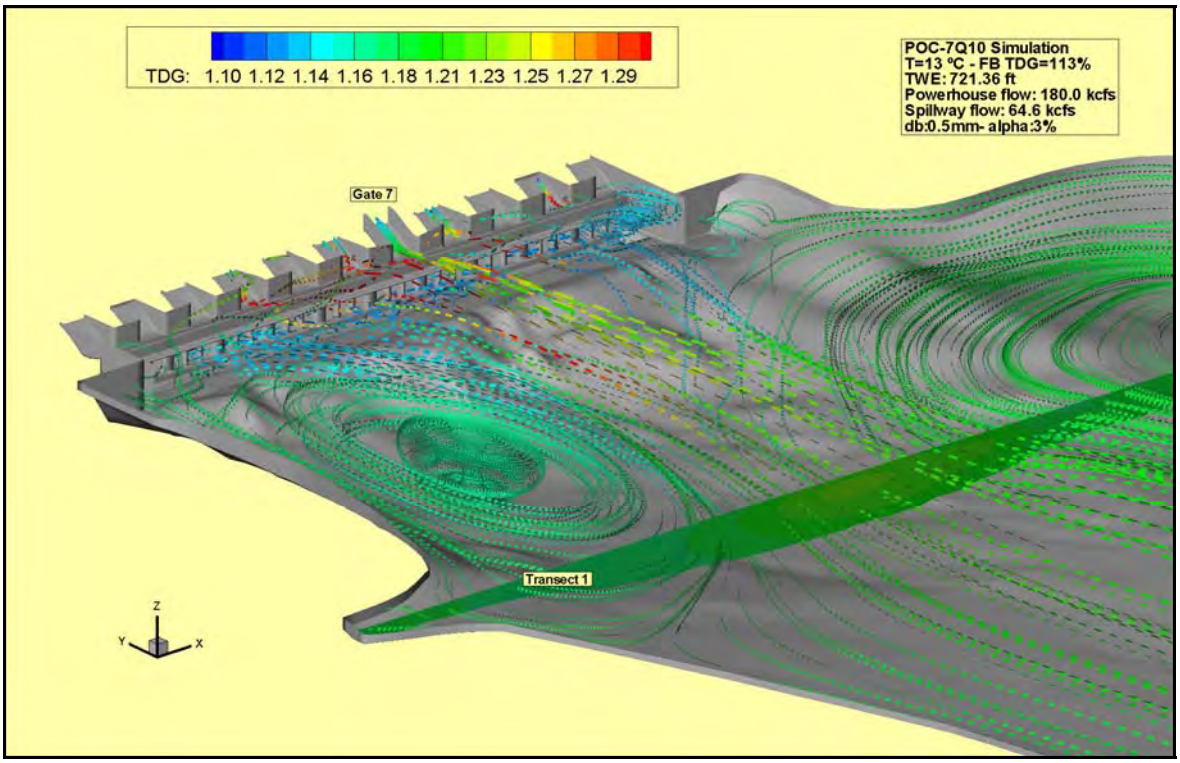

Figure 9.3-4 Streamlines colored by TDG concentration for the POC-7Q10 simulation.

9.4 Location of the compliance monitoring station

The TDG distribution at transect T3 was analyzed to evaluate the location of the tailrace TDG compliance monitoring station WELW. The standard deviation, defined as $\sigma = \sqrt{\frac{1}{N-1}\sum_{i=1}^{N}\left(C - C_{ave}\right)^2}$, and the error of the TDG predicted at the compliance monitoring station calculated from $\text{Error}(\%) = \frac{\left(C_{WELW} - C_{ave}\right)}{C_{ave}} * 100$ are tabulated in Table 9.4-1.

Table 9.4-1 Averaged predicted TDG in Transect T3 and TDG at WELW

Simulation	TDG Average	σ_{TDG}	WELW	Average-WELW Relative Difference (%)
MR1	1.179	0.00537	1.172	-0.580
MR2	1.237	0.01819	1.219	-1.459
MR3	1.207	0.00757	1.214	0.632
MR4	1.247	0.00493	1.251	0.365
MR5	1.167	0.00225	1.167	0.050
MR6	1.213	0.00103	1.212	-0.057
MR7	1.173	0.00490	1.178	0.435
MR8	1.226	0.00928	1.214	-0.920
MR9	1.229	0.00306	1.231	0.166
POC-7Q10	1.198	0.00196	1.198	0.024

In most of the cases the TDG gradient at transect T3 is small, indicating that the TDG gauge station is located in a region where substantial mixing has occurred.

10.0 DISCUSSION

A mixture two-phase flow model aimed at the prediction of TDG in the Wells tailrace was developed. Variable bubble size and gas volume fraction were used to analyze dissolution and the consequent source of TDG. The model uses an anisotropic RSM turbulence model.

The model was calibrated and validated using field data collected on May 14, May 17, June 4 June 5 and June 17, 2006 during the TDG Production Dynamics Study (EES et al., 2007). The spillway flow was spread across spillbays on June 4, concentrated through a single spillbay on May 17, June 4 and June 5, and crowned on June 17. The observed flow field in the tailrace on June 4 and June 5 was properly predicted by the model. The bubble size and gas volume fraction at the inlet were the parameters of the model. A bubble diameter of 0.5 mm and gas volume fraction of 3% in the spillbays produced TDG values that bracketed field observations.

The model captured the lateral TDG distribution and the reduction of TDG longitudinally as observed in the field. The model brackets the results of the field measurements for the validation cases with a deviation of about +/- 3% of the average TDG values for Transect 3. Numerical results obtained during calibration and validation have demonstrated that the presented model can capture the main features of the two-phase flow in the Wells tailrace and the trends of TDG values across all three transects. The model used in this study assumes that bubble size changes mainly due to mass transfer and pressure and considers that breakup and coalescence are negligible. This hypothesis is frequently used for low volume fraction flows. In this study, the gas volume fraction and bubble size were selected to be above and below the averaged TDG measured on June 4 and 5, 2006. It is expected that the inclusion of the breakup and coalescence phenomena change the bubble size distribution at the plunging jet region immediately downstream of the spillway. However, as the bubble size at the inlet was selected to bracket the field data, breakup and coalescence may play a minor role on the TDG distribution and production in the Wells tailrace.

Different spill releases and TDG production as a function of flow and tailwater elevation were analyzed to determine the spillway operation that would minimize gas saturation in the tailrace. Nine runs with two spillway configurations (spread and FG) and four total river flows were simulated in an effort to identify how sensitive the model is to various spillway operating conditions. From this analysis it was concluded that:

- For the sensitivity simulations modeled, full open gate operations result in the lowest TDG values downstream, followed by two open gates operation. The spread operation with moderate flow through each gate produced the highest TDG values as a result of more entrained air in the tailrace and smaller degasification at the free surface.

- TDG production is directly related to percentage of water spilled. In general, higher downstream TDG is observed as the spill percentage increases. Likewise, TDG production increases as the amount of spill increases. In addition, TDG levels downstream are reduced by dilution as powerhouse flow increases.

Based upon general gas dynamics defined by the results from the nine sensitivity runs a Preferred Operating Condition was selected to predict TDG in the tailrace during a 7Q10 (246 kcfs) event. The assumption was that if TDG standards can be achieved during a 7Q10 event, then the standards can be achieved at flows lower than the 246 kcfs level.

According to the numerical model results, the TDG concentration at the fixed monitoring station does not exceed 120% when the Project is operated in the preferred operating configuration during a 7Q10 flow event.

The model described above will continued to be used as a predictive numerical tool to identify additional Project operations that can be used to further reduce TDG concentration downstream of the Wells Project.

11.0 STUDY VARIANCE

There were no variances from the final FERC approved study plan for the Total Dissolved Gas Investigation.

12.0 ACKNOWLEDGMENTS

This numerical study was sponsored by Douglas PUD. The authors thank Shane Bickford, Josh Murauskas, and Bao Le for their support and cooperation to this study. The constructive suggestions of Duncan Hay of Oakwood Consulting Inc. are gratefully appreciated.

13.0 REFERENCES

Antal, S.P., R.T. Lahey Jr., and J.E. Flaherty. 1991. Analysis of Phase Distribution in Fully Developed Laminar Bubbly Two-Phase Flow, International Journal of Multiphase Flow. 17(5): 553-682

ASL Environmental Sciences Inc. 2007. Turbine discharge measurements by acoustic scintillation flow meter at Until 1 and 2, Wells Hydroelectric Project, Pateros, Washington (2006). Prepared for the Public Utility District No. 1 of Douglas County.

Carrica, P. M., D. Drew, F. Bonetto, and R.T. Lahey Jr. 1999. A Polydisperse model for bubbly two–phase flow around a surface ship. International. Journal of Multiphase Flow. 25: 257-305.

Chen, P., M.P. Dudukovic, and J. Sanyal. 2005. Three-dimensional simulation of bubble column flows with bubble coalescence and breakup. American Institute of Chemical Engineers Journal. 51(3):696-712.

Columbia Basin Environmental (CBE). 2003. Wells Dam Spillway Total Dissolved Gas Evaluation 27 May to 10 June 2003. Final Report. Prepared for Public Utility District No. 1 of Douglas County.

Columbia Basin Environmental (CBE). 2004. Wells Dam Spillway Total Dissolved Gas Evaluation 23 May to 6 June 2004. Final Report. Prepared for Public Utility District No. 1 of Douglas County.

Columbia Basin Environmental (CBE). 2006. Wells Dam Spillway Total Dissolved Gas Evaluation – 23 May to 6 June 2005, Final Report, Prepared for Douglas County PUD.

Douglas County PUD (DCPUD). 2006. Wells Hydroelectric Project. FERC Project No. 2149. Pre-Application Document.

Deckwer, W.D. 1992. Bubble Column Reactors. John Wiley & Sons.

DeMoyer, C.D., E.L. Schierholz, J.S. Gulliver, and S.C.Wilhelms. 2003. Impact of Bubble and Free Surface Oxygen Transfer on Diffused Aeration Systems. Water Research. 37(8):1890-1904.

Drew, D.A., and S.L. Passman. 1998. Theory of Multicomponent Fluids. Applied Mathematical Sciences, Springer 135.

EES Consulting, Inc., J. Carroll, ENSR, and Parametrix. 2007. Total dissolved gas production dynamics Study of the Wells hydroelectric project. Prepared for Public Utility District No. 1 of Douglas County. Kirkland, Washington.

Ferrari, G., M.S. Politano, and L. Weber. 2008. Numerical simulation of free flows on a fish bypass. Computers & Fluids. In press.

Fu, S., B.E. Launder, and D.P. Tselepidakis. 1987. Accommodating the effects of high strain rates in modeling the pressure-strain correlations. The University of Manchester Institute of Science and Technology. TFD/87/5.

Gibson, M.M., and B.E. Launder. 1978. Ground effects on pressure fluctuations in the atmospheric boundary layer. Journal of Fluid Mechanics. 86: 491-511.

Guido-Lavalle, G., P. Carrica, A. Clausse, and M.K. Qazi. 1994. A bubble number density constitutive equation, Nuclear Engineering and Design. 152: 213–224.

Hibbs, D.E., and J.S. Gulliver. 1997. Prediction of Effective Saturation Concentration at Spillway Plunge Pools. Journal of Hydraulic Engineering 123: 940-949.

Ishii, M., and N. Zuber. 1979. Drag Coefficient and Relative Velocity in Bubbly, Droplet or Particulate Flows. American Institute of Chemical Engineers Journal. 25(5):843-855.

Jakobsen, H.A., H. Lindborg, and C.A. Dorao. 2005. Modeling of bubble column reactors: progress and limitations. Industrial & Engineering Chemistry Research 44: 5107-5151.

Klinge, R. 2005. Wells Dam total dissolved gas abatement plan for 2005 and 2006 project. Prepared for Public Utility District No. 1 of Douglas County. East Wenatchee, WA

Lamont, J.C. and D.S. Scott. 1970. An eddy cell model of mass transfer into the surface of a turbulent liquid. The American Institute for Chemical Engineers Journal. 16:513-519.

Lane, G.L., M.P. Schwarz, and G.M. Evans. 2005. Numerical modeling of gas-liquid flow in stirred tanks. Chemical. Engineering. Science. 60: 2203–2214.

Launder, B. E. 1989. Second-moment closure and its use in modeling turbulent industrial flows. International Journal for Numerical Methods in Fluids 9:963-985.

Liepmann, D. 1990. The near-field dynamics and entrainment field of submerged and near surface jets. Ph.D. thesis, University of California, San Diego.

Lopez de Bertodano, M.L., R.T. Lahey Jr, and O.C. Jones. 1994. Development of a $k-\varepsilon$ model for bubbly two-phase flow. Journal of Fluids Engineering. 116: 128-134.

Mannheim, C., and L. Weber. 1997. Hydraulic Model Studies for Fish Diversion at Wanapum/Priest Rapids Development, Part XI: Spillway Deflector Design, Contracted by Public Utility District No. 2 of Grant County, Ephrata, WA. IIHR Limited Distribution Report No. 264.

Orlins, J.J. and J.S. Gulliver. 2000. Dissolved Gas Supersaturation Downstream of a Spillway II: Computational Model. Journal of Hydraulic Engineering 38: 151-159.

Politano, M.S., P.M. Carrica, C. Turan, and L. Weber. 2007a. A multidimensional two-phase flow model for the total dissolved gas downstream of spillways. Journal of Hydraulic Research 45(2): 165-177.

Politano, M.S., C. Turan, P.M. Carrica, and L. Weber. 2007b. A three-dimensional anisotropic model of the two phase flow and total dissolved gas downstream of spillways. FLUCOME.
Politano, M.S., P.M. Carrica, and J.L. Baliño. 2000. A polydisperese model of the two-phase flow in a bubble column. Heat and Technology 18(2): 101-113.

Skalski, J. R., G. E. Johnson, C. M. Sullivan, E. Kudera and M. W. Erho. 1996. Statistical evaluation of turbine bypass efficiency at Wells Dam on the Columbia River, Washington. Canadian Journal of Fisheries and Aquatic Sciences. Vol. 53, No. 10, pp. 2188 – 2198.

Takemura, F., and A. Yabe. 1998. Gas Dissolution Process of Spherical Rising Gas Bubbles. Chemical Engineering Science. 53(15):2691-2699.

Turan, C., P. M. Carrica, T. Lyons, D. Hay, and L. Weber. 2008. Study of the Free Surface Flow on an Ogee-Crested Fish Bypass. Journal of Hydraulic Engineering. 134: 1172-1175

Turan, C., M.S. Politano, P. M. Carrica, and L. Weber. 2007. Water Entrainment and Mixing due to Surface Jets. Computational Fluid Dynamics, 21: 3-4, 137-153.

Walker, D.T. 1997. On the origin of the 'surface current' in turbulent free-surface flows. Journal of Fluids Engineering 339, 275-285.

Walker, D.T., and C.Y. Chen. 1994. Evaluation of algebraic stress modelling in free-surface jet flows. Journal of Fluids Engineering 118: 48-54

Appendix A

Conditions Used for the Calibration, validation, and Sensitivity Simulations

Treatment 46 S - June 4, 2006									
Tailwater Elevation: 717.3 ft									
Powerhouse Unit Discharge (kcfs)									
U1	U2	U3	U4	U5	U6	U7	U8	U9	U10
0.0	14.7	14.7	14.4	14.7	14.7	14.8	14.8	14.4	14.7
Powerhouse Total: 131.8 kcfs									
Spillway Unit Discharge (kcfs)									
S1	S2	S3	S4	S5	S6	S7	S8	S9	S10
0.0	1.6	5.4	5.2	5.4	5.2	5.4	5.2	5.4	1.6
Spillway Total: 40.6 kcfs									
Total River Flow: 172.4 kcfs									
Forebay TDG: 111.8%									

Treatment 47 FG - June 5, 2006									
Tailwater Elevation: 720.2 ft									
Powerhouse Unit Discharge (kcfs)									
U1	U2	U3	U4	U5	U6	U7	U8	U9	U10
0.0	18.9	18.0	18.5	18.3	19.0	20.2	19.6	19.9	18.2
Powerhouse Total: 170.6 kcfs									
Spillway Unit Discharge (kcfs)									
S1	S2	S3	S4	S5	S6	S7	S8	S9	S10
0.0	1.3	0.0	2.2	0.0	2.2	42.5	2.2	0.0	1.3
Spillway Total: 51.7 kcfs									
Total River Flow: 222.3 kcfs									
Forebay TDG: 111.5%									

Treatment 1 FG - May 14, 2006									
Tailwater Elevation: 711.5 ft									
Powerhouse Unit Discharge (kcfs)									
U1	U2	U3	U4	U5	U6	U7	U8	U9	U10
0.0	15.0	15.0	14.8	0.0	0.0	0.0	0.0	14.8	15.2
Powerhouse Total: 74.8 kcfs									
Spillway Unit Discharge (kcfs)									
S1	S2	S3	S4	S5	S6	S7	S8	S9	S10
0.0	1.3	0.0	2.2	0.0	2.2	35.4	2.2	0.0	1.3
Spillway Total: 44.6 kcfs									
Total River Flow: 120.4 kcfs									
Forebay TDG: 109.1%									

Treatment 11 FG - May 17, 2006									
Tailwater Elevation: 715.4 ft									
Powerhouse Unit Discharge (kcfs)									
U1	U2	U3	U4	U5	U6	U7	U8	U9	U10
0.0	18.9	19.1	18.7	19.2	0.0	0.0	0.0	18.7	19.2
Powerhouse Total: 113.7 kcfs									
Spillway Unit Discharge (kcfs)									
S1	S2	S3	S4	S5	S6	S7	S8	S9	S10
0.0	0.9	0.0	2.2	0.0	2.2	34.1	2.2	0.0	0.9
Spillway Total: 42.6 kcfs									
Total River Flow: 157.2 kcfs									
Forebay TDG: 110.4%									

Treatment 63 C - June 17, 2006									
Tailwater Elevation: 718.6 ft									
Powerhouse Unit Discharge (kcfs)									
U1	U2	U3	U4	U5	U6	U7	U8	U9	U10
0.0	13.0	13.0	12.9	13.0	13.0	13.1	13.1	12.8	13.1
Powerhouse Total: 117.1 kcfs									
Spillway Unit Discharge (kcfs)									
S1	S2	S3	S4	S5	S6	S7	S8	S9	S10
0.0	1.7	0.0	2.2	0.0	2.2	29.8	19.9	29.8	1.7
Spillway Total: 87.4 kcfs									
Total River Flow: 205.5 kcfs									
Forebay TDG: 113.9%									

Simulation MR1									
Tailwater Elevation: 718.8 ft									
Powerhouse Unit Discharge (kcfs)									
U1	U2	U3	U4	U5	U6	U7	U8	U9	U10
0.0	20.6	20.6	20.6	20.6	20.6	20.6	20.6	20.6	20.6
Powerhouse Total: 185.5 kcfs									
Spillway Unit Discharge (kcfs)									
S1	S2	S3	S4	S5	S6	S7	S8	S9	S10
0.0	0.0	3.3	3.3	3.3	3.3	3.3	3.3	3.3	0.0
Spillway Total: 23.0 kcfs									
Total River Flow: 208.5 kcfs									
Forebay TDG: 115.0%									

Simulation MR2									
Tailwater Elevation: 721.4 ft									
Powerhouse Unit Discharge (kcfs)									
U1	U2	U3	U4	U5	U6	U7	U8	U9	U10
0.0	20.6	20.6	20.6	20.6	20.6	20.6	20.6	20.6	20.6
Powerhouse Total: 185.5 kcfs									
Spillway Unit Discharge (kcfs)									
S1	S2	S3	S4	S5	S6	S7	S8	S9	S10
0.0	0.0	8.6	8.6	8.6	8.6	8.6	8.6	8.6	0.0
Spillway Total: 60.5 kcfs									
Total River Flow: 246.0 kcfs									
Forebay TDG: 115.0%									

Simulation MR3									
Tailwater Elevation: 713.4 ft									
Powerhouse Unit Discharge (kcfs)									
U1	U2	U3	U4	U5	U6	U7	U8	U9	U10
0.0	0.0	19.2	19.2	19.2	19.2	19.2	0.0	0.0	0.0
Powerhouse Total: 96.0 kcfs									
Spillway Unit Discharge (kcfs)									
S1	S2	S3	S4	S5	S6	S7	S8	S9	S10
0.0	0.0	3.3	3.3	3.3	3.3	3.3	3.3	3.3	0.0
Spillway Total: 23.0 kcfs									
Total River Flow: 119.0 kcfs									
Forebay TDG: 115.0%									

Simulation MR4									
Tailwater Elevation: 715.9 ft									
Powerhouse Unit Discharge (kcfs)									
U1	U2	U3	U4	U5	U6	U7	U8	U9	U10
0.0	0.0	19.2	19.2	19.2	19.2	19.2	0.0	0.0	0.0
Powerhouse Total: 96.0 kcfs									
Spillway Unit Discharge (kcfs)									
S1	S2	S3	S4	S5	S6	S7	S8	S9	S10
0.0	0.0	8.6	8.6	8.6	8.6	8.6	8.6	8.6	0.0
Spillway Total: 60.5 kcfs									
Total River Flow: 156.5 kcfs									
Forebay TDG: 115.0%									

Simulation MR5									
Tailwater Elevation: 718.8 ft									
Powerhouse Unit Discharge (kcfs)									
U1	U2	U3	U4	U5	U6	U7	U8	U9	U10
0.0	20.6	20.6	20.6	20.6	20.6	20.6	20.6	20.6	20.6
Powerhouse Total: 185.5 kcfs									
Spillway Unit Discharge (kcfs)									
S1	S2	S3	S4	S5	S6	S7	S8	S9	S10
0.0	0.0	0.0	0.0	0.0	0.0	23.0	0.0	0.0	0.0
Spillway Total: 23.0 kcfs									
Total River Flow: 208.5 kcfs									
Forebay TDG: 115.0%									

Simulation MR6									
Tailwater Elevation: 721.4 ft									
Powerhouse Unit Discharge (kcfs)									
U1	U2	U3	U4	U5	U6	U7	U8	U9	U10
0.0	20.6	20.6	20.6	20.6	20.6	20.6	20.6	20.6	20.6
Powerhouse Total: 185.5 kcfs									
Spillway Unit Discharge (kcfs)									
S1	S2	S3	S4	S5	S6	S7	S8	S9	S10
0.0	0.0	0.0	0.0	0.0	0.0	60.5	0.0	0.0	0.0
Spillway Total: 60.5 kcfs									
Total River Flow: 246.0 kcfs									
Forebay TDG: 115.0%									

Simulation MR7									
Tailwater Elevation: 713.4 ft									
Powerhouse Unit Discharge (kcfs)									
U1	U2	U3	U4	U5	U6	U7	U8	U9	U10
0.0	0.0	19.2	19.2	19.2	19.2	19.2	0.0	0.0	0.0
Powerhouse Total: 96.0 kcfs									
Spillway Unit Discharge (kcfs)									
S1	S2	S3	S4	S5	S6	S7	S8	S9	S10
0.0	0.0	0.0	0.0	0.0	0.0	23.0	0.0	0.0	0.0
Spillway Total: 23.0 kcfs									
Total River Flow: 119.0 kcfs									
Forebay TDG: 115.0%									

Simulation MR8									
Tailwater Elevation: 721.4 ft									
Powerhouse Unit Discharge (kcfs)									
U1	U2	U3	U4	U5	U6	U7	U8	U9	U10
0.0	20.6	20.6	20.6	20.6	20.6	20.6	20.6	20.6	20.6
Powerhouse Total: 185.5 kcfs									
Spillway Unit Discharge (kcfs)									
S1	S2	S3	S4	S5	S6	S7	S8	S9	S10
0.0	0.0	0.0	0.0	30.3	0.0	30.3	0.0	0.0	0.0
Spillway Total: 60.5 kcfs									
Total River Flow: 246.0 kcfs									
Forebay TDG: 115.0%									

Simulation MR9									
Tailwater Elevation: 715.9 ft									
Powerhouse Unit Discharge (kcfs)									
U1	U2	U3	U4	U5	U6	U7	U8	U9	U10
0.0	0.0	19.2	19.2	19.2	19.2	19.2	0.0	0.0	0.0
Powerhouse Total: 96.0 kcfs									
Spillway Unit Discharge (kcfs)									
S1	S2	S3	S4	S5	S6	S7	S8	S9	S10
0.0	0.0	0.0	0.0	30.3	0.0	30.3	0.0	0.0	0.0
Spillway Total: 60.5 kcfs									
Total River Flow: 156.5 kcfs									
Forebay TDG: 115%									

Appendix B

Differences Between Measured and Predicted TDG Concentrations

Comparison between measured and predicted TDG on June 4, 2006

Transect	Easting (feet)	Northing (feet)	Z (feet)	TDG predicted	TDG measured	diff %	Average predicted	Average measured	Average error %
TW1P2	1878138.7	345839.8	648.7	1.238	1.173	5.58			
TW1P3	1877972.7	345812.5	648.4	1.265	1.178	7.41			
TW1P4Z1	1877766.1	345652.5	692.0	1.224	1.200	1.97			
TW1P4Z2	1877685.6	345800.1	657.0	1.190	1.197	-0.61	1.229	1.187	3.56
TW2P2	1878494.5	343593.5	675.9	1.204	1.172	2.72			
TW2P3	1878414.7	343618.3	679.9	1.230	1.174	4.78			
TW2P4	1878237.5	343582.5	698.6	1.233	1.179	4.55	1.222	1.175	4.02
WELW	1870372.9	334581.1	692.0	1.190	1.165	2.18			
TW3P2	1870323.5	334702.2	698.7	1.202	1.171	2.69			
TW3P4	1870037.3	334949.0	673.4	1.211	1.179	2.74			
TW3P5	1869929.7	335169.1	697.9	1.222	1.188	2.87	1.207	1.176	2.62

Comparison between measured and predicted TDG on June 5, 2006

Transect	Easting (feet)	Northing (feet)	Z (feet)	TDG predicted	TDG measured	diff %	Average predicted	Average measured	Average error %
TW1P2	1878138.7	345839.8	648.7	1.160	1.200	-3.38			
TW1P3	1877972.7	345812.5	648.4	1.155	1.180	-2.05			
TW1P4Z1	1877766.1	345652.5	692.0	1.153	1.158	-0.46			
TW1P4Z2	1877685.6	345800.1	657.0	1.152	1.159	-0.68	1.155	1.174	-1.66
TW2P2	1878494.5	343593.5	675.9	1.151	1.181	-2.53			
TW2P3	1878414.7	343618.3	679.9	1.152	1.182	-2.57			
TW2P4	1878237.5	343582.5	698.6	1.151	1.183	-2.73	1.151	1.182	-2.61
WELW	1870372.9	334581.1	692.0	1.149	1.173	-2.04			
TW3P2	1870323.5	334702.2	698.7	1.150	1.178	-2.35			
TW3P4	1870037.3	334949.0	673.4	1.151	1.182	-2.68			
TW3P5	1869929.7	335169.1	697.9	1.150	1.182	-2.67	1.150	1.179	-2.44

Comparison between measured and predicted TDG on May 14, 2006

Transect	Easting (feet)	Northing (feet)	Z (feet)	TDG predicted	TDG measured	diff %	Average predicted	Average measured	Average error %
TW1P1Z1	1878593.6	345704.7	692.0	1.155	1.167	-1.00			
TW1P1Z2	1878511.2	345814.2	669.1	1.159	1.167	-0.67			
TW1P2	1878138.7	345839.8	648.7	1.170	1.181	-0.96			
TW1P3	1877972.7	345812.5	648.4	1.176	1.187	-0.91			
TW1P4Z1	1877766.1	345652.5	692.0	1.173	1.163	0.88			
TW1P4Z2	1877685.6	345800.1	657.0	1.166	1.168	-0.21	1.167	1.172	-0.48
TW2P1	1878645.0	343552.6	675.6	1.162	1.167	-0.43			
TW2P2	1878494.5	343593.5	675.9	1.162	1.170	-0.71			
TW2P3	1878414.7	343618.3	679.9	1.163	1.175	-1.05			
TW2P4	1878237.5	343582.5	698.6	1.164	1.180	-1.38	1.163	1.173	-0.89
WELW	1870372.9	334581.1	692.0	1.163	1.151	1.01			
TW3P2	1870323.5	334702.2	698.7	1.162	1.165	-0.28			
TW3P3	1870104.4	334818.9	679.0	1.163	1.164	-0.12			
TW3P4	1870037.3	334949.0	673.4	1.164	1.173	-0.80			
TW3P5	1869929.7	335169.1	697.9	1.164	1.170	-0.48	1.163	1.165	-0.14

Comparison between measured and predicted TDG on May 17, 2006

Transect	Easting (feet)	Northing (feet)	Z (feet)	TDG predicted	TDG measured	diff %	Average predicted	Average measured	Average error %
TW1-1S	1878593.6	345704.7	692.0	1.147	1.163	-1.38			
TW 1-1	1878511.2	345814.2	669.1	1.156	1.161	-0.44			
TW 1-2	1878138.7	345839.8	648.7	1.183	1.166	1.45			
TW 1-3	1877972.7	345812.5	648.4	1.188	1.173	1.21			
TW1-4S	1877766.1	345652.5	692.0	1.177	1.149	2.47			
TW 1-4	1877685.6	345800.1	657.0	1.168	1.153	1.30	1.170	1.161	0.77
TW 2-2	1878494.5	343593.5	675.9	1.168	1.168	0.01			
TW 2-3	1878414.7	343618.3	679.9	1.171	1.172	-0.11			
TW 2-4	1878237.5	343582.5	698.6	1.167	1.167	0.04	1.169	1.169	-0.02
WELW	1870372.9	334581.1	692.0	1.165	1.153	1.05			
TW 3-2	1870323.5	334702.2	698.7	1.166	1.164	0.15			
TW 3-3	1870104.4	334818.9	679.0	1.167	1.162	0.47			
TW 3-4	1870037.3	334949.0	673.4	1.168	1.169	-0.11			
TW 3-5	1869929.7	335169.1	697.9	1.168	1.161	0.59	1.167	1.162	0.43

Comparison between measured and predicted TDG on June 17, 2006

Transect	Easting (feet)	Northing (feet)	Z (feet)	TDG predicted	TDG measured	diff %	Average predicted	Average measured	Average error %
TW1P1Z1	1878593.6	345704.7	692.0	1.188	1.256	-5.39			
TW1P2	1878138.7	345839.8	648.7	1.398	1.282	12.97			
TW1P3	1877972.7	345812.5	648.4	1.343	1.260	6.57			
TW1P4Z1	1877766.1	345652.5	692.0	1.284	1.217	5.54			
TW1P4Z2	1877685.6	345800.1	657.0	1.259	1.222	3.03	1.305	1.247	4.58
TW2P2	1878494.5	343593.5	675.9	1.261	1.261	-0.02			
TW2P3	1878414.7	343618.3	679.9	1.265	1.261	0.34			
TW2P4	1878237.5	343582.5	698.6	1.265	1.233	2.58	1.264	1.252	0.95
WELW	1870372.9	334581.1	692.0	1.256	1.243	1.06			
TW3P2	1870323.5	334702.2	698.7	1.264	1.249	1.16			
TW3P4	1870037.3	334949.0	673.4	1.268	1.248	1.58			
TW3P5	1869929.7	335169.1	697.9	1.269	1.238	2.53	1.264	1.245	1.58

MR1

Transect	Easting (feet)	Northing (feet)	Z (feet)	TDG predicted	Average predicted
TW1P1Z1	1878593.6	345704.7	692.0	1.169	
TW1P1Z2	1878511.2	345814.2	669.1	1.162	
TW1P2	1878138.7	345839.8	648.7	1.174	
TW1P3	1877972.7	345812.5	648.4	1.168	
TW1P4Z1	1877766.1	345652.5	692.0	1.182	
TW1P4Z2	1877685.6	345800.1	657.0	1.182	1.173
TW2P1	1878645.0	343552.6	675.6	1.170	
TW2P2	1878494.5	343593.5	675.9	1.176	
TW2P3	1878414.7	343618.3	679.9	1.187	
TW2P4	1878237.5	343582.5	698.6	1.190	1.181
WELW	1870372.9	334581.1	692.0	1.172	
TW3P2	1870323.5	334702.2	698.7	1.175	
TW3P3	1870104.4	334818.9	679.0	1.180	
TW3P4	1870037.3	334949.0	673.4	1.183	
TW3P5	1869929.7	335169.1	697.9	1.185	1.179

MR2

Transect	Easting (feet)	Northing (feet)	Z (feet)	TDG predicted	Average predicted
TW1P1Z1	1878593.6	345704.7	692.0	1.203	
TW1P1Z2	1878511.2	345814.2	669.1	1.180	
TW1P2	1878138.7	345839.8	648.7	1.240	
TW1P3	1877972.7	345812.5	648.4	1.246	
TW1P4Z1	1877766.1	345652.5	692.0	1.273	
TW1P4Z2	1877685.6	345800.1	657.0	1.278	1.237
TW2P1	1878645.0	343552.6	675.6	1.217	
TW2P2	1878494.5	343593.5	675.9	1.232	
TW2P3	1878414.7	343618.3	679.9	1.247	
TW2P4	1878237.5	343582.5	698.6	1.266	1.241
WELW	1870372.9	334581.1	692.0	1.219	
TW3P2	1870323.5	334702.2	698.7	1.223	
TW3P3	1870104.4	334818.9	679.0	1.234	
TW3P4	1870037.3	334949.0	673.4	1.244	
TW3P5	1869929.7	335169.1	697.9	1.264	1.237

MR3

Transect	Easting (feet)	Northing (feet)	Z (feet)	TDG predicted	Average predicted
TW1P1Z1	1878593.6	345704.7	692.0	1.246	
TW1P1Z2	1878511.2	345814.2	669.1	1.247	
TW1P2	1878138.7	345839.8	648.7	1.232	
TW1P3	1877972.7	345812.5	648.4	1.193	
TW1P4Z1	1877766.1	345652.5	692.0	1.181	
TW1P4Z2	1877685.6	345800.1	657.0	1.182	1.213
TW2P1	1878645.0	343552.6	675.6	1.227	
TW2P2	1878494.5	343593.5	675.9	1.216	
TW2P3	1878414.7	343618.3	679.9	1.201	
TW2P4	1878237.5	343582.5	698.6	1.185	1.207
WELW	1870372.9	334581.1	692.0	1.214	
TW3P2	1870323.5	334702.2	698.7	1.214	
TW3P3	1870104.4	334818.9	679.0	1.206	
TW3P4	1870037.3	334949.0	673.4	1.203	
TW3P5	1869929.7	335169.1	697.9	1.197	1.207

MR4

Transect	Easting (feet)	Northing (feet)	Z (feet)	TDG predicted	Average predicted
TW1P1Z1	1878593.6	345704.7	692.0	1.297	
TW1P1Z2	1878511.2	345814.2	669.1	1.295	
TW1P2	1878138.7	345839.8	648.7	1.262	
TW1P3	1877972.7	345812.5	648.4	1.230	
TW1P4Z1	1877766.1	345652.5	692.0	1.248	
TW1P4Z2	1877685.6	345800.1	657.0	1.248	1.263
TW2P1	1878645.0	343552.6	675.6	1.258	
TW2P2	1878494.5	343593.5	675.9	1.244	
TW2P3	1878414.7	343618.3	679.9	1.237	
TW2P4	1878237.5	343582.5	698.6	1.243	1.245
WELW	1870372.9	334581.1	692.0	1.251	
TW3P2	1870323.5	334702.2	698.7	1.251	
TW3P3	1870104.4	334818.9	679.0	1.247	
TW3P4	1870037.3	334949.0	673.4	1.244	
TW3P5	1869929.7	335169.1	697.9	1.239	1.247

MR5

Transect	Easting (feet)	Northing (feet)	Z (feet)	TDG predicted	Average predicted
TW1P1Z1	1878593.6	345704.7	692.0	1.158	
TW1P1Z2	1878511.2	345814.2	669.1	1.157	
TW1P2	1878138.7	345839.8	648.7	1.171	
TW1P3	1877972.7	345812.5	648.4	1.163	
TW1P4Z1	1877766.1	345652.5	692.0	1.155	
TW1P4Z2	1877685.6	345800.1	657.0	1.157	1.160
TW2P1	1878645.0	343552.6	675.6	1.168	
TW2P2	1878494.5	343593.5	675.9	1.172	
TW2P3	1878414.7	343618.3	679.9	1.170	
TW2P4	1878237.5	343582.5	698.6	1.163	1.168
WELW	1870372.9	334581.1	692.0	1.1672	
TW3P2	1870323.5	334702.2	698.7	1.16764	
TW3P3	1870104.4	334818.9	679.0	1.1681	
TW3P4	1870037.3	334949.0	673.4	1.16751	
TW3P5	1869929.7	335169.1	697.9	1.16264	1.167

MR6

Transect	Easting (feet)	Northing (feet)	Z (feet)	TDG predicted	Average predicted
TW1P1Z1	1878593.6	345704.7	692.0	1.208	
TW1P1Z2	1878511.2	345814.2	669.1	1.205	
TW1P2	1878138.7	345839.8	648.7	1.221	
TW1P3	1877972.7	345812.5	648.4	1.217	
TW1P4Z1	1877766.1	345652.5	692.0	1.205	
TW1P4Z2	1877685.6	345800.1	657.0	1.211	1.211
TW2P1	1878645.0	343552.6	675.6	1.213	
TW2P2	1878494.5	343593.5	675.9	1.215	
TW2P3	1878414.7	343618.3	679.9	1.216	
TW2P4	1878237.5	343582.5	698.6	1.213	1.214
WELW	1870372.9	334581.1	692.0	1.212	
TW3P2	1870323.5	334702.2	698.7	1.213	
TW3P3	1870104.4	334818.9	679.0	1.214	
TW3P4	1870037.3	334949.0	673.4	1.214	
TW3P5	1869929.7	335169.1	697.9	1.212	1.213

MR7

Transect	Easting (feet)	Northing (feet)	Z (feet)	TDG predicted	Average predicted
TW1P1Z1	1878593.6	345704.7	692.0	1.193	
TW1P1Z2	1878511.2	345814.2	669.1	1.192	
TW1P2	1878138.7	345839.8	648.7	1.191	
TW1P3	1877972.7	345812.5	648.4	1.165	
TW1P4Z1	1877766.1	345652.5	692.0	1.155	
TW1P4Z2	1877685.6	345800.1	657.0	1.156	1.175
TW2P1	1878645.0	343552.6	675.6	1.181	
TW2P2	1878494.5	343593.5	675.9	1.176	
TW2P3	1878414.7	343618.3	679.9	1.168	
TW2P4	1878237.5	343582.5	698.6	1.159	1.171
WELW	1870372.9	334581.1	692.0	1.178	
TW3P2	1870323.5	334702.2	698.7	1.178	
TW3P3	1870104.4	334818.9	679.0	1.173	
TW3P4	1870037.3	334949.0	673.4	1.171	
TW3P5	1869929.7	335169.1	697.9	1.167	1.173

MR8

Transect	Easting (feet)	Northing (feet)	Z (feet)	TDG predicted	Average predicted
TW1P1Z1	1878593.6	345704.7	692.0	1.180	
TW1P1Z2	1878511.2	345814.2	669.1	1.178	
TW1P2	1878138.7	345839.8	648.7	1.194	
TW1P3	1877972.7	345812.5	648.4	1.248	
TW1P4Z1	1877766.1	345652.5	692.0	1.227	
TW1P4Z2	1877685.6	345800.1	657.0	1.243	1.212
TW2P1	1878645.0	343552.6	675.6	1.210	
TW2P2	1878494.5	343593.5	675.9	1.223	
TW2P3	1878414.7	343618.3	679.9	1.244	
TW2P4	1878237.5	343582.5	698.6	1.241	1.230
WELW	1870372.9	334581.1	692.0	1.214	
TW3P2	1870323.5	334702.2	698.7	1.218	
TW3P3	1870104.4	334818.9	679.0	1.227	
TW3P4	1870037.3	334949.0	673.4	1.233	
TW3P5	1869929.7	335169.1	697.9	1.236	1.226

MR9

Transect	Easting (feet)	Northing (feet)	Z (feet)	TDG predicted	Average predicted
TW1P1Z1	1878593.6	345704.7	692.0	1.213	
TW1P1Z2	1878511.2	345814.2	669.1	1.212	
TW1P2	1878138.7	345839.8	648.7	1.218	
TW1P3	1877972.7	345812.5	648.4	1.244	
TW1P4Z1	1877766.1	345652.5	692.0	1.217	
TW1P4Z2	1877685.6	345800.1	657.0	1.228	1.222
TW2P1	1878645.0	343552.6	675.6	1.232	
TW2P2	1878494.5	343593.5	675.9	1.233	
TW2P3	1878414.7	343618.3	679.9	1.230	
TW2P4	1878237.5	343582.5	698.6	1.223	1.229
WELW	1870372.9	334581.1	692.0	1.231	
TW3P2	1870323.5	334702.2	698.7	1.231	
TW3P3	1870104.4	334818.9	679.0	1.230	
TW3P4	1870037.3	334949.0	673.4	1.229	
TW3P5	1869929.7	335169.1	697.9	1.224	1.229

POD-7Q10 Simulation

Transect	Easting (feet)	Northing (feet)	Z (feet)	TDG predicted	Average predicted
TW1P1Z1	1878593.6	345704.7	692.0	1.189	
TW1P1Z2	1878511.2	345814.2	669.1	1.188	
TW1P2	1878138.7	345839.8	648.7	1.202	
TW1P3	1877972.7	345812.5	648.4	1.199	
TW1P4Z1	1877766.1	345652.5	692.0	1.182	
TW1P4Z2	1877685.6	345800.1	657.0	1.189	1.192
TW2P1	1878645.0	343552.6	675.6	1.198	
TW2P2	1878494.5	343593.5	675.9	1.200	
TW2P3	1878414.7	343618.3	679.9	1.202	
TW2P4	1878237.5	343582.5	698.6	1.197	1.199
WELW	1870372.9	334581.1	692.0	1.198	
TW3P2	1870323.5	334702.2	698.7	1.198	
TW3P3	1870104.4	334818.9	679.0	1.199	
TW3P4	1870037.3	334949.0	673.4	1.199	
TW3P5	1869929.7	335169.1	697.9	1.194	1.198